PROJECT 1: INVESTIGATING THE POLYCLONAL NATURE OF GLIOBLASTOMA THROUGH THE DEVELOPMENT OF A 3-DIMENSIONAL SPHEROID MODEL

AND

PROJECT 2: INVESTIGATING TNF-α IN FIRST EPISODE PSYCHOSIS MEDICATION NAÏVE SCHIZOPHRENIA PATIENTS TO DEMOGRAPHICALLY CONTROLLED INDIVIDUALS AND PHARMACOLOGICAL MANIPULATION OF TNF-α RELEASE

By

KATHERINE LOUISE EALES

A thesis submitted to the University of Birmingham for the degree of MASTER OF RESEARCH

In BIOMEDICAL RESEARCH

UNIVERSITY OF BIRMINGHAM

MRC Medical Research Council

School of Cancer Sciences

School of Clinical and Experimental Medicine

College of Medical and Dental Sciences,

University of Birmingham

May 2014

PROJECT 1: INVESTIGATING THE POLYCLONAL NATURE OF GLIOBLASTOMA THROUGH THE DEVELOPMENT OF A 3-DIMENSIONAL SPHEROID MODEL

This project is submitted in partial fulfilment of the requirements for the award of the MRes

ABSTRACT

Glioblastoma (GBM) is the most malignant form of glioma with patients having a poor survival rate of 15 months post diagnosis. Metagenomics has shown that GBM is a heterogeneous disease consisting of four genetic subtypes (Proneural, Classical, Mesenchymal and Neural) characterised by diverse mutations and differential sensitivity to treatment. Understanding how these subtypes interact to promote tumour survival is imperative for the design of targeted treatments to treat the whole tumour and not specific subtypes. Previous research used adherent monolayer cultures however these do not accurately portray the complex microenvironment and 3D cell-cell interactions observed *in vivo* This study aimed to develop a 3D culture model, using 3 cell lines representative of the GBM subtypes grown as multicellular spheroids. Subtype interactions were observed using confocal microscopy and preferential subtype locations were seen within the polyclonal spheroid. Spheroids were treated with chemotherapy agent, Temozolomide (TMZ), and observations showed that the Mesenchymal subtype proliferated and relocated to the spheroid centre, potentially promoting spheroid survival. This study provides a suitable *in vitro* culture model of GBM heterogeneity, which can be further developed to improve the effectiveness of future research and the opportunity for the development of more targeted treatments.

Acknowledgments

I would first like to thank Dr Daniel Tennant and Kate Hollinshead for their supervision and guidance during this project as it has been very much appreciated. I would also like to acknowledge the rest of the GBM team and Dr Tennant's lab for their time, space and help within the lab.

I also wish to thank Dr Elena Odintsova, who kindly gave her time and assistance with the confocal microscope and who without, the imaging would not have been possible.

Finally, thanks go to the MRC for funding this investigation.

TABLE OF CONTENTS

LIST OF FIGURES

LIST OF TABLES

LIST OF ABBREVIATIONS

2D- 2-dimensional

3D- 3-dimensional

BSA- Bovine serum albumin

DMEM- Dulbecco's modified eagle medium

DMSO- Dimethyl sulfoxide

EGFR- Epidermal growth factor receptor

FACS- Fluorescent-activated cell sorting

FBS- Foetal bovine serum

GBM- Glioblastoma

GFP- Green fluorescent protein

HGG- High-grade glioma

HIF-1α- Hypoxia-inducible factor 1α

HIFs- Hypoxia-inducible factors

ICC- Immunocytochemistry

IDH1- Isocitrate dehydrogenase 1

LGG- Low-grade glioma

LMP- Low-melting point

MGMT- O^6-methylguanine DNA methyltransferase

MMR- Mismatch repair system

NF1- Neurofibromin 1

PBS- Phosphate-buffered saline

PIMO- Pimonidazole

RFP- Red fluorescent protein

RIPA- Radioimmunoprecipitation buffer

RT- Room temperature

R-T- Radiation therapy

SDS-PAGE- SDS-polyacrylamide gel electrophoresis

SDW- Sterile distilled water

SEM- Standard error of the mean

SiRNA- Small-interfering RNA

SRB- Sulforhodamine B

TCA- Triochloroacetic acid

TMZ- Temozolomide

YFP- Yellow fluorescent protein

1. INTRODUCTION

1.1 Glioblastoma

Glioblastoma (GBM) is the most severe type of glioma, a class of malignant brain tumours derived from glial cells[1, 2]. The cancer has a significantly poor survival prognosis of less than one year from time of diagnosis[3]. Even with multimodal treatment strategies, the median survival time is around 15 months, with as little as 3-5% survival over 36 months[4]. Despite brain tumours affecting more people under 40 years old than any other cancer, less than 2% of cancer research funding is dedicated to brain tumour research[5]. Due to the severity of this condition, it is imperative that further research is conducted into the causes of GBM and potential treatments.

Gliomas have been histologically classified according to the World Health Organisation (WHO) into astrocytomas, oligodendrogliomas and mixed oligoastrocytomas[2, 6]. These tumours are then graded according to severity based on information obtained from a tumour biopsy[2]. Low-grade gliomas (LGGs), designated as grades I/II, are slow growing but may progress to more aggressive tumours[2]. Grade III/IV tumours are fast-progressing, high-grade gliomas (HGGs), with the most malignant grade IV glioblastoma accounting for 82% of gliomas[7]. Around 90% of GBMs are believed to arise *de novo* (primary GBM)[8, 9] i.e. without any clinical evidence of a preceding lower grade tumour, whereas 10% arise from progression from LGGs (secondary GBM)[9, 10]. Genetic studies have shown that primary and secondary tumours have distinct genetic profiles that largely differ from each other[8, 11], (figure 1).

Figure 1: The genetic pathways of Gliomas (Ohgaki et *al.*, 2013 [8]). Schematic documenting the genetic mutations involved in the generation of primary and secondary glioblastomas. Note that despite both originating from glial progenitor cells, primary and secondary GBM have separate, distinctive differences in the mutations present and also the time course of tumour progression.

GBM has a significant impact on the quality of life of both the patient and their relatives and since primary GBM is most common in elderly patients[2, 8], it is thought that GBM incidence could rise with an ever-increasing ageing population[7]. This only emphasises that more research needs to be conducted to be able to better diagnose and develop improved treatment strategies for GBM in the near future.

1.2 Importance of Tumour Heterogeneity and Genetic Subtypes in Glioma

Tumour heterogeneity is important in glioma research as different cells have characteristically different phenotypes with regards to survival and response to treatment[12]. Tumours are not solely comprised of homotypic cells but are more commonly an ensemble of different cell types that differ in genetic morphology, which is important for tumour invasiveness, metastatic behaviour and ultimately drug resistance[13]. Tumours vary not only between patients, but also within the same organ, known as inter-tumour heterogeneity[14]. Cells from different locations within a tumour have also been shown to portray a different genetic profile (intra-tumour heterogeneity)[14]. Defining these genetic profiles can assist in not only diagnosing glioma but also in predicting patient's response to therapy[15].

Development of next generation sequencing technologies over the past decade[16], has allowed an integrated approach, using metagenomic and metatranscriptomic analyses[17], to explore heterogeneity in GBM[1]. The Cancer Genome Atlas defined four genetic subtypes (Verhaak Classification), which allowed for the first time to categorise the extensive inter-tumoural heterogeneity observed in GBM[4, 18, 19], table 1.

	Proneural	Classical	Mesenchymal	Neural
Amplifications	PDGFRA (4q12)	EGFR (97%) Chromosome 7	MET CDK6	
Mutations	IDH1 point mutations (R132) PDGFRA TP53 PIK_3R1/CA	EGFR	NF1 PTEN RB1	
Deletions		CDKN2A/2B Chromosome 10 loss	Homozygous deletion NF1	
Gene Expression	↑OLIG2 ↑NKX_{2-2} ↓CDKN1A	↑NES ↑Notch ↑Sonic Hedghog	↓NF1 CH13L1 MET	NEFL GABRA1 SYT1 SLC12AS
Gene Signature	Oligodendrocytic	Astrocytic	Cultured astroglial	Enrichment in neuronal genes

Table 1: Genetic alterations classifying Glioma subtypes. Table 1 shows the gene amplifications, mutations, deletions and expression characterising four GBM subtypes as defined by the Verhaak Classification system.

The Proneural subclass characteristically display a point mutation in the isocitrate-dehydrogenase 1 (IDH1) gene, the earliest detectable mutation in LGGs[8] and consequently seen in 80% of secondary GBMs, compared to 5% of primary GBMs[10, 20]. Mutations in IDH1 are generally associated with an increase in the overall survival, after combined surgery and radiotherapy, from an average of 11.3 months to 27.1 months[20]. Thus, IDH1 mutations are a strong predictor of a more favourable prognosis and a highly selective molecular marker of secondary GBM. The Classical subgroup is defined by high-level amplification of epidermal growth factor receptors (EGFRs) present in 40-50% of glioblastomas[21], predominately primary GBMs, but also in a minority of secondary GBMs[9]. The Mesenchymal subgroup is distinguished by homozygous deletions/mutations in the neurofibromin1 gene, NF1[19]. Other mesenchymal markers are also highly expressed corresponding to a higher level of necrosis and inflammation[19]. The Neural subtype is

categorised by expression of neuronal markers such as NEFL, SYT1 and GABRA1 and is most similar to normal brain tissue[19].

A study conducted by Sottoriva *et al.,* 2013[12] showed that in 6 out of 10 tumours analysed, fragments taken from the same tumour were classified into at least 2 subgroups, suggesting that clonal interactions are potentially important for tumour survival. Selective pressures such as chemotherapy treatment, allow for populations of tumour cells that have acquired genetic alterations to survive, rendering them resistant to that treatment[12, 22]. The resistant tumour cells can co-operate with other subtypes present and even alter the tumour microenvironment to facilitate overall survival[13]. EGFR mutations have shown to confer resistance to treatment and have actually been detected before treatment has commenced[14, 23]. Inter-clonal co-operativity and mutualistic interactions are thought to a method of maintaining heterogeneity and promoting tumour growth[14, 24] consequently leading to recurrence[25]. Despite this, there is optimism that a stratified treatment approach could potentially be derived according to the patient subtype to retard inter-clonal co-operativity[14]. It is therefore imperative that tumour heterogeneity and clonal interactions are further investigated.

1.3 Treatment Strategy

Treating GBM is problematic since tumour cells are highly aggressive and particularly resistant to therapy[26]. This becomes a significant issue because invasive and irradiating treatment can consequently damage surrounding healthy tissue, which the brain cannot adequately repair posing an important question of the necessity of aggressive treatments.

The first line of treatment for glioma is surgical resection. Tumours are first graded in malignancy with the highest grade being reported, however many reports discussing the heterogeneous nature of gliomas suggest single biopsies underestimate the mutational heterogeneity, giving a misleading prognosis[27]. A clinical study[28, 29] has shown that complete tumour resection is needed to benefit survival however, unfortunately due to high invasion into surrounding tissue, complete resection is often impossible[1].

Following surgery, the patient undergoes successive rounds of combined radiation therapy (RT) and chemotherapy. Stupp *et al.,* 2005[3] investigated the benefit of combined RT and chemotherapy and consequently showed a significant increase in the 2-year survival rate from 10.4% with radiotherapy alone to 26.5% when treated with RT and chemotherapy in combination. The current chemotherapy reagent is Temozolomide (TMZ) which, following administration, methylates DNA at positions N^7 and O^6 of guanine residues and O^3 of adenine residues[30]. The mismatch repair (MMR) system, designed to repair DNA, fails at incorporating a complementary base pair to the methylated residues, consequently inducing DNA lesions along the strand. These lesions accumulate inhibiting successful DNA replication, triggering tumour cell apoptosis[31]. Some tumour cells however are resistant to TMZ-induced damage. The O^6-methylguanine DNA methyltransferase (MGMT) gene encodes DNA repair enzyme that specifically removes methyl groups present at the O^6 position of guanine, thus repairing TMZ-induced adducts[32]. However, epigenetic silencing of the MGMT promoter region via methylation, apparent in approximately 45-50% of GBM patients[33-35], prevents expression of MGMT, therefore restoring sensitivity to TMZ. Hence, MGMT promoter methylation has shown to greatly benefit patients treated with TMZ[36], as seen in a clinical study conducted by Hegi *et al.,* 2005[37].

Treatment stratification is particularly important, as different glioma subtypes have been shown to respond differently to chemotherapy. It has been shown that the Proneural subtype does not respond to aggressive treatment[19]. Similarly, patients that do not have methylated MGMT undergo the same aggressive procedure even though it provides no additional benefit to their survival[28, 37]. Considering chemotherapy cycles are severely debilitating and costs the NHS around £12,000 per patient[38], both health organisations and patients will benefit from the ability to characterise different forms of GBM, providing a more targeted and effective approach to treatment.

1.4 Investigating Glioma Heterogeneity *in vitro*

1.4.1 Adherent monolayer cultures

In vitro cell culture has proved to be an invaluable technique for investigating many cellular processes[39, 40]. Previous research has utilised an adherent monolayer technique, however this has recently been questioned as to whether this method accurately represents *in vivo* observations[40]. 2-dimensonal (2D) cultures do not accurately represent the microenvironment and architecture present in intact tissue[41] which are important for processes such as proliferation, adhesion and migration[42] that influence cell infiltration and invasion. The many parameters that dynamically impact these factors can be seen in figure 2. Consequently, a more biologically relevant model of cell culture is required to provide an increased insight into many cellular processes[43].

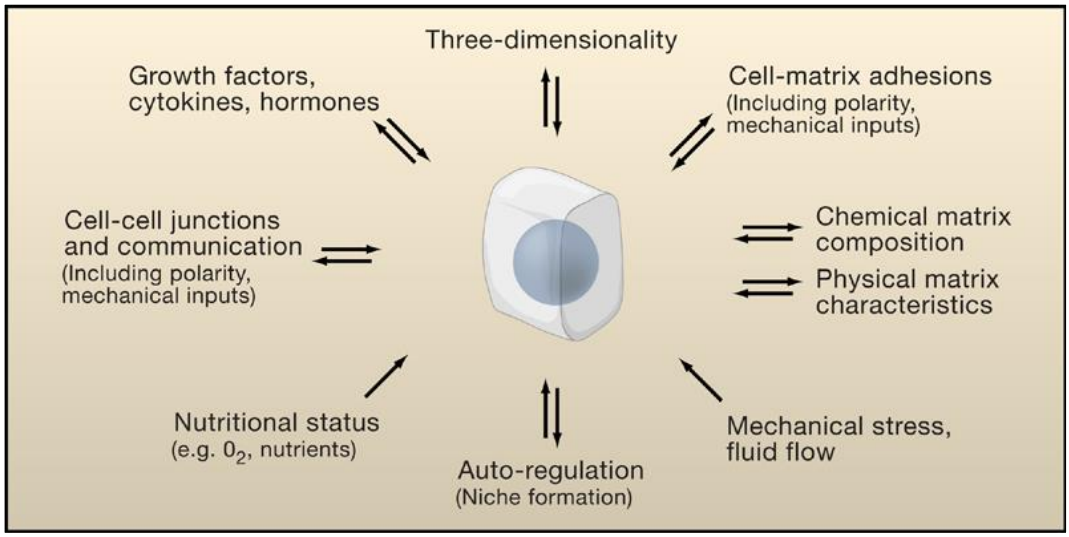

Figure 2: Environmental factors influencing cell growth and behaviour (Yamada et al.,[44]). There are many aspects that affect the spatial and temporal growth of cells, which is absent in adherent monolayer cultures. 3D culture models better represent *in vivo* cell behaviour since these influential factors are introduced. Tumour cells are known be dynamically influenced by the surrounding microenvironment and neighbouring host cells, ultimately manipulating tumour growth, invasiveness and malignancy. The microenvironment is not a heterogeneous environment and fluctuations in factors such as oxygen pressure, growth factors and density of blood vessels can allow selective pressures on different mutations and thus manifest different tumour phenotypes[14, 24] and responses to therapy.

1.4.2 3D Cell Culture

3-dimensional (3D) cell culture was first described more than 40 years ago by Sutherland *et al.*, 1971[45] who cultured Chinese hamster V79 lung cells in suspension using spinner flasks and noted these cells formed multicellular aggregates that resembled the small nodules seen in human carcinomas. Since, many methods have been developed including the hanging-drop method[46], microfluidic channels[39], reconstituted basement membrane (Matrigel)[42] and the liquid-overlay technique. Yuhas *et al.*, 1977[47, 48] described this technically simple method of seeding cell suspensions onto a thin layer of agarose or gelatinous material. This then allows

cells to spontaneously aggregate rather than adhere to the culture vessel due to the fact that the adhesive forces between the cells is greater than that onto which they are seeded[43]. The cellular aggregates that form are known as multicellular spheroids and provide a 3D *in vitro* model that allows spatial and temporal organisation of cell growth[39, 40].

Tumour spheroids display similar growth kinetics and morphological characteristics to that of *in vivo* tumours[49, 50]. The size and growth rate largely depends on cell type however an average size of more than 100-150 μm is generally accepted as a spheroid. As the spheroid grows in size, a nutrient, metabolite and oxygen concentration gradient is generated across the spheroid which establishes spatially separate regions of cells that are comparably observed within *in vivo* tumours[43]. These three structurally distinct regions involve an outer peripheral layer of proliferating cells, an inner core of tightly packed viable but hypoxic and quiescent cells and a central core of necrotic cells, which have died from deprivation of oxygen and nutrients[51, 52] (figure 3).

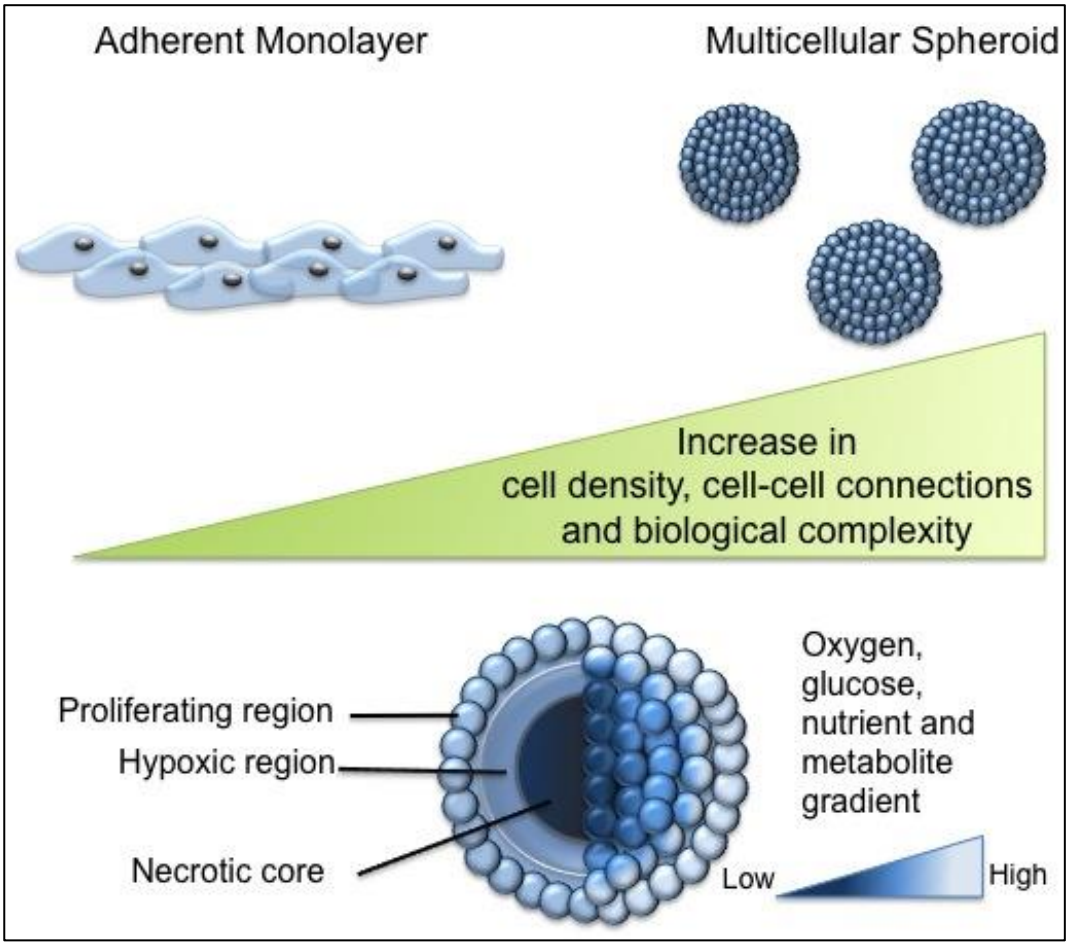

Figure 3: Multicellular spheroid characteristics (based on Ota and Miki, 2012[53]). Adherent monolayers do not exhibit the high biological complexity, increased cell density and cellular connections as observed in multicellular spheroids. Upon growth of 3D spheroids, a steep oxygen, glucose, nutrient and metabolite concentration gradient is generated which results in a stratified arrangement of cells. The outer layer consists of viable and proliferating cells, underneath is a layer of quiescent and hypoxic layer of cells and in the central region of the spheroid is generally a core of necrotic and dead cells that have been deprived of oxygen and other nutrients needed for survival.

Many studies have used homotypic spheroid models, for investigation into influence of metabolic and oxygen gradients on therapeutic treatments[54]. However, it is becoming increasingly popular to introduce other interacting cell types to generate a heterotypic polyclonal co-culture. This provides a more representative model since many tumours are

known to exude heterogeneity, as previously discussed. By providing a 3D model of different cell types, the diverse cellular interactions, localisations and co-dependencies can be investigated.

This 3D spheroid co-culture method can be applied to create an *in vitro* model of glioma. De Witt Hamer *et al.*, 2008[55] analysed the genetic profile of glioma 2D monolayer cultures, spheroid cultures and cultures derived from primary tumours, and showed that the genomic profile of glioma subtypes is preserved in 3D multicellular spheroids however lost in short-term 2D culture. By being able to recapitulate this heterogeneity seen within GBM using known proportions of glioma cell lines representative of the different subtypes, the clonal relationships can be analysed in a controlled manner, which has yet to be investigated[14, 24].

2. AIMS AND HYPOTHESES

2.1 Aims

The aims of this project were to:

- To develop a method for 3D culturing of polyclonal spheroids to provide a more representative *in vitro* model of GBM.
- To use this model to assess the heterogeneity, morphology and subtype interactions of three glioma cell lines representative of the different GBM subtypes.
- To investigate the different responses to chemotherapy treatment (TMZ) in each of the subtypes both individually and also within the polyclonal spheroid model.

2.2 Hypotheses

It was hypothesised that the three subtypes will exhibit differential morphology when grown as spheroids with a stratified arrangement of cells, including an apparent necrotic core due to central oxygen and nutrient deprivation. It is also hypothesised that the subtypes will have diverse locations within the polyclonal spheroid that can potentially contribute to overall spheroid viability. Furthermore, upon addition of chemotherapy reagent Temozolomide, the different cell lines will exhibit a varied sensitivity, as seen in patient tumours[19], but could potentially co-operate when grown as a polyclonal spheroid to permit survival.

3. MATERIALS AND METHODS

3.1 Glioma Cell Lines

Three different cell lines, U343-YFP, U373-RFP and U87 IDH1-Mutant-GFP, were selected to investigate the aims outlined in section 2.1. Table 2 shows the characteristics of each cell line.

Cell Line	U87 IDH1-Mutant-GFP	U343-YFP	U373-RFP
Representative Subtype	Proneural	Classical	Mesenchymal
Representative Characteristic	Mutation in IDH1 (R132H)	High EGFR expression	Low NF1 expression
Fluorescent tag	Green Fluorescent Protein	Yellow Fluorescent Protein	Red Fluorescent Protein

Table 2: Glioma cell line characteristics. Three glioma cell lines were selected, each with a defining characteristic best representative of a different GBM subtype. The U87 cell line had been engineered to overexpress mutant IDH1, which is characteristically seen in the Proneural GBM subtype. The U343-YFP cell line was selected as it had high EGFR expression therefore making it best representative of the Classical subtype. Finally U373-RFP cells were designated to be best representative of the Mesenchymal GBM subtype due to low NF1 expression. Furthermore, each of the cell lines had been engineered to endogenously express a fluorescent protein, for identification during confocal microscopy. In addition, a fourth cell line, U87 IDH1-WT-GFP, was used as a control for U87 IDH1-Mutant-GFP.

It has been shown that the IDH1 mutation cannot be propagated in culture[56] and so the U87 line had been previously generated to stably overexpress $IDH1^{R132H}$ or $IDH1^{WT}$ [57]. Additionally, each cell line had been formerly engineered within the laboratory to endogenously express a fluorophore allowing for identification via confocal microscopy. Cell lines were sorted by fluorescent-activated cell sorting (FACS) to distinguish the highest fluorophore expressing cells so that these cells could be selected and maintained in culture.

3.2 Cell Culture

3.2.1 Adherent Monolayer Culture

All glioma cells lines were cultured in Dulbecco's Modified Eagle Medium (DMEM; Hyclone Thermo scientific, SH30285.01) supplemented with 10% foetal bovine serum (FBS; Hyclone Thermo Scientific, SV30160.03) and 2 mM L-Glutamine at 37°C, 21% O_2 and 5% CO_2. Cells were subject to routine mycoplasma testing in case of contamination.

3.2.2 Spheroid Cell Culture

To obtain spheroids, individual cell lines (listed above) were grown on 0.5% agarose plates using the liquid-overlay method[47]. Agarose plates were made using 0.5% low-melting point agarose (LMP; Promega, V2111) in DMEM which had been pre-heated to 60°C. 10mls of 0.5% agarose/DMEM solution was then plated onto a 10 cm sterile petri dish and left to set. Once cells had been trypsinised and counted using Countess® Automated Cell Counter (Life Technologies), $1x10^6$ cells of each cell line was seeded onto individual 10 cm 0.5% agarose plate. The plates were then topped up to 20 ml with DMEM creating an aqueous overlay in which 3D spheroids could develop. The plates were left undisturbed for 2-4 days (37°C, 5% CO_2). U87 IDH1-WT-GFP and U87 IDH1-Mutant-GFP lines formed large multicellular spheroids within 2 days, before embedded into the 0.5% agarose layer. The U343-YFP and U373-RFP spheroids took 3-4 days to form. Polyclonal spheroids were generated by mixing equal number of cells ($1x10^6$ cells) from U87 IDH1 Mutant-GFP, U343-YFP and U373-RFP lines in a total 20 ml medium. Spheroids were left undisturbed for 3 days (37°C, 5% CO_2).

3.3 Spheroid Immunocytochemistry (ICC)

Spheroids were transferred and filtered through a 40 μm cell strainer to retain any spheroids above this size. The cell strainer containing the spheroids was then inverted over a conical tube and washed with phosphate-buffered saline (PBS) to collect the spheroids. 1 ml of PBS containing the spheroids was then transferred to a microcentrifuge tube and cells were stained with either Pimonidazole (PIMO) or hypoxia-inducible factor 1α (HIF-1α) to act as markers for hypoxia.

PIMO staining was achieved using a Hydroxyprobe™-1 kit (Hydroxyprobe, Burlington MA, USA). Pimonidazole-HCL (200 μM) was added to spheroids in PBS and incubated (37°C, 1 hour). Afterwards, or if not staining with PIMO, spheroids were subject to 10% formalin fixation for 1 hour at room temperature (RT). Following fixation, spheroids were centrifuged (0.8 rpm, 1 minute) and formalin was removed by aspiration. Spheroids were then subjected to permeabilisation using 250 μl 0.1% Triton-X-100 in PBS (20 minutes, RT). The 0.1% Triton-X-100-PBS solution was aspirated following centrifugation (0.8 rpm, 1 minute) and primary antibody was added to spheroids and kept at 4°C in the dark overnight. For PIMO staining, the primary antibody was 1:400 dilution of IgG1 mouse monoclonal antibody in PBS-0.5% Tween (PBS-T). For HIF-1α staining, purified mouse anti-human HIF-1α (BD Transduction, 610959) was used at 1:50 dilution in 0.5% BSA, PBS-T. Prior to addition of HIF-1α, spheroids were blocked in 5% BSA, PBS-T for 1 hour.

After overnight incubation, the primary antibody was removed and anti-mouse IgG (H+L) DyLight 649 fluorescent secondary antibody (Vector labs, DI-2649) was added at a 1:100 dilution in PBS-T (2 hours, RT). Spheroids were centrifuged (0.8 RPM, 1 min) and 500μl of

PBS was added. To stain for DNA, 1 drop of Hoechst 33342 (NucBlue® live cell stain ready probes™, Life Tech, R37605) dye was added for 20 minutes at RT. Following this, 250µl of spheroids were transferred to 1 well on an 8 well chamber slide and 200µl of 1% LMP agarose/PBS was added on top.

3.4 Confocal Microscopy

3.4.1 Acquisition Parameters

A Zeiss LSM-510 confocal microscope was used to visualise the morphology and clonal interactions of the fluorescently labelled, agarose-embedded spheroids. The acquisition parameters used are shown in table 3.

Fluorophore	**Hoechst-33342**	**GFP**	**YFP**	**RFP**	**DyLight - 649**
Excitation Laser	343	488	488	543	633
Fluorophore Spectral Range (nm)	Ex_{max}- 343 Em_{max}- 483	Ex_{max}- 488 Em_{max}- 509	Ex_{max}- 514 Em_{max}-527	Ex_{max}- 555 Em_{max}- 584	Ex_{max}- 654 Em_{max}- 673
Lens	20x EC Plan-Neofluar objective				
Pinhole	Optical size (monoclonals) 1.8 Airy Units (polyclonals)				
Gain	Adjusted per channel to avoid saturation in pixel intensity				
Resolution	512 x 512				
Scan speed	5				
Data Depth	12 bit				

Table 3: Confocal microscopy parameters. Table showing the specific parameters of the confocal microscope used for imaging the monoclonal and polyclonal spheroids. A 2D image was taken approximately mid-way through the spheroid, where the necrotic core was visible.

3.4.2 Imaging Polyclonal Spheroids

Imaging of the polyclonal spheroids required application of a computer algorithm because the emission spectra from GFP and YFP fluorophores have high spectral overlap (figure 4). Therefore it was not possible to distinguish clearly between the fluorophores and the resulting image showed signal bleed through from one fluorophore into the detection channel of the other fluorophore.

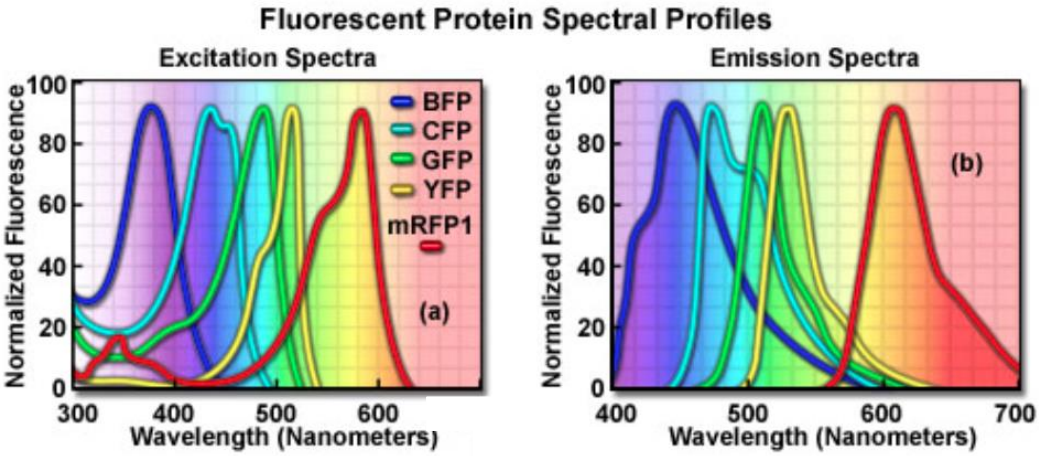

Figure 4: Excitation and emission spectra of common fluorescent proteins (Olympus[58]). Image shows excitation and emission wavelengths for common fluorescent proteins. It is apparent that GFP and YFP fluorophores have very close excitation and emission maximum values resulting in spectral overlap. It is therefore difficult to distinguish between the fluorescence from fluorophores when imaged in combination.

A process called emission fingerprinting (figure 5) was employed to resolve the fluorescent contribution from each fluorophore[59]. Spheroids were first imaged with only one fluorophore present and an emission spectrum was saved as a reference in a spectral database. The lambda-unmixing programme was then applied when imaging the fluorophores in combination. A lambda-coded projection of the image was produced and compared to the reference spectra for each of the fluorophores. The spectra could then be separated by an

algorithm called linear unmixing. The resulting image produced a multichannel image displaying the fluorescence from each fluorophore separately.

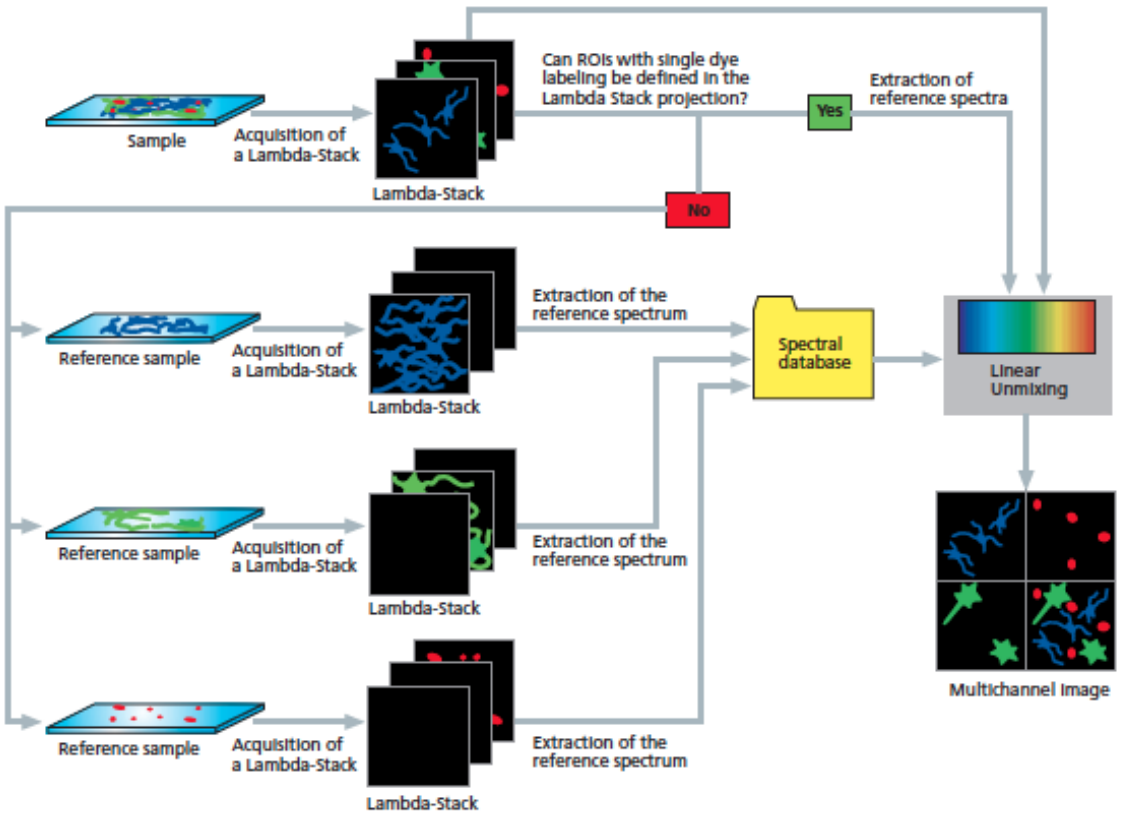

Figure 5: Schematic of emission fingerprinting procedure (Zeiss[59]). Samples are imaged individually as providing a reference emission spectrum. When the sample is imaged in the presence of all fluorophores, unmixing can be applied. Linear unmixing records the spectral profiles at each individual pixel and can therefore assign colours by consulting the reference spectra, in regions that would normally appear mixed.

Emission spectra of the imaging controls used can be seen in figure 6.

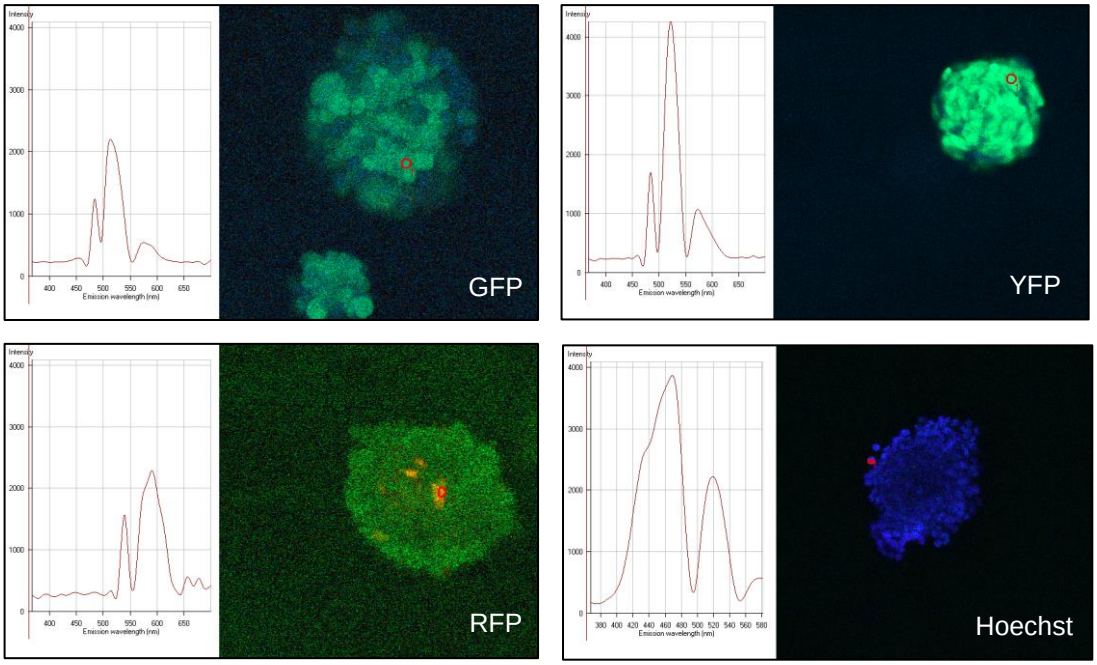

Figure 6: Reference emission spectra from the individual fluorophores used in emission fingerprinting. Spheroids were fixed in the presence of one fluorophore. A region of interest with the brightest fluorescence was selected and an emission spectrum was generated. These spectra were recorded in a spectral database for use in emission fingerprinting to separate the spectral overlap of the GFP and YFP fluorophores.

3.5 Western Blotting

3.5.1 Protein Extraction

To determine whether each cell line was representative of a glioma subtype, Western blotting was performed on protein extracted from each cell line. DMEM was removed and the cells washed three times with 1x PBS. 200 µl of radioimmunoprecipitation assay (RIPA) buffer (50 mM Tris/HCL pH 7.5, 150 mM NaCl, 0.1% SDS, 1 mM EDTA pH 8, 0.5% sodium deoxycholate and 1% Triton-X-100) with added protease inhibitor cocktail (Sigma, P8340) was used to lyse the cells. The cells were then scraped, harvested and kept on ice for 20 minutes. Following this, the cells were centrifuged (13,000 rpm, 15 minutes, 4°C) and

supernatant was then carefully transferred to a new microcentrifuge tube. Protein concentration was determined using Novagen BCA protein assay kit (Calbiochem, 71285-3). Samples were then diluted in Laemmli buffer 2x concentrate (Sigma-Aldrich, S3401-1VL) to normalise protein concentration.

3.5.2 SDS-PAGE, Protein Transfer and Antibody Incubation

15 µg of protein from each cell line was resolved by SDS-polyacrylamide gel electrophoresis (SDS-PAGE). Proteins were then transferred at 100 V (1 hour) onto nitrocellulose membrane.

Following transfer, non-specific antibody binding was blocked by washing the blot in 5% milk-PBS-T (1 hour, RT). Primary antibodies in 5% milk-PBS-T, were incubated overnight at 4°C. Anti-NF1 (Abcam, ab30325), anti-EGFR (Santa-Cruz, SC-03) and anti-IDH1 R132H (Dianova, DIA H09) were used at a 1:500 dilution. Anti-actin (Sigma, A4700) was used as a loading control (1:2000). Following primary antibody incubation, blots were washed with PBS-T three times and then probed with horseradish peroxidase-conjugated secondary antibody (Cell Signalling, anti-mouse IgG HRP-linked, #7076 or anti-rabbit IgG HRP-linked, #7074) at a 1:3000 dilution in PBS-T (1 hour, RT). Blots were then washed with PBS-T and developed using Amersham ECL Prime Western Blotting Detection Reagent (GE Healthcare Life Sciences, RPN2232).

3.6 Temozolomide Sensitivity Assays

3.6.1 Adherent Monolayer Sensitivity Assay

For monolayer TMZ sensitivity assays, the U373-RFP cell line was seeded at a density of $1x10^4$ while the U343-YFP and U87-IDH1-Mutant-GFP were seeded at a density of $3x10^4$

into each well of a 12 well plate. Varying densities were used to account for the U373-RFP line growing at a significantly higher rate (previous observations).

Two separate 12-well plates were prepared, one for TMZ treatment and one for a dimethyl sulfoxide (DMSO) control. A DMSO control was required since TMZ is diluted in DMSO and therefore the degree of cell death observed solely in the presence of DMSO needs to be accounted for. The 12-well plates were incubated at 37˚C overnight. Following incubation, the medium was removed and cells were treated with either DMSO or TMZ. 1 ml of 0.3, 0.5 and 1 mM of TMZ in DMEM was added in triplicate. 0 mM TMZ was used as a control. On the other 12-well plate, 1 ml of 0.3, 0.5 and 1% DMSO, alongside a 0% DMSO control was added in triplicate. The cells were then incubated (37°C) for 72 hours. After 72 hours, 20% ice-cold triochloroacetic acid (TCA; Sigma-Aldrich, T0699) was added to each well to terminate the treatment. Plates were then incubated for 30 minutes at 4°C. The TCA was removed and the wells washed carefully three times with sterile distilled water (SDW). The plates were then left to dry for 2-3 hours. When dry, 0.4% Sulforhodamine B (SRB) in 1% acetic acid was added to each well and incubated (10 minutes, RT). Following incubation, the SRB solution was removed and plates washed 4-5 times with 1% acetic acid. Plates were left to dry overnight at RT. The following day, SRB stained wells were dissolved using 50 mM Tris/HCL pH8.8 and 100 µl of each well was transferred to a 96-well plate. The absorbance was then recorded at 495 nm on a microplate reader and cell viability calculated for each cell line.

3.6.2 Polyclonal TMZ Sensitivity

Polyclonal spheroids were created as described in section 3.2.2, and left to form on stationary agarose plates for 3 days. Following spheroid formation, spheroids were retained on agarose plates and treated with either 1% DMSO (control) or 1 mM TMZ. Spheroids were incubated for 72 hours at 37˚C, 5% CO_2. Spheroids were then harvested and subject to ICC (section 3.3). Confocal microscopy was used to visualize the morphological changes (section 3.4).

3.7 Analysis of Spheroid Morphology

To calculate total spheroid and spheroid core volume, the diameter was calculated for each spheroid from confocal microscopy images using ImageJ (NIH). For each spheroid two perpendicular diameters were recorded and a mean diameter calculated. This was repeated to calculate the necrotic core volume. The volume of the spheroid and necrotic core were then calculated using the equation[26, 60, 61]:

$$Volume = \frac{4}{3}\pi r^3$$

To calculate the spheroid wall thickness, spheroid images were divided into four and a measurement was taken from the outer edge to the necrotic core in each of the quarters. A mean width for each spheroid was then calculated using each of the quarters of the spheroid. Each image was calibrated to the scale bar.

3.8 Statistical Analyses

All statistical tests were performed using GraphPad Prism v6 for Macintosh (GraphPad Software, La Jolla California USA). Unpaired T-tests with unequal standard deviation (SD; Welch's correction) were performed.

4. RESULTS

4.1 Spheroid Optimisation

In order that a suitable *in vitro* model of GBM might be obtained, it was essential that the spheroid culture method was optimised. Initially, spheroids were cultured in spinner flasks for 7 days before extraction for confocal microscopy. Spheroids cultured using this method grew well however, when examined, were small in size and appeared non-viable. To overcome this, the liquid-overlay culture method was considered which produced, a high yield of viable spheroids after an incubation period of 2 days and therefore was adopted for subsequent experiments.

Images produced from cultures stained with PIMO, designed to identify regions of hypoxia, demonstrated a faint signal and high background fluorescence. This was an issue as it prevented hypoxic regions from being clearly identifiable, thereby hindering analysis. To overcome this, the dilution of primary antibody was increased and the fixative used during ICC was changed from Acetone/Methanol to 10% formalin, which allows better sample preservation[58]. Although these changes produced clearer confocal images, PIMO still did not produce adequate staining and so HIF-1α was used as a marker for hypoxia, which produced clearer images. The confocal imaging also required optimisation, as previously described, and the permeabilisation time with Triton-X-100 was increased from 5 to 20 minutes to increase Hoechst 33342 dispersion.

4.2 Western Blotting to Confirm GBM Subtype Representation

Western blotting was used to confirm that the cell lines used had protein expression representative of the GBM subgroups, (table 2). Representative blots (figure 7) showed the

U343-YFP line expressed high levels of EGFR compared to the other cell lines. NF1 protein showed differential expression in the U373-RFP line in three experiments and would need to be repeated to confirm that this protein has been mutated. A R132H IDH1 mutation was detected in the U87-IDH1 mutant cell line but not the others, confirming that this cell line is characteristic of the Proneural subtype.

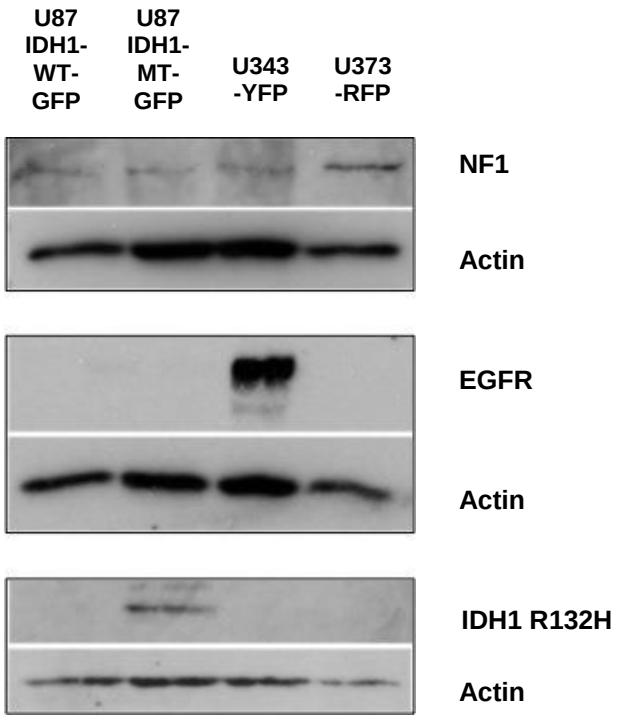

Figure 7: Western blots to confirm cell lines are representative of GBM subtypes. Protein was harvested from each cell line (three individual culture passages for U87 IDH1-WT-GFP, U87 IDH1-Mutant-GFP and U373-RFP, 2 individual passages for U343-YFP). 15 µg of protein was separated by SDS-PAGE gel electrophoresis. Subsequent blots were probed for NF1 (319 kDa), EGFR (170 kDa) and IDH1 Mutant (R132H; 47 kDa). Actin (42 kDa) was used as a loading control. It is apparent that NF1 loss was not seen in the U373-RFP cell line, however a lower level of expression was observed in an additional experiment. EGFR expression was high in the U343-YFP cell line, indicating that this cell line is representative of the Classical GBM subtype. An antibody against the mutant form of IDH1 confirmed that the U87 IDH1-Mutant-GFP cells express the IDH1 mutant enzyme.

4.3 Differential Morphology of Glioma Cell Lines

Brightfield microscopy was used to examine growth of the glioma cells as adherent monolayers and multicellular spheroids. As seen in figure 8, the U87 IDH1-WT-GFP cell line is different to the U87 IDH1-Mutant in both monolayers and spheroids. The U87 IDH1-Mutant-GFP cells typically displayed a spindle-like morphology and were slower growing. The U343-YFP cell line as adherent monolayers exhibited the slowest growth and when cultured in suspension, formed smaller, compact spherical spheroids. Conversely, the U373-RFP cells exhibited very quick growth as monolayers and exhibited a punctate spheroid structure with individual cells visible on the spheroid periphery.

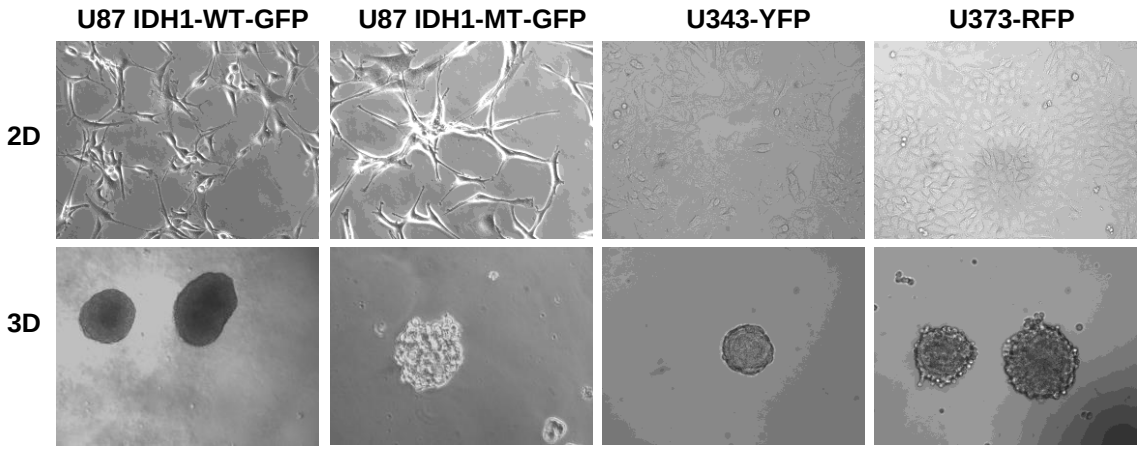

Figure 8: Morphology of glioma cell lines as adherent monolayers and multicellular spheroids. Distinctive morphology is exhibited in each cell line as adherent monolayers but also as multicellular spheroids. Magnification 20x.

4.4 Monoclonal Spheroid Morphology

Confocal microscopy was used to examine monoclonal spheroid morphology (figure 9).

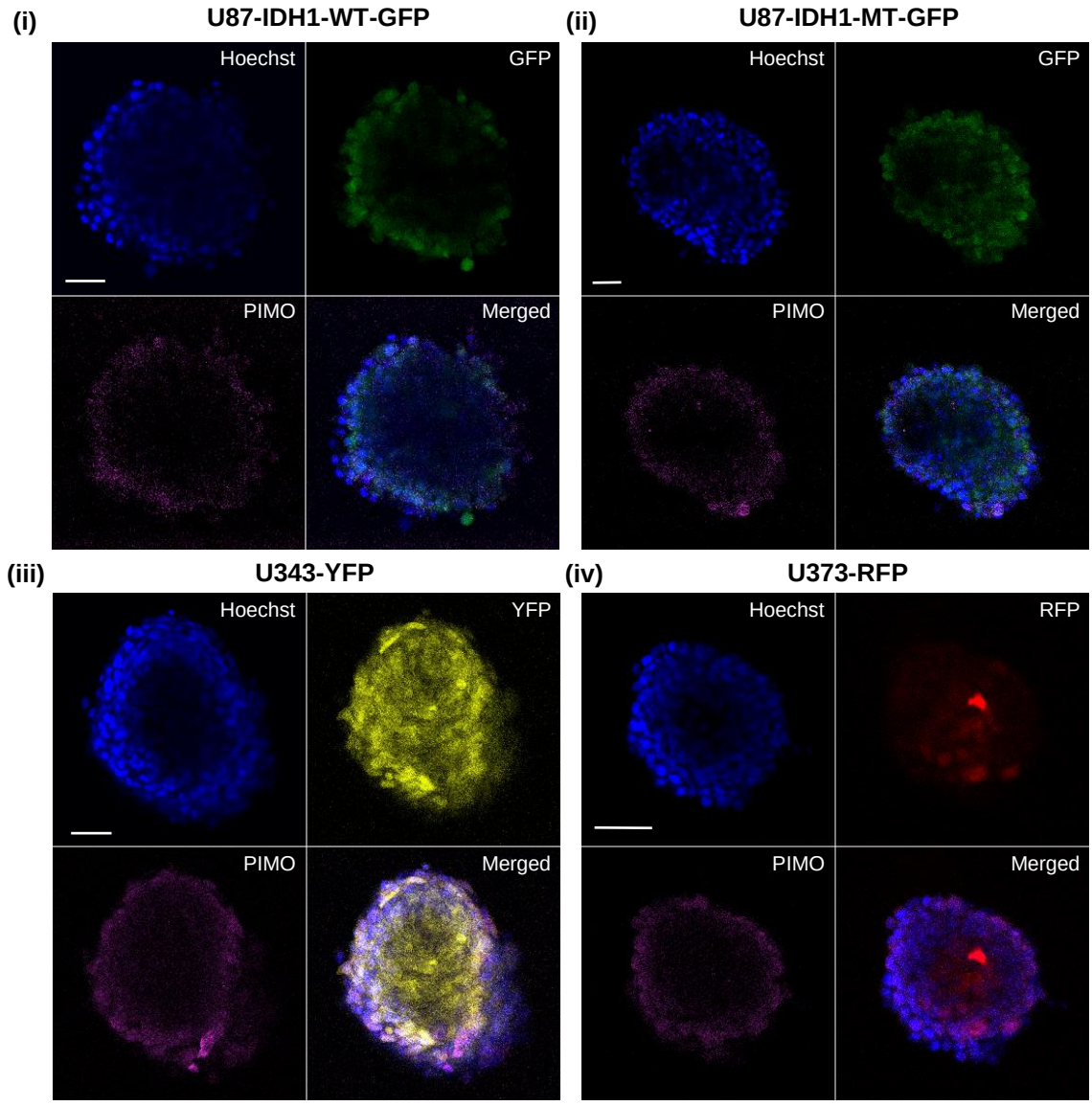

Figure 9: Monoclonal spheroid morphology. Hoechst stain indicates the presence of DNA. It can be seen that there is a central core devoid of staining in the spheroids, indicating cell necrosis. PIMO staining indicates a region of hypoxic cells surrounding the necrotic core **(i) U87 IDH1-WT-GFP monoclonal spheroid.** A small layer of proliferating cells can be seen on the outer edge of the spheroid, with a large necrotic core. **(ii) Monoclonal spheroid of the U87 IDH1-Mutant-GFP cells.** The spheroid has a high cell density and has a smaller necrotic core compared to the U87 IDH1-WT-GFP spheroid. A hypoxic rim is seen to surround the spheroid to the outer spheroid periphery. **(iii) Representative image of U343-YFP monoclonal spheroids**. It is apparent that the necrotic core is surrounded by a wall of high cell density. PIMO staining indicates that these cells are very hypoxic. No evidence for the existence of a layer of non-hypoxic cells was visible in the outer periphery. **(iv) Representative image of the U373-**

RFP monoclonal spheroids. These spheroids had the smallest volume with a densely packed outer layer of cells and smaller necrotic core. As seen in the U87 IDH1- Mutant-GFP and U343-YFP spheroids, the cells are hypoxic to the outer spheroid edge. Scale bar represents 50μm.

U87 IDH1-WT-GFP cells formed spheroids with a large volume and a distinctively large necrotic core (figure 9(i)). Cells appeared to be loosely packed together, with a thin outer layer of proliferating cells. A hypoxic rim was seen below the spheroid periphery, detected by PIMO staining. The U87 IDH1-Mutant-GFPs (figure 9(ii)) however demonstrated a denser, tightly packed spheroid, with a smaller necrotic core. The hypoxic region was observed to be towards the outer edge of the spheroid, compared to the IDH1-WT, indicating that a greater volume of spheroid was more hypoxic. However more replicates are needed to confirm these observations. The U343-YFP cell line (figure 9(iii)), were considerably smaller with a tightly packed outer layer of proliferating/hypoxic cells and a smaller necrotic core. The hypoxic region was very pronounced around the outer edge of the spheroid indicating these spheroids were very hypoxic. U373-RFP spheroids (figure 9(iv)), demonstrated similar morphological characteristics to U343-YFP spheroids.

4.5 Polyclonal Spheroid Morphology and Growth Characteristics

After 3 days growth, spheroids were imaged using brightfield microscopy to observe their morphology (figure 10A).

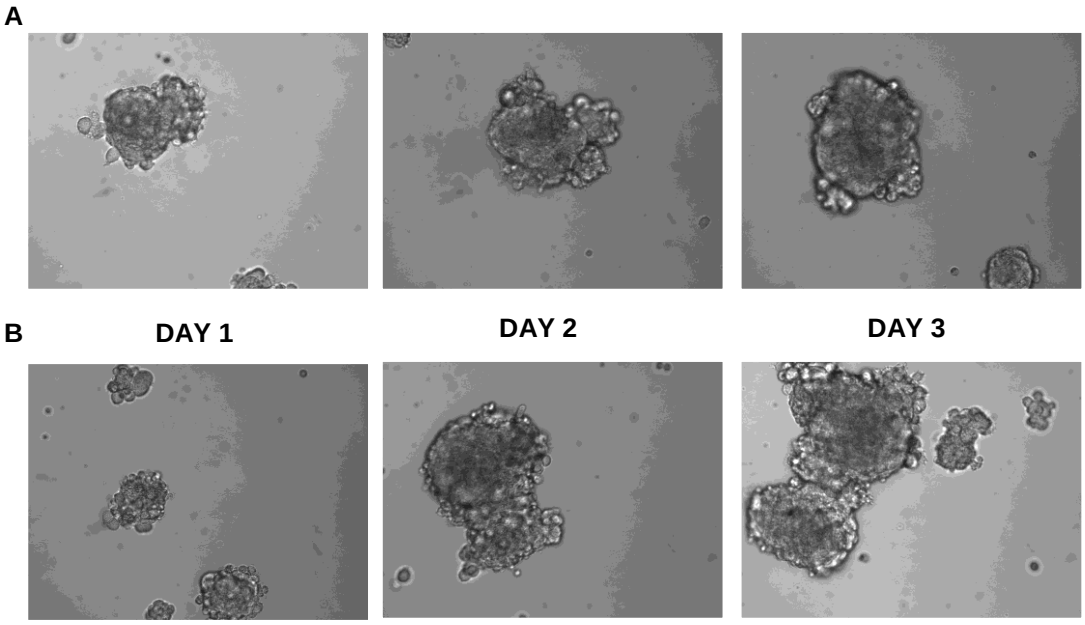

Figure 10: Polyclonal spheroid morphology. Polyclonal spheroids were generated by mixing 1 x 10^6 cells from each of the glioma cell lines. **(A)** Representative images of polyclonal spheroids after 3 days growth on stationary agarose plates. The spheroids formed dense cores, with clusters of cells around the outside of the spheroid. **(B)** Representative images of polyclonal spheroid growth over 3 days. Initially, the cells formed small cellular aggregates, which by day 2 formed a much larger, more defined solid spheroid. By the day 3, the spheroids had more cells situated around the outer edge and also were prone to aggregation. Spheroids were used 3 days after seeding because the spheroids started to embed themselves into the agarose after this time. Magnification 20x.

There is a clear difference in the polyclonal spheroid morphology (figure 10) compared to the monoclonal spheroids (figure 8). Polyclonal spheroids were formed of a solid core of cells, surrounded by smaller, punctate clumps of cells located on the periphery. Figure 10B shows this structural formation over the growth period of 3 days.

4.6 Subtype Interactions Within Polyclonal Spheroids

Confocal microscopy allowed for the different subtypes interactions to be identified. Due to the high spectral overlap of GFP and YFP fluorophores, the different subtypes could not be resolved (figure 11).

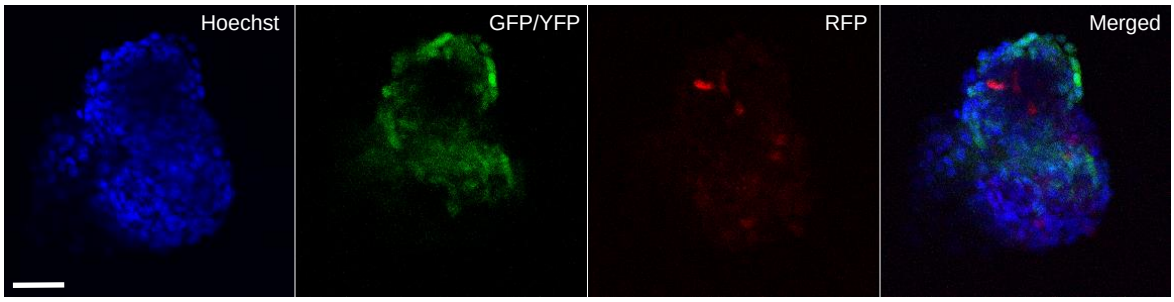

Figure 11: Polyclonal spheroid before separation of GFP/YFP fluorophores. It is apparent that the fluorescence from the GFP and YFP fluorophores could not be distinguished from one another, producing one image with fluorescence from both fluorophores, as opposed to two separate images as expected. Therefore the clonal interactions could not be determined. Scale bar represents 50µm.

Figure 12 shows representative images of the polyclonal spheroids following separation of the fluorophores. These spheroids were very cell dense, with little or no necrotic core present. The U373-RFP and U87 IDH1-Mutant-GFP cells appear to localise together whereas there is a distinct location of the U343-YFP cells. In every image analysed (N=18), from 3 independent experiments, the U343-YFP cells were situated on the outer spheroid, indicating a possible important function.

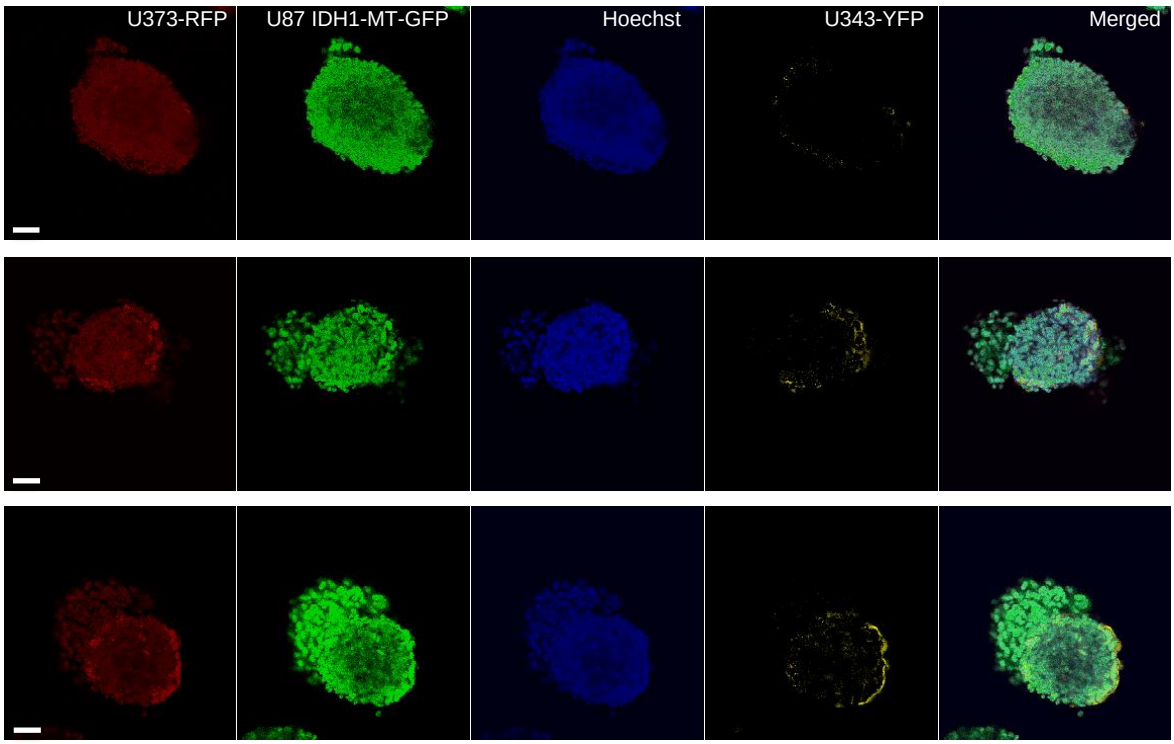

Figure 12: Confocal images showing subtype interactions in polyclonal spheroids. Representative images of polyclonal spheroids showing the interactions and locations of the cell lines representative of the four GBM subtypes. U373-RFP and U87 IDH1-Mutant-GFP were observed to co-localise. The U343-YFP cells however demonstrated a clear and distinctive location around the outer periphery of the spheroid suggesting a specialised function of this representative GBM subtype. The spheroids also lacked a distinctive necrotic core, as shown by Hoechst dye penetrating to the spheroid centre. 3 independent experiments were performed, 18 images. Scale bar represents 50 µm.

Staining for hypoxic regions could not be processed in the same confocal channel, thus the polyclonal spheroids, from the same experiments as above, were individually imaged for Hoechst and hypoxia staining (figure 13).

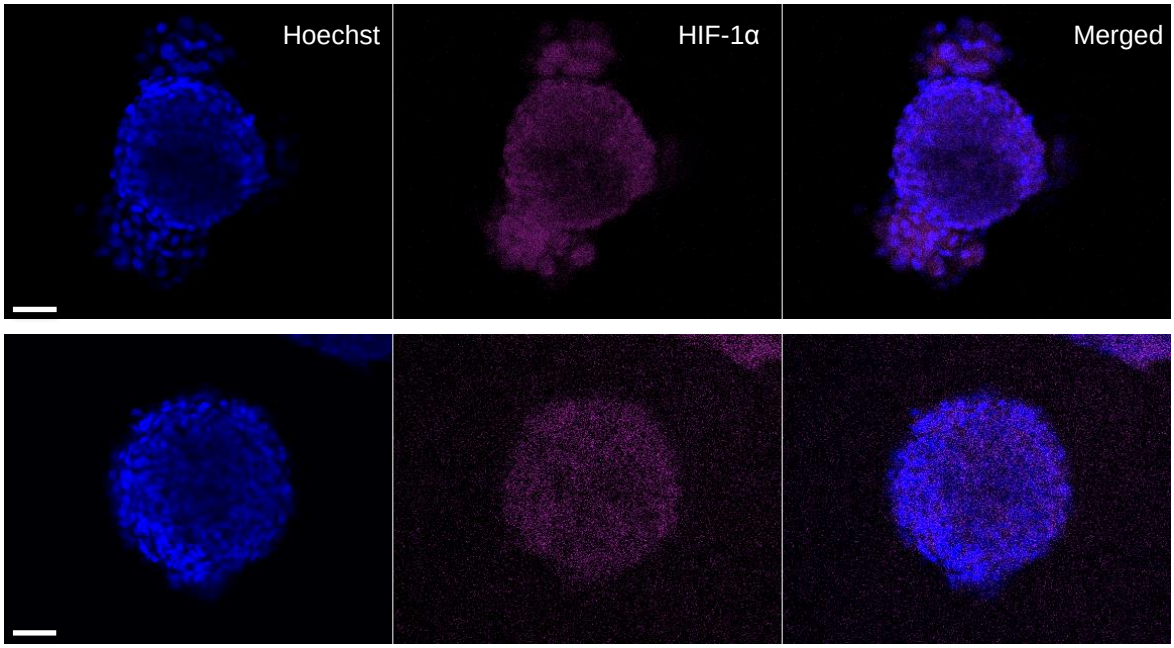

Figure 13: Polyclonal spheroids are mainly hypoxic with little necrosis present. Representative images showing polyclonal spheroids stained with Hoechst 33342 and for hypoxic regions with HIF-1α. These spheroids were very dense, with smaller necrotic cores as the Hoechst dye was observed to penetrate to the centre of the spheroids. Hypoxia staining was very strong throughout the spheroid indicating that the polyclonal spheroids were almost entirely hypoxic compared to the monoclonal spheroids seen in figure 9, where only a layer of hypoxic cells were seen. These images were used for quantitative analysis of the polyclonal morphology. 3 independent experiments were performed, 18 images. Scale bar represents 50µm.

4.7 Analysis of Monoclonal and Polyclonal Morphological Characteristics

Spheroid morphology was quantitatively analysed (figure 14). Spheroid diameter of U87 IDH1-WT-GFP and-Mutant-GFP spheroids was larger than both the U343-YFP and U373-RFP spheroids, with the U373-RFP being the smallest polyclonal spheroid, however was not statistically significant. The U87 IDH1-Mutant-GFP spheroids had the largest spheroid volume, tightly packed and exhibited a high cell density, (figure 9(ii)). U373-RFP produced the smallest spheroid, which were significantly ($p=0.0038$) smaller than the polyclonal

spheroids. The volume of the necrotic core was also measured and the U87 IDH1-WT-GFP appeared to demonstrate the largest core volume. The U87 IDH1-Mutant-GFP spheroids however had considerably smaller necrotic core volume compared with other spheroids, despite having the largest overall volume. However, these observations were not statistically significant as more replicates are needed. The U373-RFP exhibited the smallest necrotic core, being the smallest spheroid overall. The polyclonal spheroids also demonstrated typically small necrotic cores (figure 12).

The necrotic core to spheroid volume ratio was calculated demonstrating that the U87 IDH1-WT-GFP spheroids had the largest necrotic core, with 27% of the spheroid being necrotic. The other spheroids however had a much smaller degree of necrosis, with polyclonal spheroids having on average 8.5±1.7% necrosis. U87 IDH1-WT-GFP spheroids had the thinnest layer of proliferating and hypoxic cells whereas, conversely, the U87 IDH1-Mutant-GFP had the thickest cell wall amongst the monoclonal spheroids. The polyclonal spheroids had the thickest cell wall that was particularly cell dense and also highly hypoxic.

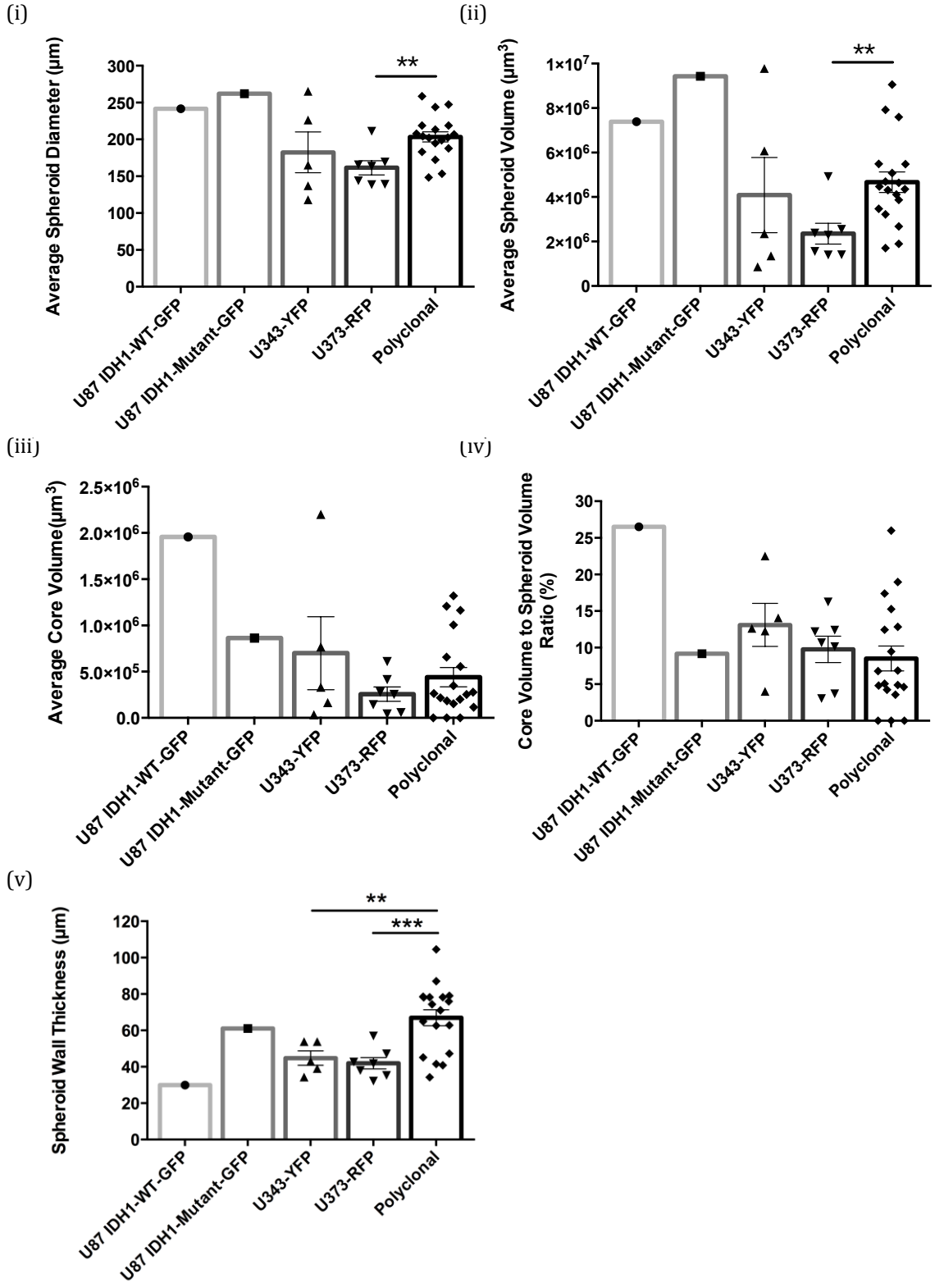

Figure 14: Quantitative analysis of monoclonal and polyclonal spheroid characteristics. (i) Mean spheroid diameter. U87 IDH1-WT-GFP and –Mutant-GFP were seen to produce the largest spheroids of the 4 monoclonal subgroups

(U87-IDH1-WT-GFP: 241.6 µm, 1 image; U87 IDH1-Mutant-GFP: 262.1 µm, 1 image; U343-YFP: 182.4 ± 27.66 µm, 5 images; U373-RFP: 161.6 ± 9.61 µm, 7 images) and Polyclonals (203.5 ± 6.88 µm, 18 images). However the difference between U373-RFP and the polyclonal spheroids was the only one that was statistically significant (unpaired T-test, P value= 0.0038). (**ii) Mean spheroid volume.** U87 IDH1-WT-GFP and U87 IDH1-Mutant-GFP expressed the largest volume of the spheroids (U87-IDH1-WT-GFP: 7.39 x 10^6 μm^3, 1 image; U87 IDH1-Mutant-GFP: 9.43 x 10^6 μm^3, 1 image; U343-YFP: 4.09 ± 1.62 x 10^6 μm^3, 5 images; U373-RFP: 2.36 ± 0.47 x 10^6 μm^3, 7 images; Polyclonals: 4.67 ± 0.46 x 10^6 μm^3, 18 images) though, as shown with the mean spheroid diameters, only the difference observed between U373-RFP and the polyclonals was significant (unpaired T-test, P value= 0.0025). **(iii) Mean necrotic core volume.** U87 IDH1-WT-GFP spheroids exhibited a large area of necrosis compared to the U373-RFP and polyclonal spheroids, which had smaller cores. (U87-IDH1-WT-GFP: 1.96 x $10^6 \mu m^3$, 1 image; U87 IDH1-Mutant-GFP: 0.86 x $10^6 \mu m^3$, 1 image; U343-YFP: 0.70 ± 0.40 x $10^6 \mu m^3$, 5 images; U373-RFP: 0.26 ± 0.08 x 10^6 μm^3, 7 images; Polyclonals: 0.44 ± 0.10 x $10^6 \mu m^3$, 18 images)**. (iv) Necrotic core to total spheroid volume ratio.** U87 IDH1-WT-GFP spheroids had the largest ratio compared to the other spheroids (U87 IDH1-WT-GFP: 26.5 %, 1 image; U87 IDH1-Mutant-GFP: 9.2%, 1 image; U343-YFP: 13.1 ± 2.9%, 5 images; U373-RFP: 9.8 ± 1.8%, 7 images; Polyclonals: 8.5 ± 1.7%, 18 images). **(v) Spheroid wall thickness.** The spheroid wall thickness was measured from the spheroid periphery to the necrotic core. Polyclonal spheroids had the thickest cell wall (66.9 ± 4.40 µm, 18 images), which was statistically significant compared with U343-YFP (unpaired T-test, P value= 0.002) and U373-RFP (unpaired T-test, P value= 0.0001) spheroids whereas the U87 IDH1-WT-GFP spheroid had a comparatively thinner cell wall (29.9 µm, 1 image), despite having a greater overall volume. Other monoclonal spheroids had cell wall thicknesses that fell between this range (U87 IDH1-Mutant-GFP: 61.0 µm, 1 image; U343-YFP: 44.8 ± 3.93 µm, 5 images; U373-RFP: 42.0 ± 3.12 µm, 7 images) though none of these differences were found to be significantly different. Bars show the mean values for each measurement. Error bars represent ±SEM.

4.8 Temozolomide Sensitivity Assays of Monoclonal Adherent Monolayers

TMZ sensitivity of each cell line was investigated when grown as adherent monolayers (figure 15). It is clear from this data that the most sensitive was U373-RFPs, which showed an average 33% cell death with increasing concentrations of TMZ. The U87 IDH1-Mutant-GFP and U343-YFP cell lines however were less sensitive to TMZ treatments with only 22% cell death after treatment with1 mM TMZ.

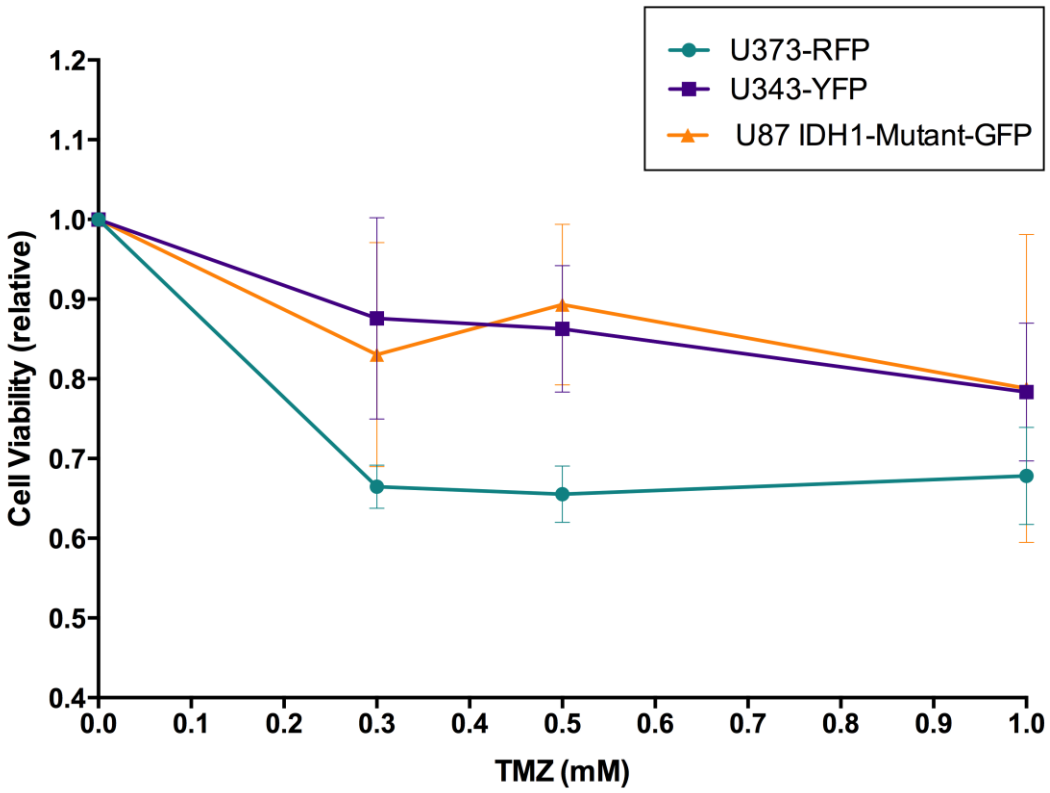

Figure 15: Glioma cell lines show differential sensitivity to TMZ treatment as adherent monolayers. Each cell line was subject to TMZ treatment for 72 hours after which the cell viability was measured using a SRB assay. U373-RFP cells were more sensitive to 0.3, 0.5 and 1mM TMZ treatments (0.3 mM- 0.67 ± 0.03, 0.5 mM- 0.66 ± 0.04, 1 mM- 0.68 ± 0.06) compared with both the U87 IDH1-Mutant-GFP (0.3 mM- 0.83 ± 0.14, 0.5 mM- 0.89 ± 0.10, 1 mM- 0.79 ± 0.19) and U343-YFP (0.3 mM- 0.88 ± 0.13, 0.5 mM- 0.86 ± 0.08, 1 mM- 0.78 ± 0.08) cell lines. Despite there being a strong distinction between the mean cell viability of these spheroids, they were not found to be significantly different). 4 independent experiments were conducted for U373-RFP and U343-YFP cell lines and 3 independent experiments for U87 IDH1-Mutant-GFP cells. Error bars represent ±SEM.

4.9 Polyclonal Spheroid Growth and Morphology Following TMZ Treatment

Polyclonal spheroids treated with 1 mM TMZ were examined using brightfield microscopy to investigate whether there was any noticeable difference in spheroid morphology (figure 16).

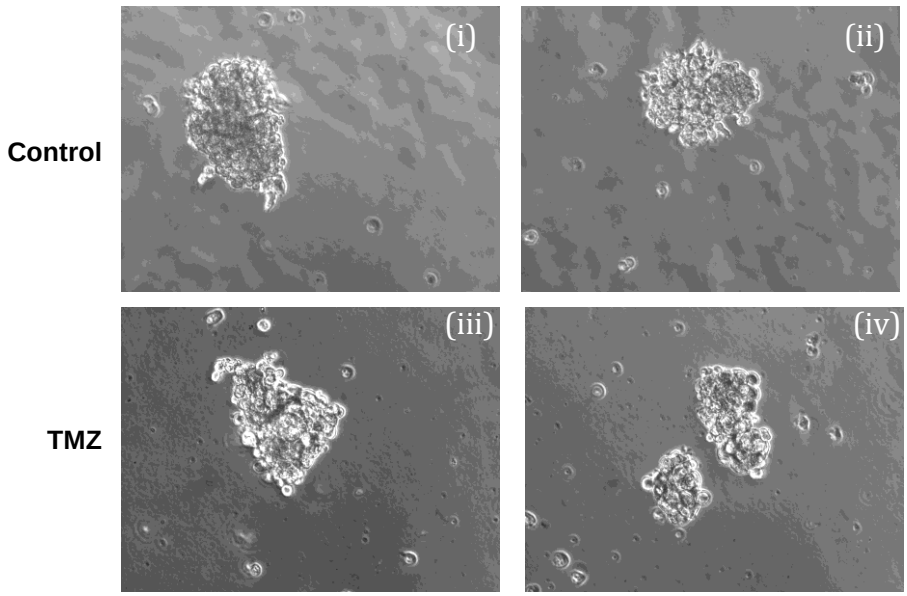

Figure 16: Morphology of polyclonal spheroids following TMZ treatment. Polyclonal spheroids were seeded and left to grow for 3 days on stationary agarose plates so that spheroids could form, after which they were treated with 1 mM TMZ (iii and iv) or DMSO (control; i and ii) for 72 hours. There was no apparent difference in spheroid morphology between these treatments as complete spheroids were retained in both conditions. It should be noted however, that upon addition of TMZ, more single cells and small cellular aggregates were present compared to the control condition, indicating that there may have been more dissolution of the spheroids upon TMZ treatment.

Following immunocytochemistry, polyclonal spheroids with and without TMZ treatment were imaged using confocal microscopy (figure 17). In the control condition, the U343-YFP cell line was situated on the far edge of the spheroid, as seen with the polyclonals (figure 12). It should be noted that there were very few U343-YFP cells incorporated into the spheroid. The quantity and location of the U343-YFP cells was observed in every control image taken, from 2 experiments. A defined necrotic core was seen within these spheroids, which were surrounded by a tightly packed layer of U373-RFP and U87 IDH1-Mutant-GFP cells. Upon TMZ treatment however the necrotic core was observed to be considerably larger and the

layer of proliferating cells on the edge of the spheroid were reduced. TMZ treated spheroids also demonstrated the proliferation and dramatic relocation of the U343-YFP cell line. In all images, U343-YFP cells appeared to have increased and relocated to fill the central core of the spheroid. This is remarkably different to the control and polyclonal spheroids.

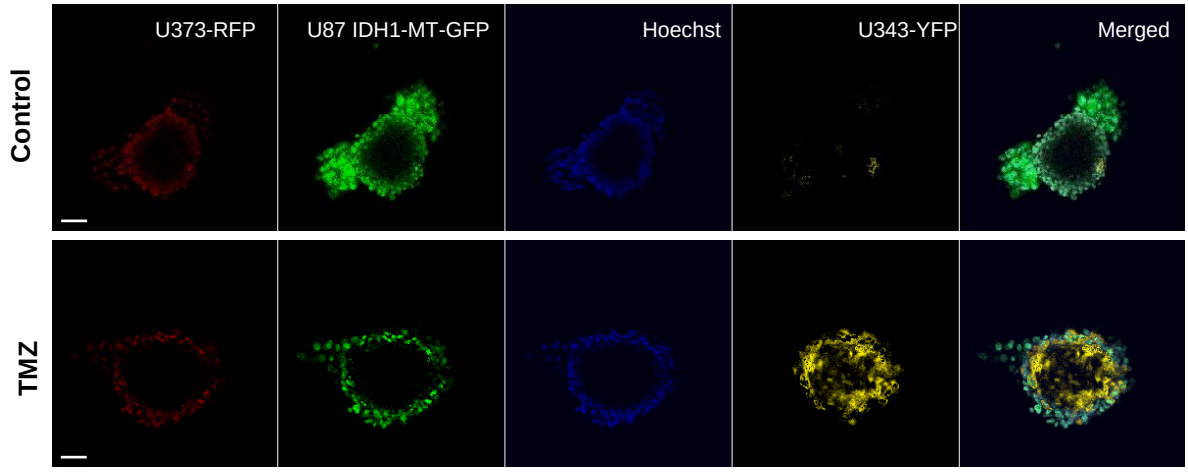

Figure 17: TMZ treatment of polyclonal spheroids causes a dramatic proliferation and relocation of the U343-YFP cells. In the control condition, the U373-RFP and U87 IDH1-Mutant-GFP localised in similar regions of the spheroid. The U343-YFP had a similar location as seen previously (figure 12), situated around the outside of the spheroid. There was also a reduced amount of these cells present in these spheroids. A large necrotic core was present in these spheroids, which had not been observed in previous polyclonal images, suggesting that this may be due to the presence of DMSO, or the longer period of growth on the agarose plates. Upon addition of 1 mM TMZ (72 hours incubation) however, there was a noticeable relocation and proliferation of the U343-YFP cells into the central core of the spheroids suggesting the possibility of a specialised function to these cells. The spheroid walls appear to be thinner than seen in the control with a larger necrotic core, although it was filled with U343-YFP cells. Scale bar represents 50 µm.

4.10 Analysis of Polyclonal Spheroid Morphology Following TMZ Treatment

Quantitative analysis of spheroid morphology following TMZ treatment was performed (figure 18). After TMZ treatment, the mean diameter of the polyclonal spheroids increased in

size compared to the control, however was not significantly different. Spheroid volume showed that after TMZ treatment the volume increased, however was not significant. Analysis of the necrotic core volume again showed that the core was significantly larger upon TMZ treatment, although the core was filled with U343-YFP cells, which was not apparent in the control spheroids. Analysis of the percentage of core to the total volume showed that TMZ treated spheroids to have significantly (p=0.003) larger core than control spheroids, being around 50% of the total spheroid volume. Finally, cell wall diameter was measured which showed that the control spheroids had a thicker layer of cells surrounding the necrotic core compared to the TMZ treated spheroids, however results were non-significant. In the confocal images (figure 17) it can be seen that there is a reduction in the presence of the U373-RFP cells on the outside of the spheroid, which could potentially be linked to its sensitivity to TMZ treatment showed in figure 15.

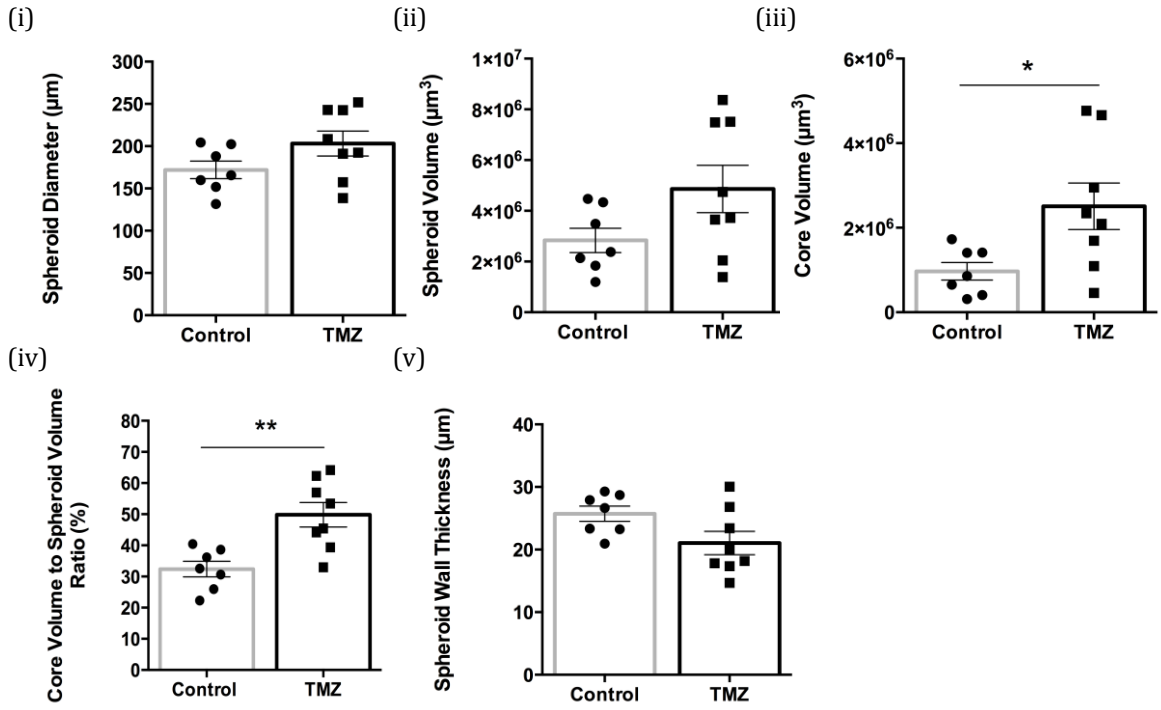

Figure 18: Quantitative analysis of polyclonal spheroid morphology after TMZ treatment. (i) Mean spheroid diameter. The mean spheroid diameter increased upon TMZ treatment however was not significant compared to the control condition (Control: 172 ± 10.3 µm, 7 images; TMZ: 203.2 ± 14.7 µm, 8 images). **(ii) Mean spheroid volume.** The average spheroid volume was determined and demonstrated an apparent increase with the addition of TMZ (Control: 2.83 ± 0.48 x 10^6 μm^3, 7 images; TMZ: 4.87 ± 0.94 x10^6 μm^3, 8 images). **(iii) Mean necrotic core volume.** A significant increase (unpaired T-Test, P value=0.0285) was observed in the necrotic core volume with TMZ compared to the control (Control: 0.97 ± 0.21 x 10^6 μm^3, 7 images; TMZ: 2.51 ± 0.55 x 10^6 μm^3, 8 images). (**iv) Necrotic core to total spheroid volume ratio.** The mean core to volume ratio demonstrated that there is significant increase (unpaired T-test, P value=0.003) in the percentage of necrosis of the overall spheroid with TMZ treatment (Control: 32.4 ± 2.5%, 7 images; TMZ: 49.8 ± 3.9%, 8 images). **(v) Spheroid wall thickness.** The mean wall thickness of the spheroids was seen to decrease upon TMZ treatment, however this was not significant compared to the control condition (Control: 25.7 ± 1.2 µm, 7 images; TMZ: 21.1 ± 1.9 µm, 8 images). 2 independent experiments were conducted. Bars show the mean values for each measurement. Error bars represent ±SEM.

5. DISCUSSION

5.1 Representation of GBM Subtypes Through Cell Lines

Understanding the polyclonal nature and heterogeneity of GBM is imperative for determining effective treatments tailored to patients. To investigate clonal interactions, a representative *in vitro* model which expresses the different GBM subtypes is required as current models do not accurately represent *in vivo* gliomas. Three cell lines, U87 IDH1-Mutant-GFP, U343-YFP and U373-RFP, were chosen in this project to best represent GBM subtypes in a polyclonal spheroid model.

Western blotting (figure 7) confirmed that the U343-YFP cell line highly expressed EGFR protein, which is characteristic of the Classical GBM subtype (table 1). It has previously been reported that, when culturing glioma cells, Chromosome 7p amplification, containing the EGFR gene locus, can be lost within short-term culture[55, 56]. However, during this experiment high EGFR expression was conserved despite continuous culture. Therefore, the U343-YFP line preserved a typical characteristic best representative of the Classical GBM subtype during this investigation.

The U87 IDH1-Mutant-GFP cell line was confirmed to express the mutated IDH1 enzyme (figure 7). Like EGFR, it has been shown that IDH1 mutations cannot be sustained in culture conditions[56]. Therefore, the U87 IDH1-Mutant-GFP cell line had been engineered[57] to overexpress the IDH1 mutant and these results confirm that the introduced mutation was sustained through cell passages. This cell line is therefore representative of the Proneural subtype.

NF1 expression was shown to be differentially expressed in the U373-RFP cell line across three experiments performed within this project and would therefore require further investigation to confirm that this cell line is representative of the Mesenchymal subtype, as believed. This cell line should be sequenced to ensure the NF1 deletion is present and Western blotting performed with more harvested protein, potentially with a different NF1 antibody to test antibody specificity. In addition, other proteins characteristic of the Mesenchymal subtype, for example the presence of markers such as CH13L1 and cadherin-11[62], could be investigated. It should not however be assumed that these cell lines are exact representations of each GBM subtype as they do not exhibit all mutations and amplifications present in *in vivo* tumours. Nevertheless, these cell lines are considered to provide a good representation of glioma subtypes to develop a suitable *in vitro* model to study GBM heterogeneity.

5.2 Monoclonal Spheroid Morphology

Tumour growth is typically defined by an exponential growth phase of proliferating cells, followed by a decline in cell proliferation generally associated with the increase of quiescent, non-proliferating cells within the spheroid outer region and necrotic cells within the spheroid core[50]. This stratified arrangement is dependent on factors including cell type, density and nutrient consumption rates[50]. Figure 9 shows these differences observed in monoclonal spheroid morphology. The U87 IDH1-WT-GFP cells quickly formed large spheroids with an extensive area of necrosis, a rim of hypoxic and potentially quiescent cells and a single layer of proliferating cells. These observations suggest that these spheroids were able to quickly exhaust nutrients and oxygen, resulting in a large proportion of cell death. Comparing the U87 IDH1-WT-GFP to the IDH1-Mutant-GFP spheroids, there was a distinct difference in morphology. In the presence of mutant IDH1, the spheroids were denser, with the cells tightly

packed together forming a thicker wall of proliferating/quiescent cells surrounding a smaller necrotic core. Spheroids were also hypoxic to the outer edge, which was not seen in the U87 IDH1-WT-GFP spheroids. These observations suggest that the presence of mutant IDH1 permitted better survival of the spheroid due to the smaller proportion of necrotic cells present. Research has documented that the presence of mutant IDH1 enzyme is required for IDH1 mutated tumour cell growth[63] and an inhibitor of R132H-mutated IDH1 delayed cell growth[64], suggesting that mutated IDH1 promotes growth, sustaining tumour viability.

Compared to the U87 IDH1-WT-GFP or –Mutant-GFP monoclonal spheroids, the U343-YFP and U373-RFP cells formed much smaller and tightly packed spheroids, with a considerably thicker cell wall and smaller necrotic core, showing a distinctive difference in morphology between these cells lines. The presence of a smaller necrotic core also suggests that these spheroids are better at surviving under reduced oxygen and nutrient conditions, which may influence the polyclonal spheroid survival.

Analysis of the U373-RFP cell line (figure 9) demonstrated that RFP fluorescence was particularly irregular. Despite being cultured in medium containing puromycin, which allowed for selection of RFP expressing cells, the overall fluorescent labelling was not uniform. To improve this, U373-RFP cells could be re-sorted using FACS to select the highest RFP expressing cells. If the fluorescence of this tag could not be optimised, different fluorescent tags could be used such as improved variants of RFP, DsRed or mCherry (emission maximum values of 592nm and 610nm respectively), which would not interfere with emission spectra of the other fluorescent tags and should facilitate imaging.

All cell lines were seen to not emit Hoechst fluorescence in the central region of the spheroids, indicating necrotic and dead cells (figure 9). However, YFP, and in some regions RFP, were still expressed in the central spheroid core indicating potentially viable cells. This suggests that perhaps Hoechst was not able to fully penetrate and bind to DNA in the spheroid centre due to spheroid thickness. Weiswald *et al.*, 2010[65] investigated the optimal immunocytochemistry parameters for intact spheroids. They found that simultaneously fixing and permeabilising the spheroids in a solution of paraformaldehyde and Triton-X-100, followed by dehydration in methanol allowed complete dye penetration whilst retaining spheroid structure[65]. A future improvement however, would be to combine fixation and permeabilisation steps and extend incubation time as described in Weiswald *et al.*, 2010[65]. Nevertheless, when imaging polyclonal spheroids (figures 12 and 13) it is apparent that Hoechst is present in the spheroid centre. However, to ensure that Hoechst infiltration is not a problem when imaging the monoclonal spheroids, a different dye could be used in combination to check cell viability. NucRed® Dead 647 ReadyProbes® Reagent (Life Technologies) could be used after spheroid fixation, and would bind to nuclear DNA in cells with compromised cell membranes, hence staining for the presence of dead cells.

5.3 Relationship of Subtypes Within Polyclonal Spheroids

Confocal microscopy showed that there was a differential location of the subtypes within the polyclonal spheroid model. It is apparent (figure 12) that U373-RFP and U87 IDH1-Mutant-GFP cells co-localise forming a tight, cell-dense spheroid body, with little to no necrosis. This shows that these cells are able to survive in oxygen and nutrient deprived environments and promote the overall spheroid survival. This is an example of mutualism where different subtypes are positively interacting to benefit the survival of other clones, therefore providing an evolutionary advantage of the tumour. The entire spheroid is seen to be very hypoxic,

noted by the presence of HIF-1α (figure 13) suggesting that these spheroids could potentially be using this as a mechanism of survival. Tumour hypoxia is present within solid tumours due to large amounts of oxygen being consumed during the tumours rapid proliferation. Within gliomas, the majority of tumour cells in grade IV GBM are known to be hypoxic[66] compared to lower grades. Additionally, the presence of moderate to severe hypoxia has been correlated with a more aggressive tumour behaviour[66] and increased resistance to radiation and chemotherapy[67]. To overcome the limited oxygen supply and reduce cell death, tumour cells are known to alter their metabolism to sustain proliferation. Hypoxia-inducible factors (HIFs), induced under hypoxic conditions, play a key role in this altered metabolism since they up-regulate genes key for tumour survival, such as those involved in invasion, and also glycolytic genes, which manage survival upon reduction in oxygen availability[68].

HIF-1α has been shown to be located in areas adjacent to necrosis and also within invading tumour cells situated at the spheroid periphery[67, 71]. This is interesting because results (figure 12) demonstrate the distinctive location of potentially very hypoxic U343-YFP cells on the invading edge. This clonal interaction and location is particularly important, as these cells are known to overexpress EGFR. Constant activation of the EGF receptor activates downstream cascades that promote tumourigenesis, anti-apoptosis, invasion and can lead to uncontrolled cell proliferation[9]. Studies, such as those conducted by Okada *et al.*, 2003, showed that cells containing an EGFR-amplification were preferentially located in clusters on the outer, invading edge of the tumour compared to relatively small amounts located in the solid tumour core. The results of this investigation corroborate these findings as the EGFR expressing U343-YFP cells were observed on the outer spheroid edge (figure 12). This might suggest

that these cells have a specific role within the polyclonal spheroid, promoting infiltration of into surrounding tissue.

This apparent co-operation between the subclones is particularly important when relating to GBM patients since differential treatment sensitivity has been shown[19]. Because these clones work together to benefit the survival of the tumour, further investigation is needed to determine a method of treatment that will dissolve these specific pro-survival interactions thus targeting the whole tumour and not individual subtypes.

5.4 Issues Relating to Confocal Microscopy Issues and Analysis

Problems were encountered whilst using confocal microscopy to investigate the clonal relationships. Fluorescence from GFP and YFP tagged cells could not be separated due to overlapping emission spectra. This problem was resolved using a computer algorithm to separate the fluorescence. Although this is a valid method, there could be debate as to whether the fluorophores have been entirely separated. Therefore, to confirm the cell locations within the spheroid model, untagged U343 cells could be incorporated instead. Cells would then be probed for EGFR, since they highly express the protein, and then detected using the DyLight-649 secondary antibody, which emits fluorescence in the far-red region. Consequently, there would be no risk of spectral overlap, providing absolute conformation of subtype locations. For a more long-term solution, the cells would ideally be designed to express a more compatible range of fluorescent tags, though this would require further investigation.

To quantitatively analyse monoclonal and polyclonal morphologies, total spheroid and necrotic core volumes were measured (section 3.8)[60]. However this method may not be the best to accurately calculate spheroid volume as these cell cultures are not perfect spheroids or

uniform in size. Therefore, an improved method may be to use computational programming and imaging software to calculate the area of spheroid slices and 3D reconstruction to calculate overall volume.

5.5 Differential Sensitivity of Glioma Subtypes to Temozolomide Treatment

Inter- and intra-tumoral heterogeneity is known to comprise treatment strategies since tumour cells often develop resistance mechanisms (section 1.2). Different glioma subtypes can exhibit a differing response to chemotherapy and radiotherapy[19] however GBM patients are treated with the same aggressive course of treatment, regardless of subtype. Therefore, it is important that this varied response to treatment is investigated.

Temozolomide sensitivity was investigated in each subtype grown as adherent monolayers. Figure 15 shows that the most sensitive of the three cell lines to 72-hour treatment of TMZ was U373-RFP (Mesenchymal subtype). U87 IDH1-Mutant-GFP and U343-YFP cells were more resistant to TMZ treatment, and only exhibited around 20% cell death with 1 mM TMZ. These cells are potentially more hypoxic, as seen with HIF-1α localisation (figures 9, 12 and 13), and because the IDH1 mutation is thought to promote stabilised expression of HIF-1α. Studies have also shown that TMZ treatment can up-regulate many HIF-1α target genes[72], contributing to increased resistance by inducing cell cycle arrest of tumour cells and therefore providing protection against agents such as TMZ, that induce cellular apoptosis[71]. To confirm this hypothesis, TMZ sensitivity assays could be combined with either a small-interfering RNA designed to target HIF-1α or a small molecule inhibitor such as Chetomin, which disrupts the HIF pathway, attenuating HIF expression[73]. TMZ sensitivity in glioma cells has been shown to be increased upon inhibition of HIF-1α and shown to be a possible target in glioma treatment[74].

Additionally, MGMT status of glioma cells lines should be determined to see if this is causing TMZ resistance, observed in the U87 IDH1-Mutant-GFP and U343-YFP cells (figure 15). According to Verhaak *et al*., 2010[19] the Proneural subclass do not benefit from TMZ treatment compared to other subgroups. This is seen within the 2D sensitivity experiments (figure 15) in this project. Because TMZ treatment in patients is usually combined with a course of radiotherapy to provide the best survival outcome[3], future experiments should also compare sensitivity with radiation, both alone and combined with TMZ.

TMZ sensitivity of the polyclonal spheroids was examined using confocal microscopy. The data (figure 17) show that in the control condition U343-YFP cells are again situated on the invading edge of the spheroid and are small in number. A large necrotic core was present in these spheroids, which was not apparent in the untreated polyclonal cultures. This is potentially explained by cell death by DMSO addition or because spheroids were left for a further three days, after the initial two day growth phase, which may have allowed a steeper oxygen gradient to form across the spheroid.

With TMZ treatment there was a pronounced relocation and proliferation of the U343-YFP cells (figure 17). The spheroid core also significantly increased in size, however U343-YFP cells were observed within this core. This suggests that these cells are part of a mechanism benefiting the overall survival of the spheroid model. EGFR amplifications, as previously discussed, induce cell proliferation and can influence tumour cell survival, invasiveness and most importantly, resistance to treatment[75]. Therefore the data from this project suggests that amplification in EGFR signalling provides an important mechanism of resistance to TMZ treatment. Further experiments are required to investigate whether it is EGFR signalling

which is responsible for this dramatic relocation and proliferation of U343-YFP cells. A selective EGFR inhibitor such as Erlotinib[76] or Imantinib should be used to investigate whether inhibition of EGFR would inhibit the relocation of these cells. Additionally, the U87 cell line could be engineered to overexpress EGFR to see if these cells could proliferate and migrate to the spheroid core upon TMZ treatment. Furthermore, there was no visible staining of DNA from U343-YFP cells in the spheroid centre (figure 17). To check the cell viability, a TUNEL assay or detection of Capase-3, which detects the presence of apoptotic cells, could be performed. Combined, these experiments would be able to confirm that EGFR is a key mediator in this interesting response to TMZ treatment. A further experiment of interest would be to use live-cell imaging to observe real-time alterations and migrations of the subclones upon treatment. This would give great indication as to when EGFR expressing cells relocate and how they proliferate to benefit the overall spheroid survival.

6. CONCLUSION

The data presented in this investigation suggests that 3D cell culturing produces a more representative model of GBM compared with existing 2D models. Initial observations using this model suggest that different glioma subtypes exhibit distinct morphologies both in monoclonal and polyclonal communities. However, certain problems were encountered during analysis (sections 3.4.2 and 5.4), which require optimisation in order to improve the effectiveness of this model. Furthermore, an improved spheroid co-culture model could be developed by introducing microglial cells to provide a comparable tumour microenvironment for the spheroids. Moreover, GBM tumour spheroids could be created using tumour fragments obtained from patient resections, along with the creation of a microenvironment, would provide an even more representative *in vitro* model of GBM.

Polyclonal TMZ studies showed a novel subtype interaction, where U343-YFP cells dramatically proliferated and relocated to the spheroid core, suggesting a mechanism of spheroid survival under adverse conditions. However. additional experiments are needed to this further investigate this observation. Nevertheless, this work represents a significant improvement into how GBM is investigated *in vitro* and, with further development, will increase our understanding of glioma heterogeneity resulting in more effective therapy for GBM patients.

7. LIST OF REFERENCES

1. Goffart, N., Kroonen, J. and Rogister, B. (2013) *Glioblastoma-Initiating Cells: Relationship with Neural Stem Cells and the Micro-Environment.* Cancers, **5**(3): p. 1049-1071.
2. Nupponen, N.N. and Joensuu, H. (2006) *Molecular pathology of gliomas.* Current Diagnostic Pathology, **12**(5): p. 394-402.
3. Stupp, R., et al. (2005) *Radiotherapy plus concomitant and adjuvant temozolomide for glioblastoma.* New England Journal of Medicine, **352**(10): p. 987-996.
4. McNamara, M.G., Sahebjam, S. and Mason, W.P. (2013) *Emerging Biomarkers in Glioblastoma.* Cancers, **5**(3): p. 1103-1119.
5. The Brain Tumour Charity. (2014) *The About Us Bit | The facts about brain tumours*. http://www.thebraintumourcharity.org/about-us/The-facts Last accessed (14.05.14)
6. Kleihues, P., et al. (1995) *Histopathology, classification, and grading of gliomas.* Glia, **15**(3): p. 211-221.
7. Omuro, A. and DeAngelis, L.M. (2013) *Glioblastoma and other malignant gliomas: a clinical review.* JAMA, **310**(17): p. 1842-1850.
8. Ohgaki, H. and Kleihues, P. (2013) *The definition of primary and secondary glioblastoma.* Clinical Cancer Research, **19**(4): p. 764-772.
9. Olar, A. and Aldape, K.D. (2014) *Using the molecular classification of glioblastoma to inform personalized treatment.* The Journal of Pathology, **232**(2): p. 165-177.
10. Hartmann, C., et al. (2013) *Long-Term Survival in Primary Glioblastoma With Versus Without Isocitrate Dehydrogenase Mutations.* Clinical Cancer Research, **19**(18): p. 5146-5157.
11. Dresemann, G. (2010) *Temozolomide in malignant glioma.* OncoTargets and Therapy, **3**: p. 139-146.
12. Sottoriva, A., et al. (2013) *Intratumor heterogeneity in human glioblastoma reflects cancer evolutionary dynamics.* Proceedings of the National Academy of Sciences, **110**(10): p. 4009-4014.
13. Bonavia, R., Cavenee, W.K. and Furnari, F.B. (2011) *Heterogeneity maintenance in glioblastoma: a social network.* Cancer Research, **71**(12): p. 4055-4060.
14. Inda, M.-d.-M., Bonavia, R. and Seoane, J. (2014) *Glioblastoma Multiforme: A Look Inside Its Heterogeneous Nature.* Cancers, **6**(1): p. 226-239.
15. Dehais, C., et al. (2006) *Prognostic stratification of patients with anaplastic gliomas according to genetic profile.* Cancer, **107**(8): p. 1891-1897.
16. Fisher, R., Pusztai, L. and Swanton, C. (2013) *Cancer heterogeneity: implications for targeted therapeutics.* British Journal of Cancer, **108**(3): p. 479-485.

17. Navin, N., et al. (2010) *Inferring tumor progression from genomic heterogeneity.* Genome Research, **20**(1): p. 68-80.
18. McLendon, R., et al. (2008) *Comprehensive genomic characterization defines human glioblastoma genes and core pathways.* Nature, **455**(7216): p. 1061-1068.
19. Verhaak, R.G., et al. (2010) *Integrated Genomic Analysis Identifies Clinically Relevant Subtypes of Glioblastoma Characterized by Abnormalities in PDGFRA, IDH1, EGFR and NF1.* Cancer Cell, **17**(1): p. 98-110.
20. Nobusawa, S., et al. (2009) *IDH1 mutations as molecular signature and predictive factor of secondary glioblastomas.* Clinical Cancer Research, **15**(19): p. 6002-6007.
21. Szerlip, N.J., et al. (2012) *Intratumoral heterogeneity of receptor tyrosine kinases EGFR and PDGFRA amplification in glioblastoma defines subpopulations with distinct growth factor response.* Proceedings of the National Academy of Sciences, **109**(8): p. 3041-3046.
22. Sottoriva, A., Vermeulen, L. and Tavaré, S. (2011) *Modeling evolutionary dynamics of epigenetic mutations in hierarchically organized tumors.* PLoS Computational Biology, **7**(5), e1001132: p. 1-11.
23. Nguyen, K.S.H., Kobayashi, S. and Costa, D.B. (2009) *Acquired Resistance to Epidermal Growth Factor Receptor Tyrosine Kinase Inhibitors in Non-Small-Cell Lung Cancers Dependent on the Epidermal Growth Factor Receptor Pathway.* Clin Lung Cancer, **10**(4): p. 281-289.
24. Marusyk, A. and Polyak, K. (2010) *Tumor heterogeneity: causes and consequences.* Biochimica et Biophysica Acta (BBA)-Reviews on Cancer, **1805**(1): p. 105-117.
25. Nickel, G.C., et al. (2012) *Characterizing mutational heterogeneity in a glioblastoma patient with double recurrence.* PloS One, **7**(4), e35262: p. 1-8.
26. Günther, W., et al. (2003) *Temozolomide induces apoptosis and senescence in glioma cells cultured as multicellular spheroids.* British Journal of Cancer, **88**(3): p. 463-469.
27. Gerlinger, M., et al. (2012) *Intratumor heterogeneity and branched evolution revealed by multiregion sequencing.* New England Journal of Medicine, **366**(10): p. 883-892.
28. Clarke, J., Butowski, N. and Chang, S. (2010) *Recent advances in therapy for glioblastoma.* Archives of Neurology, **67**(3): p. 279-283.
29. Stummer, W., et al. (2006) *Fluorescence-guided surgery with 5-aminolevulinic acid for resection of malignant glioma: a randomised controlled multicentre phase III trial.* The Lancet Oncology, **7**(5): p. 392-401.
30. Friedman, H.S., Kerby, T. and Calvert, H. (2000) *Temozolomide and treatment of malignant glioma.* Clinical Cancer Research, **6**(7): p. 2585-2597.

31. D'Atri, S., et al. (1998) *Involvement of the mismatch repair system in temozolomide-induced apoptosis.* Molecular Pharmacology, **54**(2): p. 334-341.
32. Stupp, R., van den Bent, M.J. and Hegi, M.E. (2005) *Optimal role of temozolomide in the treatment of malignant gliomas.* Current Neurology and Neuroscience Reports, **5**(3): p. 198-206.
33. Kitange, G.J., et al. (2009) *Induction of MGMT expression is associated with temozolomide resistance in glioblastoma xenografts.* Neuro-oncology, **11**(3): p. 281-291.
34. Ramirez, Y.P., et al. (2013) *Glioblastoma Multiforme Therapy and Mechanisms of Resistance.* Pharmaceuticals, **6**(12): p. 1475-1506.
35. Zhang, J., et al. (2010) *Acquired resistance to temozolomide in glioma cell lines: molecular mechanisms and potential translational applications.* Oncology, **78**(2): p. 103-114.
36. Chen, Y., et al. (2013) *MGMT promoter methylation and glioblastoma prognosis: A systematic review and meta-analysis.* Archives of Medical Research, **44**(4): p. 281-290.
37. Hegi, M.E., et al. (2005) *MGMT gene silencing and benefit from temozolomide in glioblastoma.* New England Journal of Medicine, **352**(10): p. 997-1003.
38. Dinnes, J., et al. (2001) *The effectiveness and cost-effectiveness of temozolomide for the treatment of recurrent malignant glioma: a rapid and systematic review*. Health Technology Assessment, **5**(13): p.1-6.
39. Fennema, E., et al. (2013) *Spheroid culture as a tool for creating 3D complex tissues.* Trends in Biotechnology, **31**(2): p. 108-115.
40. Haycock, J.W. (2011) *3D cell culture: a review of current approaches and techniques*. 3D Cell Culture, Springer. p. 1-15.
41. Kim, J.B. (2005) *Three-dimensional tissue culture models in cancer biology*. Seminars in Cancer Biology, **15**: p. 365-377.
42. Manome, Y., et al. (2010) *Three-dimensional cell culture of glioma and morphological comparison of four different human cell lines.* Anticancer Research, **30**(2): p. 383-389.
43. Bates, R.C., Edwards, N.S. and Yates, J.D. (2000) *Spheroids and cell survival.* Critical Reviews in Oncology/Hematology, **36**(2): p. 61-74.
44. Yamada, K.M. and Cukierman, E. (2007) *Modeling tissue morphogenesis and cancer in 3D.* Cell, **130**(4): p. 601-610.
45. Sutherland, R.M., McCredie, J.A. and Inch, W.R. (1971) *Growth of multicell spheroids in tissue culture as a model of nodular carcinomas.* Journal of the National Cancer Institute, **46**(1): p. 113-120.
46. Timmins, N.E. and Nielsen, L.K. (2007) *Generation of multicellular tumor spheroids by the hanging-drop method*. Tissue Engineering, Springer. p. 141-151.

47. Yuhas, J.M., et al. (1977) *A simplified method for production and growth of multicellular tumor spheroids.* Cancer Research, **37**(10): p. 3639-3643.
48. Corcoran, A., et al. (2003) *Evolution of the brain tumour spheroid model: transcending current model limitations.* Acta Neurochirurgica, **145**(9): p. 819-824.
49. Ivascu, A. and Kubbies, M. (2006) *Rapid generation of single-tumor spheroids for high-throughput cell function and toxicity analysis.* Journal of Biomolecular Screening, **11**(8): p. 922-932.
50. Sutherland, R.M. (1988) *Cell and environment interactions in tumor microregions: the multicell spheroid model.* Science, **240**(4849): p. 177-184.
51. Hamilton, G. (1998) *Multicellular spheroids as an in vitro tumor model.* Cancer Letters, **131**(1): p. 29-34.
52. Sutherland, R., et al. (1981) *Spheroids in cancer research.* Cancer Research, **41**(7): p. 2980-2984.
53. Ota, H. and Miki, N. (2012) *Microtechnology-based three-dimensional spheroid formation.* Frontiers in Bioscience (Elite edition), **5**: p. 37-48.
54. Hirschhaeuser, F., et al. (2010) *Multicellular tumor spheroids: an underestimated tool is catching up again.* Journal of Biotechnology, **148**(1): p. 3-15.
55. Hamer, P.D.W., et al. (2008) *The genomic profile of human malignant glioma is altered early in primary cell culture and preserved in spheroids.* Oncogene, **27**(14): p. 2091-2096.
56. Piaskowski, S., et al. (2011) *Glioma cells showing IDH1 mutation cannot be propagated in standard cell culture conditions.* British Journal of Cancer, **104**(6): p. 968-970.
57. Bralten, L.B., et al. (2011) *IDH1 R132H decreases proliferation of glioma cell lines in vitro and in vivo.* Annals of Neurology, **69**(3): p. 455-463.
58. Olympus Inc. (2014) *Olympus Microscopy Resource Center | Confocal Microscopy - Fluorophores for Confocal Microscopy*. http://www.olympusmicro.com/primer/techniques/confocal/fluorophoresintro.html. Last accessed (14.05.14).
59. Zeiss. (2014) *Spectral Separation of Multifluorescence Labels with the LSM 510 META* 27. http://www.well.ox.ac.uk/_asset/file/spectral-seperation-with-510-meta.pdf. Last accessed (14.05.14).
60. Darling, J., Oktar, N. and Thomas, D. (1983) *Multicellular tumour spheroids derived from human brain tumours.* Cell Biology International Reports, **7**(1): p. 23-30.
61. Vinci, M., et al. (2012) *Advances in establishment and analysis of three-dimensional tumor spheroid-based functional assays for target validation and drug evaluation.* BMC Biology, **10**(29): p. 1-20.

62. Kaur, H., et al. (2012) *Cadherin-11, a marker of the mesenchymal phenotype, regulates glioblastoma cell migration and survival in vivo.* Molecular Cancer Research, **10**(3): p. 293-304.
63. Jin, G., et al. (2012) *Mutant IDH1 is required for IDH1 mutated tumor cell growth.* Oncotarget, **3**(8): p. 774-782.
64. Rohle, D., et al. (2013) *An inhibitor of mutant IDH1 delays growth and promotes differentiation of glioma cells.* Science, **340**(6132): p. 626-630.
65. Weiswald, L.-B., et al. (2010) *In situ protein expression in tumour spheres: development of an immunostaining protocol for confocal microscopy.* BMC Cancer, **10**(106): p. 1-11.
66. Evans, S.M., et al. (2004) *Hypoxia is important in the biology and aggression of human glial brain tumors.* Clinical Cancer Research, **10**(24): p. 8177-8184.
67. Yang, L., et al. (2012) *Hypoxia and hypoxia-inducible factors in glioblastoma multiforme progression and therapeutic implications.* Experimental Cell Research, **318**(19): p. 2417-2426.
68. Greijer, A., et al. (2005) *Up‐regulation of gene expression by hypoxia is mediated predominantly by hypoxia‐inducible factor 1 (HIF‐1).* The Journal of Pathology, **206**(3): p. 291-304.
69. Zhao, S., et al. (2009) *Glioma-derived mutations in IDH1 dominantly inhibit IDH1 catalytic activity and induce HIF-1α.* Science, **324**(5924): p. 261-265.
70. Frezza, C., Tennant, D.A. and Gottlieb, E. (2010) *IDH1 mutations in gliomas: when an enzyme loses its grip.* Cancer Cell, **17**(1): p. 7-9.
71. Semenza, G.L. (2000) *Hypoxia, clonal selection, and the role of HIF-1 in tumor progression.* Critical Reviews in Biochemistry and Molecular Biology, **35**(2): p. 71-103.
72. Fisher, T., et al. (2007) *Mechanisms operative in the antitumor activity of temozolomide in glioblastoma multiforme.* The Cancer Journal, **13**(5): p. 335-344.
73. Kessler, J., et al. (2010) *HIF-1α inhibition by siRNA or chetomin in human malignant glioma cells: effects on hypoxic radioresistance and monitoring via CA9 expression.* BMC Cancer, **10**(1): p. 605.
74. Li, L., et al. (2006) *Hypoxia-inducible factor-1 inhibition in combination with temozolomide treatment exhibits robust antitumor efficacy in vivo.* Clinical Cancer Research, **12**(15): p. 4747-4754.
75. Hatanpaa, K.J., et al. (2010) *Epidermal growth factor receptor in glioma: signal transduction, neuropathology, imaging, and radioresistance.* Neoplasia, **12**(9): p. 675-684.

76. Brown, P.D., et al. (2008) *Phase I/II trial of erlotinib and temozolomide with radiation therapy in the treatment of newly diagnosed glioblastoma multiforme: North Central Cancer Treatment Group Study N0177.* Journal of Clinical Oncology, **26**(34): p. 5603-5609.

PROJECT 2: INVESTIGATING TNF-α IN FIRST EPISODE PSYCHOSIS MEDICATION NAÏVE SCHIZOPHRENIA PATIENTS TO DEMOGRAPHICALLY CONTROLLED INDIVIDUALS AND PHARMACOLOGICAL MANIPULATION OF TNF-α RELEASE

This project is submitted in partial fulfilment of the requirements for the award of the MRes

ABSTRACT

Schizophrenia is a psychotic disorder affecting approximately 1% of the global population. Schizophrenia is a heterogeneous disease with a complex aetiology including neurotransmitter abnormalities, viral infection and genetic predisposition. More recently, research focus has shifted to investigate the role of the immune system in schizophrenia development. Studies report an elevation in pro-inflammatory cytokines, such as tumour necrosis factor-α (TNF-α), in patients with schizophrenia. However, there is a level of ambiguity within these studies as factors such as medication can significantly affect cytokine levels and have often not been controlled for in previous studies. This study aimed to resolve this uncertainty by investigating TNF-α release from monocytes obtained from medication-naïve patients, which had been demographically matched to healthy individuals. Results showed a small, but non-significant increase in TNF-α release. Additionally, it has been shown that the nicotinic acetylcholine receptor (nAChR) is important in cytokine regulation and following activation, inhibits pro-inflammatory cytokine release. This study also investigated a nAChR activator, 4BP-TQS in cytokine release and results showed a significant reduction in TNF-α production from THP-1 monocytes. Further investigation of nAChR agonists is desirable in schizophrenia research to provide an alternative anti-inflammatory treatment to relieve negative symptoms associated with increased inflammation.

Acknowledgments

I would first like to thank Professor Nicholas Barnes and Dr Rachel Upthegrove for providing the opportunity to undertake this project and for their guidance during this investigation. I would also like to thank Dr Rumel Ahmed, Dr Gillian Grafton and the rest of Professor Barnes' lab for their time, space and assistance within the lab.

I also wish to thank Lindsay Durant, who kindly gave her time, assistance and facilities to perform the flow cytometry and cell-viability analysis in this project.

Finally, thanks go to the MRC for funding this investigation.

TABLE OF CONTENTS

LIST OF FIGURES

LIST OF TABLES

LIST OF ABBREVIATIONS

4BP-TQS- (4-(4-bromophenyl)-3a,4,5,9b-tetrahydro-3H-cyclopenta[c]quinoline-8-sulfonamide

5-HT- Serotonin

ACh- Acetylcholine

BMI- Body mass index

CNS- Central nervous system

DMSO- Dimethyl sulfoxide

ELISA- Enzyme-Linked Immunosorbent Assay

FACS- Fluorescent-activated cell sorting

FEP- First-episode psychosis

HI-FBS- Heat inactivated- foetal bovine serum

IL-1β- Interleukin–β

IL-4- Interleukin-4

IL-6- Interleukin-6

IL-10- Interleukin-10

IL-11- Interleukin-11

LPS- Lipopolysaccharide

MLA- Methyllycaconitine

nAChR- Nicotinic acetylcholine receptor

NAM- Negative allosteric modulator

NF-κB- Nuclear factor kappa-light-chain-enhancer of activated B cells

PAM- Positive allosteric modulator

PBMC- Peripheral blood mononuclear cell

PBS- Phosphate-buffered saline

Pen/Strep- Penicillin/Streptomycin

PTX- Picrotoxin

RT- Room temperature

SEM- Standard error of the mean

SD- Standard deviation

TNF-α- Tumour necrosis factor-α

1. INTRODUCTION

1.1 Schizophrenia

Schizophrenia is a serious psychotic disorder affecting approximately 1% of the global population[1] and generally manifests as a psychotic episode in late adolescence or early adulthood[1]. Clinical schizophrenia is diagnosed following periodic occurrence of these psychotic episodes over a six-month period[2]. Symptoms of schizophrenia are characterized into 3 classes, positive, negative and cognitive[3]. Positive symptoms are generally only exhibited in schizophrenic patients and include delusions, extreme paranoia, disorganised thought and visual and auditory hallucinations; otherwise known as psychosis[1]. Negative symptoms, refer to mental processes normally observed in the healthy population but are absent in patients. These symptoms include social and emotional withdrawal, apathy, lack of motivation and anhedonia[1]. Cognitive symptoms include dissolution of neurological processes such as memory and attention. Collectively, the broad spectrum of these symptoms can severely impair everyday activities for patients such as employability[4] and maintaining social relationships[5] and therefore it is imperative that effective treatments are designed to target all classes of symptoms.

There are many theories concerning schizophrenia aetiology and how early psychosis can progress to clinical schizophrenia. To date, the majority of schizophrenia research has focused on neurotransmitter abnormalities within the dopaminergic[6, 7] and glutamatergic systems[8], viral infection[9, 10] and genetic influence[11] on disease development. Historical research involving monozygotic twin and adoption studies have shown a strong genetic predisposition to schizophrenia as the risk of a relative of a schizophrenic individual developing the disorder is approximately 80%[12]. Although a large number of studies have identified genetic variants

that increase the susceptibility of developing schizophrenia, such investigations only explained a small minority of cases[11, 13]. It therefore seems apparent that schizophrenia is a heterogeneous disease with a complex aetiology. More recently, research focus has diverted to the contribution of the immune system within disease development.

1.2 Immune Dysregulation Theory of Schizophrenia Aetiology

1.2.1 Inflammation and Role of Cytokines

Inflammation is an immediate biological mechanism designed to protect and induce healing in response to harmful physiological stimuli, such as tissue damage, invasive pathogens and cellular stress[14]. It is first initiated by the organism's innate immune system that recruits cellular components such as monocytes (which can differentiate into macrophages,) granulocytes, dendritic cells and natural killer cells, to the site of infection or injury[14, 15]. These immune cells then recognise and eliminate potential pathogens typically through release and increased production of cytokines (figure 1).

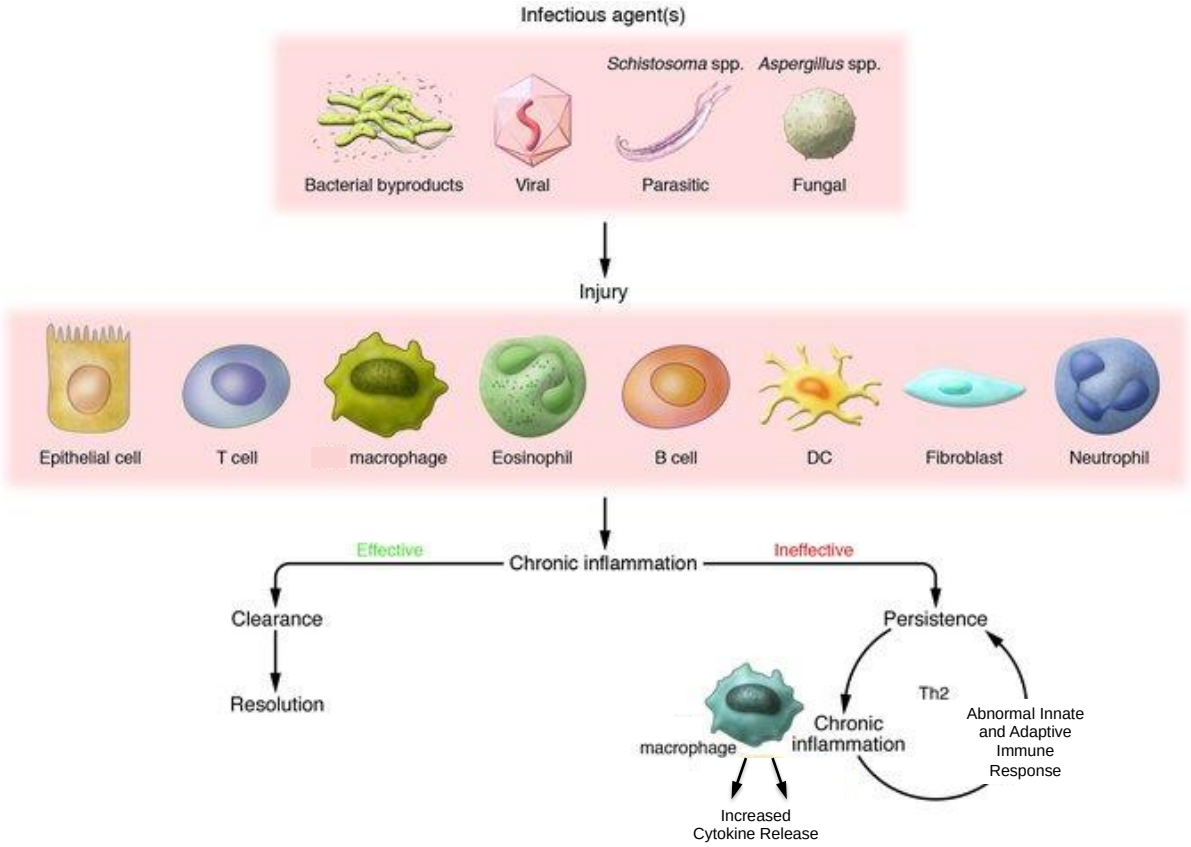

Figure 1: Cellular components of the host response to invasive and cellular stress (adapted from Meneghin and Hogaboam, 2007[16]). Pathogen infection, along with tissue injury and cellular stress is known to induce a host response in order to provide effective clearance of pathogens and healing of the damaged sites. The innate immune system, consisting of cellular components such as monocytes, macrophages, dendritic cells and granulocytes (neutrophils, basophils and eosinophils), are activated and secrete immunomodulating proteins causing the protective inflammatory response. If inflammation persists however, due to ineffective clearance and dysregulation of the innate and adaptive (consisting of immune 'memory' cells, such as B and T cells) systems, chronic inflammation can occur, which underlies many inflammatory disorders.

Cytokines are a diverse category of immunomodulating proteins that include interleukins, chemokines, interferons and tumour necrosis factors. These signalling proteins modulate the interactions and effects of target cells, which is crucial in producing a host response to invasive and damaging stimuli. Cytokines are divided into two general classes, pro- and anti-

inflammatory[17], corresponding to their effect. Pro-inflammatory cytokines include molecules such as tumour necrosis factor-α (TNF-α), interleukin-1β (IL-1β) and interleukin-6 (IL-6). Principally produced from activated macrophages, their primary function is to elevate systemic inflammation inducing responses such as pyrexia, cachexia, cell death and pathological pain[17]. Conversely, anti-inflammatory cytokines such as interleukin-4 (IL-4), interleukin-10 (IL-10) and interleukin-11 (IL-11), act to regulate the pro-inflammatory response by suppressing pro-inflammatory cytokine expression and reduce neuropathic pain[17].

The inflammatory process in healthy individuals is tightly controlled by homeostatic processes, resulting in affective pathogen clearance and tissue healing procedures whilst preventing excessive inflammation[1, 18]. Acute inflammation however can develop into chronic systemic inflammation due to prolonged activation of the innate immune system and dysregulation of immune cells[1], resulting in a sustained over-expression of pro-inflammatory cytokines.

1.2.2 Cytokine Imbalance in Schizophrenia

Recently, studies have investigated the role of cytokines and systemic inflammation in schizophrenia pathology[14, 15, 19, 20]. Results have shown a significant expression of pro-inflammatory cytokines, their receptors and activity, above that of background levels, in the serum and cerebrospinal fluid of schizophrenia patients[14]. Cytokines are known to have additional roles other than regulating the immune system, as they are also important for communication between the immune and central nervous systems[21] (CNS). Cytokines have a key function in neurodevelopmental processes such as synaptogenesis in foetal development

and regulation of synaptic plasticity, neurotransmission and neurogenesis in later life[22, 23]. It is believed that the immune response created from pre-natal viral exposure could subsequently interfere with brain development, and may result in an increased risk of developing schizophrenia[24, 25]. Therefore, imbalance in these key regulators could result in the neuroanatomical changes apparent in individuals with schizophrenia. Additionally, this may cause an abnormal and more aggressive inflammatory response from chronically activated monocytes and macrophages and an imbalance in T-cell subsets from the adaptive immune system[15]. Consequently, excessive release of cytokines could potentially contribute to many schizophrenia symptoms. Supporting this theory, studies have shown that peripheral administration of pro-inflammatory agents can induce the innate immune system to cause a 'sickness-behaviour' which when persistent, can develop into negative symptoms such as social deficits and anhedonia[1, 26], seen in schizophrenia. Table 1 shows a list of cytokines commonly altered in schizophrenia.

Cytokine	Main Cellular Source	Biological Function	Effect in Schizophrenia
IL-1β	Activated monocytes/macrophages, microglia and endothelial cells	Promote fever, stimulate release of pro-inflammatory cytokines, activation of T/B cells	↑ (serum/plasma) ↑/↓ (CNS)
IL-2	T-cells (T_H1)	Activation, growth and differentiation of T-cells, stimulate natural killer cells and neutrophils to stimulate pro-inflammatory cytokines.	↑/--- (CNS)
IL-6	Activated monocytes and macrophages, T-cells (T_H2/T_H17)	Promote fever, activate T-cells, stimulation of immunoglobulin-G production	↑ (serum/plasma)
IL-10	Activated monocytes and macrophages, T cells (T_H2), B-cells	Inhibition of pro-inflammatory cytokine synthesis, promotion of humoral immune repsonses	↑ (serum/plasma)
TNF-α	Activated monocytes and macrophages, T-cells (T_H1), natural killer cells, endothelial cells, microglia	Promote fever, direct cytotoxic effects, activation on monocytes, lymphocytes and endothelial cells	↑/ --- (serum/plasma)

Table 1: Cytokines implicated in the inflammatory response of schizophrenia (adapted from Meyer et al., 2011[1]). Table summarises a selection of cytokines, their main cellular source and biological functions found to be altered within the peripheral (serum/plasma) or central nervous systems (CNS) of schizophrenic patients. ↑ denotes a significant elevation, ↓ denotes a significant reduction in cytokine levels. There is ambiguity however in some of the findings such as TNF-α levels, as it has been found to be significantly elevated in some studies, however others have recorded a non-significant change (---).

1.3 Role of Nicotinic Acetylcholine Receptors in Schizophrenia

1.3.1 P50 Auditory Gating Deficits in Schizophrenia Patients

Nicotinic acetylcholine receptors (nAChRs) are of particular interest within schizophrenia research as they have been implicated in numerous pathological and pathophysiological neurological functions such as learning and memory, attention and arousal and modulation of synaptic transmission[27].

Nicotinic acetylcholine receptors are pentameric, ligand-gated ion channels consisting of a homomeric or heteromeric conformation from a selection of 16 subunits[28]. They are best known for their function in synaptic transmission following activation from endogenous neurotransmitter acetylcholine (ACh, figure 2). Nicotinic acetylcholine receptors are differentiated from muscarinic acetylcholine receptors as nAChRs can also be activated by the alkaloid, nicotine and other cholinergic agonists[29].

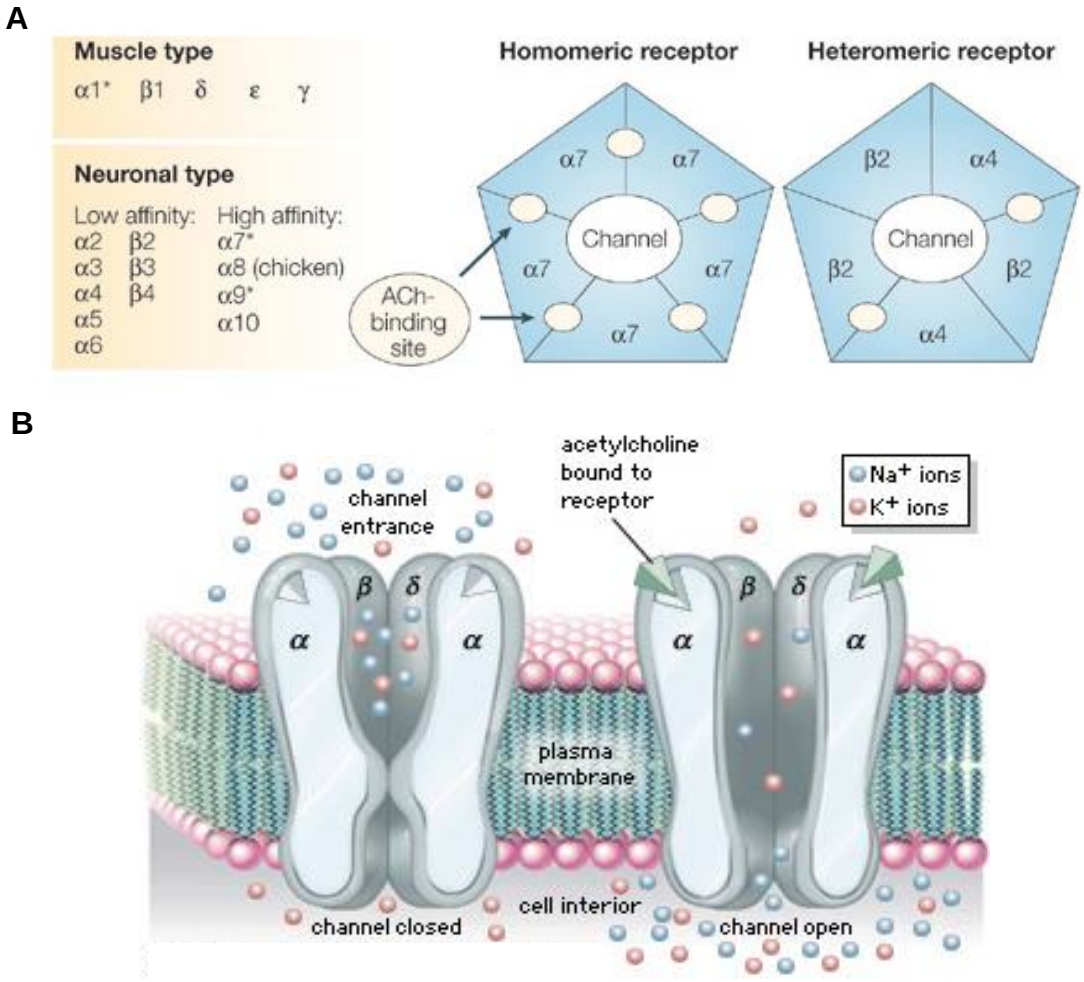

Figure 2: Acetylcholine receptor composition (adapted from Ulloa, 2005[30] and Erulkar and Lentz, 2013[31]). (A) Nicotinic acetylcholine receptors are either homomeric or heterometric pentamers consisting of a wide variety of subunits including α (1-10) β (1-4) γ, δ and ε subunits. Subunits co-assemble to create an array of subtypes which all have diverse biological and pharmacological

behaviours. Receptor affinity is related to the binding potential of receptor antagonist α-bungratoxin, which can specifically bind to neuronal nicotinic acetylcholine receptor α 1, 7 and 9 subunits. Nicotinic receptors can also exist in a homomeric conformation of α7 subunits. **(B)** Acetylcholine, and other nicotinic receptor agonists can bind to specific sites within the receptor subunits. This binding activates the receptor channel so it exists in an open conformation allowing positively charged ions, such as Na^+, K^+ and even Ca^{2+} to flow through the channel pore into the cell, mediating synaptic transmission.

It has been documented that many cognitive deficits observed in neurological disease such as Parkinson's disease and schizophrenia are often associated with attenuated cholinergic activity and deregulation of neuronal nAChRs[28, 29]. Major positive neurological indicators of schizophrenia include psychotic episodes with prominent auditory hallucinations (see section 1.1). It is known that schizophrenia patients have deficits in neurological sensory (auditory) gating which filters out any redundant or superfluous stimuli from the surrounding environment, preventing flooding of extraneous information into the brain[32]. Individuals suffering from schizophrenia are unable to filter auditory stimuli that have been presented 50 ms from one another whereas healthy individuals would generally regard the second stimuli to be redundant (figure 3)[33]. The P50 deficit has become one of the most recognized neurological markers concomitant with schizophrenia, as it is prominent in over 75% of patients[33].

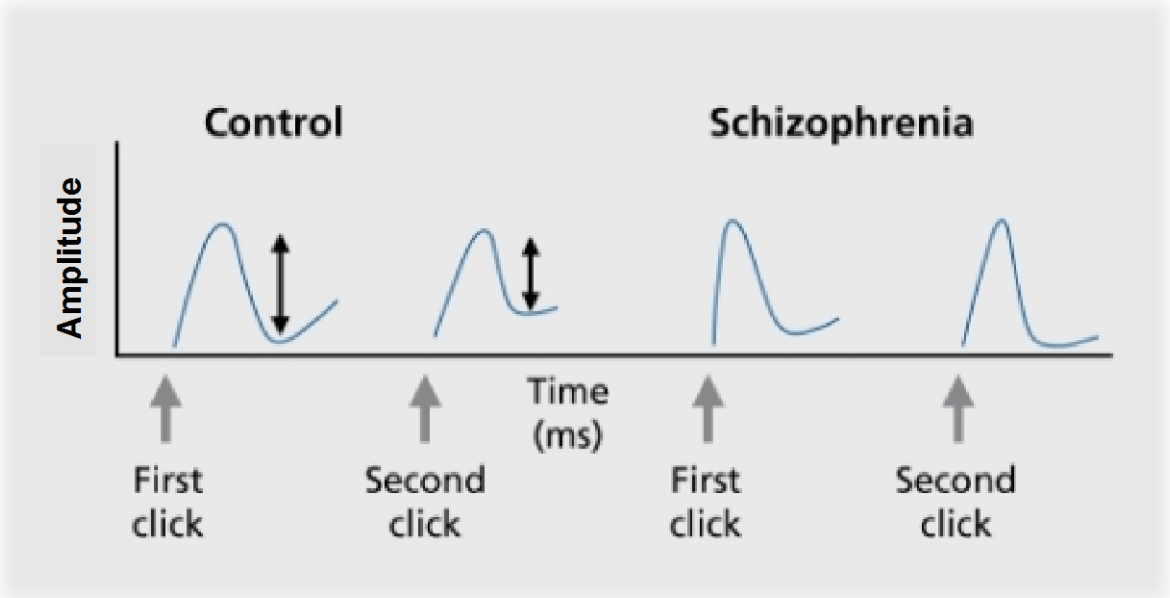

Figure 3: The P50 sensory gating deficit in schizophrenia (taken from Berrettini and Wade, 2005[34]). Upon testing auditory sensory gating in individuals, 2 auditory stimuli are provided 50 ms apart. In healthy individuals, the evoked response, measured using scalp electrodes, to the second click is reduced in amplitude compared to the first click. This is to prevent overload of information into the brain and consequently the second stimulus is considered to be redundant since it occurs close to the first stimulus. This effect is considered to be the electrophysiological signature of sensory gating. In schizophrenic individuals however, the amplitude of the P50 wave of the second auditory stimulus is comparable to the first stimulus and is therefore considered to be a failure in sensory gating.

It has been documented that stimulation of nAChRs via its agonist nicotine, can normalise and correct the P50 deficit[33, 35]. Epidemiological studies show that nicotine dependence is particularly high within schizophrenic individuals, as it has been reported that around 80% of patients[36] frequently smoke compared to 25-30% of the general population[37] suggesting that this in an effective self-medicated treatment for schizophrenia sufferers[38]. However, nicotine has only been shown to relieve the effects of abnormal sensory gating for around 30 minutes after which the deficit returns[33], which could suggest why chain smoking is so prevalent

within patients[39]. Animal studies have shown that this gating deficit may be due to reduced function of nAChR in schizophrenia[36]. This is mirrored in post-mortem studies of brain tissue from schizophrenic individuals as a 50% reduction in the expression of low-affinity nicotinic acetylcholine receptors has been documented compared to healthy controls[33, 36, 40].

In addition to the function of nAChRs within the CNS, nicotinic AChRs have also been found to be expressed in non-neuronal cells, such as cells within the immune system, and are believed in play a role in the regulation of anti-inflammatory effects[27].

1.3.2 nAChRs in the Immune System

The nAChRs expressed on component cells of the innate immune system, such as monocytes and macrophages, have recently been a focus within schizophrenia research[15, 41, 42].

The cholinergic anti-inflammatory pathway is particularly important within regulating the inflammation response as it acts as an endogenous mechanism to regulate overactive innate immune responses and prevent release of pro-inflammatory cytokines[43], therefore attenuating the inflammation response so chronic inflammation does not occur. This reflex is induced upon increased levels pro-inflammatory cytokines, which can activate receptors situated on vagal nerves[44]. This inflammation response within the CNS can then alter the immune response through release of acetylcholine, which can significantly inhibit release of TNF-α and other pro-inflammatory cytokines from immune cells[45, 46], figure 4.

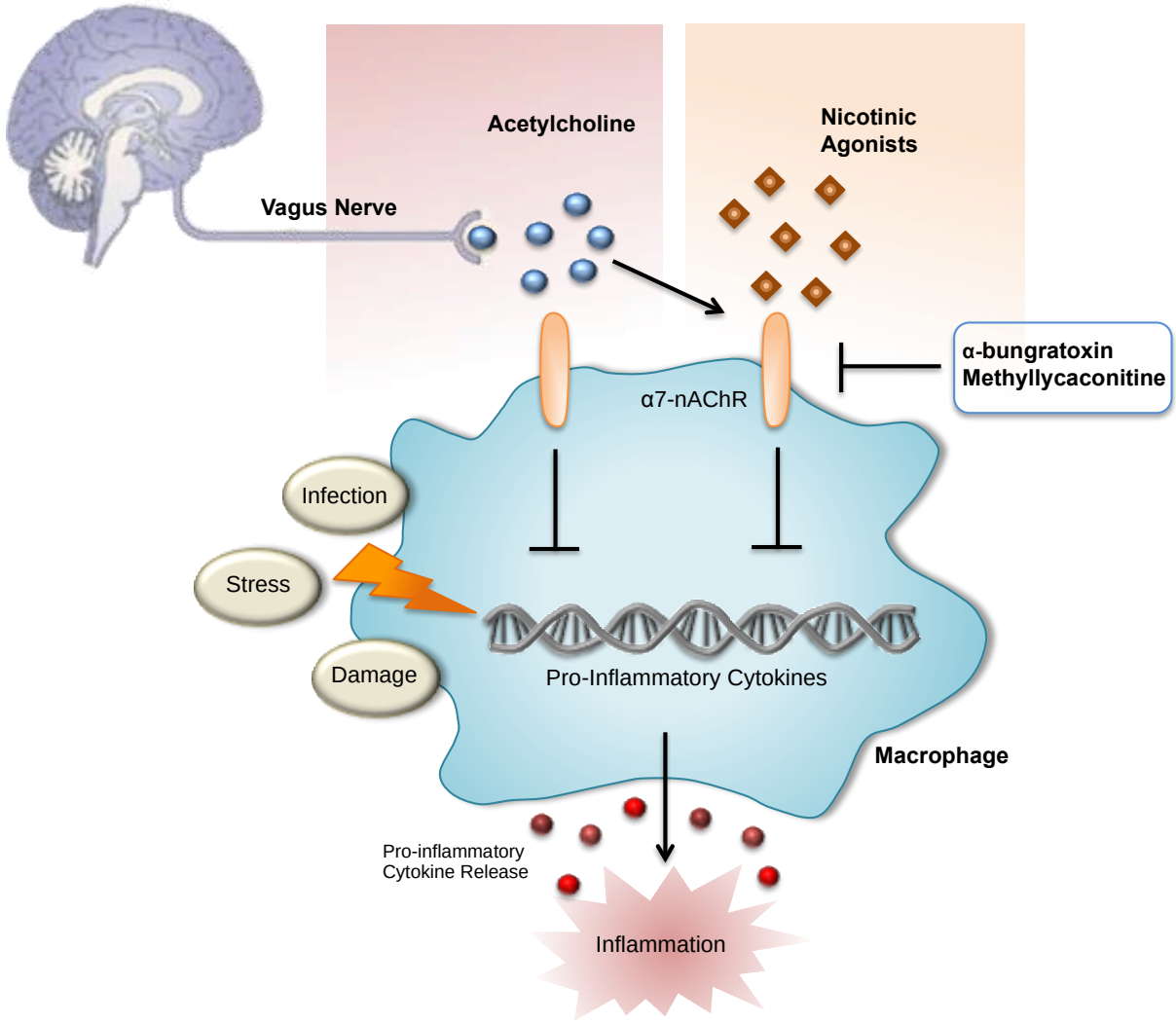

Figure 4: Inhibition of pro-inflammatory cytokine release from macrophages via activation of nicotinic acetylcholine receptors (based on Ulloa, 2005[30]). Activation of the Vagus nerve, by stimuli such as cellular stress, causes release of the neurotransmitter acetylcholine, which consequently causes activation of nicotinic acetylcholine receptors present on immune cells such as macrophages, inhibiting the production of pro-inflammatory cytokines through reduced activation of the nuclear factor kappa-light-chain-enhancer of activated B cells (NF-κB) pathway. Nicotine and nicotinic agonists have been shown to be more selective cholinergic agonists acting through α7nAChRs and are more effective at inhibiting pro-inflammatory cytokine release.

Monocytes and differentiated macrophages have predominately been shown to be involved in release of pro-inflammatory cytokines within the innate immune system[42]. Within

schizophrenia patients a noticeable increase in the number of monocytes has been documented[42, 47]. Additionally, irregularities in circulating monocytes have been seen within patients[42], which could consequently result in increased release of pro-inflammatory cytokines, creating an elevated inflammatory response. Many studies however document that cytokine release from these cells is inhibited upon activation of the α7-homomeric nAChRs[44, 48]. Therefore, because nicotine stimulation of α7-nAChRs has been shown to reduce pro-inflammatory cytokine release and improve cognitive defects seen in schizophrenia patients[49], further investigation concerning the role and therapeutic potential of nicotinic acetylcholine receptor agonists may provide a multimodal treatment for treatment and relief of schizophrenia symptoms.

1.4 Contrasting Results Within Schizophrenia Research

Many meta-analysis studies documenting cytokine levels in schizophrenia patients have reported a significant elevation in the serum, plasma and macrophage levels of pro-inflammatory cytokines such as IL-1β, IL-6 and TNF-α[14, 20, 21]. However the strength of the conclusions from these studies may be questioned as cytokine release is affected by various factors, which are not consistently controlled for[14, 15]. For example, the effects of current anti-psychotic medicine, such as clozapine, have been shown to elevate levels of TNF-α instead of reduce[50].

Additionally, many studies have recorded cytokine levels from different stages of disease progression and therefore some patients may have had longer exposure to anti-psychotic medicines, which would affect data analysis[14]. Other studies have aimed to correct for this by investigating patients that have experienced their first psychotic episode (first-episode

psychosis; FEP) although many patients have actually recently commenced treatment or analysed in a 'drug-free' state, however been previously taken medication[14, 19]. Therefore it is important when investigating the true effects of inflammation in schizophrenia, that FEP patients who are neuroleptic-naïve and have never commenced treatment are studied.

Other patient demographics such as illicit drug use[51, 52] age[21], gender[14] body mass index (BMI)[53] and smoking-status[54] are also known to dramatically affect levels of pro-inflammatory cytokines in patient blood and historically have not always been accounted for during studies. The BMI of a patient for example, is important when measuring cytokine levels as it is known that obesity can cause an inflammatory response in many metabolic tissues[53, 55]. Consequently, systemic cytokine levels have been shown to be considerably elevated in obese individuals, therefore not providing a true representation of cytokine level in regards to schizophrenia. Furthermore, as previously discussed, nicotine plays a large role in self-medication of schizophrenia patients[56], resulting in a reduced inflammatory response, again obscuring the true cytokine response as a result of schizophrenia.

TNF-α is one of the most common pro-inflammatory cytokines researched and dysregulation of TNF-α levels have been associated with diseases such as Alzheimer's[57] and inflammatory bowel disease[58]. Within schizophrenia however, there is ambiguity over the regulation of TNF-α. A large number of studies have documented TNF-α elevation in patients[1, 19, 41, 59] however other studies have shown no significant alteration[21]. This uncertainty could be a result from the influence of the above factors that may have not been controlled for. Therefore to improve success of future research in resolving schizophrenia aetiology and developing

potential treatments, it is imperative that differential expression of TNF-α is first elucidated using FEP neuroleptic-naïve patients who are demographically matched to healthy individuals.

2. AIMS AND HYPOTHESES

2.1 Aims

The aims of this project were to:

- Investigate TNF-α release from stimulated monocytes harvested from whole blood obtained from 10 neuroleptic-naïve FEP patients and compare to 9 healthy individuals which had been matched for age, gender, BMI and smoking-status.
- Use an *in vitro* culture model, representative of primary monocytes, to observe any differences in monocytic TNF-α release in the presence of a variety of pharmacological compounds.

2.2 Hypotheses

It was hypothesised that, according to previous research, TNF-α levels produced from stimulated monocytes, will be increased amongst the schizophrenia patients compared to the healthy controls. The use of FEP neuroleptic-naïve cases (demographically matched with the control samples) in this study will provide a better representation of the differential expression of TNF-α associated with schizophrenia and a greater understanding of the role of inflammatory cytokines in this disease. Additionally, through the use of a monocytic cell line, the TNF-α levels released from stimulated cells are likely to be altered within the presence anti-psychotic drugs and nAChR agonists, and could therefore be investigated further as potential anti-inflammatory treatments for schizophrenia. This would be of significant benefit since many atypical antipsychotics, such as clozapine, are associated with serious side-effects and can potentially increase TNF-α levels over time.

3. MATERIALS AND METHODS

3.1 Cell Culture

THP-1 cells, a human monocytic cell line, were cultured in suspension in RPMI-1640 medium (containing L-Glutamine and sodium bicarbonate; Sigma-Aldrich, R8758) supplemented with 10% heat-inactivated foetal bovine serum (HI-FBS) and 1% penicillin/streptomycin (Pen/Strep). Cultures were incubated at 37˚C, 5% CO_2.

3.2 LPS Stimulation of THP-1 Cells

The endotoxin lipopolysaccharide (LPS; Sigma-Aldrich, L2630) from *Escherichia coli* is a major inducer of TNF-α and was used to stimulate THP-1 cells to produce an inflammatory response. THP-1 cells were centrifuged at 400 G, 5 minutes, after which the supernatant was removed and cell pellet suspended in RPMI-1640 (10% HI-FBS, 1% Pen/Strep). Cells were counted using a haemocytometer and seeded into a 48-well plate at a density of 2.5×10^5 cells per well. To determine the optimal stimulation time and LPS concentration which would evoke optimum TNF-α production, cells were stimulated at 37˚C, 5% CO_2 with 0, 1, 10 and 100 ng/mL LPS for 1, 2, 4, 8 and 24 hours. At each time point, the cell suspension was removed and centrifuged (300 G, 5 minutes). The supernatant was then transferred, taking care to not disturb the THP-1 pellet, to a new 48-well plate and kept at -80˚C until needed to quantify TNF-α concentration using Enzyme-Linked Immunosorbent Assay (ELISA) analysis (see section 3.7).

3.3 THP-1 Stimulation in the Presence of a Range of Pharmacological Agents

Following determination of the optimal LPS concentration and stimulation time, THP-1 cells were stimulated with LPS and a range of drugs to observe any changes in TNF-α production.

THP-1 cells were seeded at density 2.5 x 10^5 cells per well onto two 48-well plates, which were stimulated (one plate with 10 ng/mL the other with 100 ng/mL LPS) for 4 hours (37˚C, 5% CO_2). Table 2 shows the drug concentrations and corresponding vehicle control used.

Drug	4BP-TQS	5-HT and 5-Chloroindole	PNU 282987 and PAM 120596	Clozapine
Concentration (μM)	30	3 (5-HT) 10 (5-chloroindole)	10 (PNU) 1 (PAM)	1
Vehicle Control	0.3 % DMSO	0.1 % DMSO	0.1 % DMSO	0.01% Water

Table 2: Concentrations of pharmacological agents used to assess TNF-α levels from LPS- stimulated THP-1 cells. Table showing the concentrations at which the agents in this study, (4-(4-bromophenyl)-3a,4,5,9b-tetrahydro-3H-cyclopenta[c]quinoline-8-sulfonamide (4BP-TQS), 5-HT (serotonin), 5-Chloroindole, PNU-282987, PAM-120598, and clozapine were used, with the corresponding vehicle control, dimethyl sulfoxide (DMSO) or water, for each condition. Each condition was replicated 5 times.

Following 4-hour stimulation, plates were centrifuged (300 G, 5 minutes) and supernatants removed and stored at -80˚C until cytokine quantification.

3.4 THP-1 Stimulation in the Presence of 4BP-TQS

3.4.1 4BP-TQS Concentration Curve

A concentration curve was produced to determine the lowest but effective concentration of 4BP-TQS. The minimum effective concentration is important to determine to ensure the effect is due to the drug and not from high cytotoxic concentrations. THP-1 cells were seeded into a 48-well plate at a density of 2.5 x 10^5 cells per well. Table 3 shows the concentrations and vehicle controls used.

Condition	4BP-TQS					Cycloheximide	Stimulation Control
Concentration (µM)	1	3	10	30	100	25	-
Vehicle Control	1% DMSO					0.25% Ethanol	-
LPS	100 ng/mL					100 ng/mL	100 ng/mL

Table 3: 4BP-TQS concentration curve. 1, 3, 10, 30 and 100 µM of 4BP-TQS was added to THP-1 cells. 1% DMSO was added to serve as a vehicle control for 4BP-TQS. 100 ng/mL of LPS was added to all conditions to stimulate the cells. 100 ng/mL LPS was also added to cells in the absence of 4BP-TQS to serve as a stimulation control. In addition, cells were also stimulated with 25 µM cycloheximide (Sigma-Aldrich, C7698) and 100 ng/mL LPS to act as a positive control of cell death to check cell viability using fluorescent-activated cell sorting (FACS). A 0.25% ethanol vehicle control was used. Each condition was performed in triplicate.

Cells were incubated (37˚C, 5% CO_2) for 4 hours. Following incubation, the plate was centrifuged (300 G, 5 minutes) after which supernatants extracted and kept at -80˚C until TNF-α quantification. THP-1 cell pellets were suspended in phosphate-buffered saline (PBS) and taken for fluorescent-activated cell sorting (FACS) analysis (described in section 3.5) to check cell viability.

3.4.2 THP-1 Stimulation With 4BP-TQS and Picrotoxin

To investigate whether the effect of 4BP-TQS on THP-1 TNF-α release could be blocked, varying concentrations of picrotoxin (PTX) was added in combination with 30 µM 4BP-TQS. THP-1 cells were seeded in a 48-well plate at a density of 2.5 x 10^5 cells per well. Table 4 shows the concentrations and vehicle controls for each condition.

PTX	300 nM	1 µM	3 µM	3 µM	-
4BP-TQS	30 µM	30 µM	30 µM	-	30 µM
Vehicle control	0.3 % DMSO				
LPS Stimulation	100 ng/mL	100 ng/mL	100 ng/mL	-	100 ng/mL

Table 4: Concentrations of PTX used in combination with 4BP-TQS. Table shows concentrations of PTX added to THP-1 cells stimulated with 100 ng/mL LPS in combination with 30 µM 4BP-TQS. 3 µM PTX was added to cells without 4BP-TQS and LPS stimulation, to ensure that the PTX was not causing an effect on the TNF-α release. Similarly, 100 ng/mL LPS was added in the absence of 4BP-TQS and PTX to serve as a stimulation control. Each condition was performed in triplicate.

Cells were then stimulated accordingly and incubated (37˚C, 5% CO_2) for 4 hours. Following stimulation, the plate was centrifuged (300 G, 5 minutes) after which supernatants were extracted and stored at -80˚C until needed.

3.4.3 THP-1 Stimulation With 4BP-TQS and Methyllycaconitine

THP-1 cells were stimulated with 4BP-TQS and methyllycaconitine (MLA) to see if the effect of 4BP-TQS could be inhibited. THP-1 cells were seeded in a 48-well plate at a density of 2.5 x 10^5 cells per well. Table 5 shows drugs concentration and vehicle controls used.

Drug	4BP-TQS	MLA	4BP-TQS and MLA
Concentration	10 µM	100 nM	10 µM (4BP-TQS) 100 nM (MLA)
Vehicle Control	0.1% DMSO	0.01% Water	0.1% DMSO and 0.01% Water

Table 5: Concentrations of MLA and 4BP-TQS incubated with LPS-stimulated THP-1 cells. Table showing concentrations of MLA and 4BP-TQS added to 100 ng/mL LPS-stimulated THP-1 cells and the appropriate vehicle control for each condition. 100 ng/mL LPS was added in the absence of 4BP-TQS and MLA to serve as a stimulation control. Each condition was replicated 5 times.

Cells were then stimulated with 100 ng/mL LPS and incubated (37˚C, 5% CO_2) for 4 hours. Following stimulation, the plate was centrifuged (300 G, 5 minutes) after which supernatants were extracted and stored at -80˚C until needed.

3.5 Fluorescent-Activated Cell Sorting (FACS)

To ensure that concentrations of 4BP-TQS were not toxic to THP-1 cells, thereby affecting TNF-α release, THP-1 cell viability was checked via FACS following 4BP-TQS stimulation.

After stimulation for 4 hours (section 3.4.1), cells were centrifuged at 300 G, 5 minutes. Supernatants were then removed and kept for ELISA analysis. The resulting THP-1 cell pellets were suspended in 270 µL PBS/2% bovine serum albumin (BSA). The cell suspension was transferred to a FACS tube where 30 µl of SYTOX Blue (final concentration of 0.125 µM; Life Technologies, S34857) was added for 5 minutes. SYTOX Blue dead cell stain is able to penetrate and stain nucleic acid in cells with comprised plasma membranes. When a 405 nm violet laser is shone on the sample, the nucleic acids within the dead cells fluoresce, and is detected in the violet channel of the CyAn Advanced Digital Processing (ADP) High-Performance Flow Cytometer (Beckman-Coulter). Figure 5 shows an example of SYTOX Blue fluorescence.

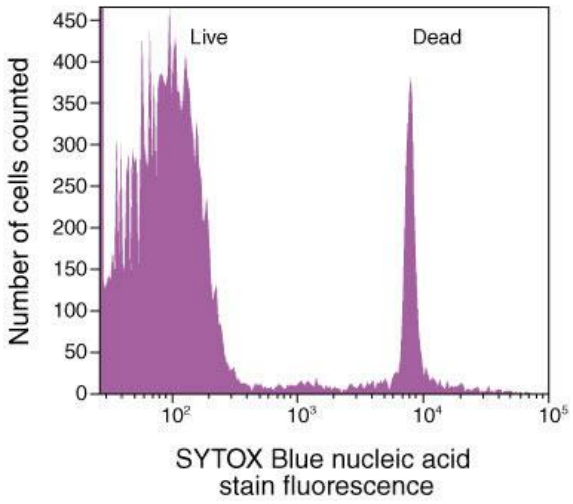

Figure 5: SYTOX Blue dead cell stain (taken from Life Technologies[60]). Schematic shows fluorescence of cells analysed on a flow cytometer equipped with a 405 nm violet diode laser. The dead cell population can easily be distinguished from the live cells by a sharp peak around 10^4.

The forward and side scatter of the cells was measured for each of the samples and the fluorescence from the SYTOX Blue recorded. Data generated was consequently imported and processed using Summit software (v4.3, Beckman-Coulter), where the mean percentage of cell death was determined for each condition.

3.6 Peripheral Blood Mononuclear Cell (PBMC) Purification

3.6.1 Monocyte Purification Using Ficoll-Paque and Plastic Adherence Methods

Blood was acquired from 10 patients with medication-naïve FEP, meeting research diagnostic criteria for schizophrenia[61], and 9 demographically controlled individuals, matched for age, gender, body mass index (BMI) and smoking-status. Blood was collected in vacutainers coated with an anti-coagulant EDTA, to prevent blood clotting. Blood samples were blinded and sent to the laboratory to harvest monocytes using the Ficoll-Paque density gradient

centrifugation method. Ficoll-Paque allows separation of blood components by density, forming distinctive layers of component blood cells, which can then be individually isolated. Whole blood was carefully layered on top of 25 mL Ficoll-Paque (GE healthcare, 17-1440-03), in a 50 mL conical tube. It is important there is minimal mixing of the two layers to obtain good separation of the blood. The sample was then centrifuged (900 G (no brake), 25 minutes). Following centrifugation, the blood was seen to clearly separate into its different constituent parts (figure 6).

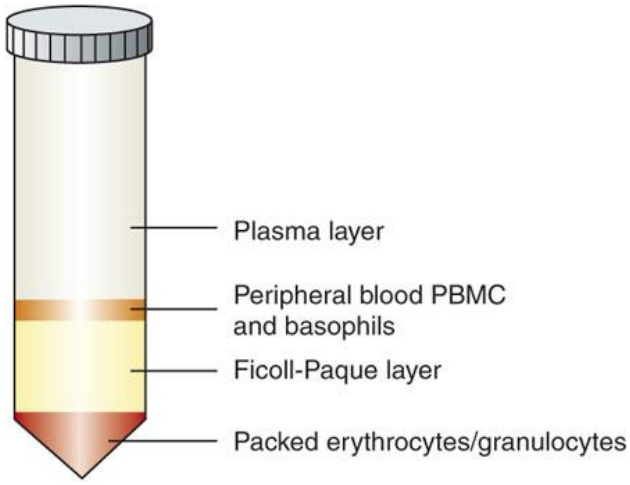

Figure 6: Ficoll-Paque density centrifugation of whole blood (taken from Munoz and Leff, 2007[62]). Following centrifugation at 900 G for 25 minutes, whole blood is separated by density allowing clear identification of its constituent parts. To harvest peripheral blood mononuclear cells, the plasma/serum fraction is removed and the underlying PBMC layer is removed and subsequently purified to obtain primary monocytes.

The plasma layer was carefully removed and kept for future analysis. The PBMC layer underneath was harvested and transferred to a new conical tube. RPMI-1640 (1% Pen/Strep) was then added to top up the PBMC fraction to 50 mL. The sample was then centrifuged (400 G, 5 minutes). The supernatant was subsequently removed, leaving the PBMC pellet. The pellet was then suspended in 50 mL RPMI-1640 (1% Pen/Strep), and centrifuged (400 G, 5

minutes). This step was repeated until the medium was clear (approximately 2 washes). The washes are important to remove any contaminating Ficoll-Paque, platelets and plasma proteins. Following the final wash, the supernatant was removed and the PBMC pellet was suspended in 1 mL RPMI-1640 (+10% HI FBS, 1% Pen/Strep) and cells counted. For monocyte purification, cells were suspended to a density of 3 x 10^6 cells/mL and 500 µL was added to each well of a 48-well plate. Cells were then incubated (37˚C, 5% $C0_2$) for 1 hour so that the monocytes could adhere. Following incubation, the medium was removed and monocytes were washed three times with 500 µL RPMI-1640 (+10% HI FBS, 1% Pen/Strep), to rid of any contaminant cells such as lymphocytes.

3.6.2. LPS Stimulation of Monocytes

Following purification, adhered monocytes were stimulated with 10 ng/mL LPS for 24 hours. Following incubation, plates were centrifuged (300 G, 5 minutes). The supernatant was then removed and kept at -80˚C until needed for ELISAs. Samples required processing 24 hours after they were obtained and were collected over a 12-month period. Previously 14 out of 19 samples had been collected, processed in the lab, and stimulated supernatants had been frozen until analysed simultaneously for TNF-α levels.

3.7. Enzyme-Linked Immunosorbent Assay (ELISA)

3.7.1. ELISA Protocol

ELISAs were performed to detect the concentration of human-TNF-α released from the THP-1 stimulation experiments and schizophrenia patient and control monocytes.

ELISAs were conducted according to manufacturers instructions (ELISA Human TNF-α Max^{TM}; Biolegend, 430201). First, a 96-well plate was coated in 100 µl of capture antibody (1:200 dilution in 1x coating buffer) and incubated overnight (4˚C). Following incubation, the plate was washed four times with wash buffer (1x PBS + 0.05% Tween). 200 µl of 1x assay diluent (10% FBS in PBS) was added to each well and incubated at room temperature (RT) for 1 hour with shaking. This was to block any non-specific antibody binding. The plate was then washed four times with wash buffer. Following, 100 µL of TNF-α standards and samples (which had been diluted in 1x assay diluent to be in the ELISA detection range) were added to the appropriate wells and incubated at RT for 2 hours with shaking. After incubation, the plates were washed four times with wash buffer. 100 µL of detection antibody (1:200 dilution in 1x assay diluent) was added to each well and incubated at RT for 1 hour with shaking. The plate was then washed four times with wash buffer. 100 µL of diluted Avidin-HRP solution (1:1000 dilution in 1x assay diluent) was then added to each well and incubated at RT for 30 minutes with shaking. After, the plates were washed five times, soaking the plates for 30 seconds per wash. Finally 100 µL of TMB substrate solution (Bethyl Laboratories, 130221) was added to each well and incubated in the dark for between 10-25 minutes, until the desired colour had developed. To stop the reaction, 100 µL of stop solution (2 N H_2SO_4) was added to each well. The absorbance was then read on a microplate reader (Multiskan EX, Thermo) at 450 nm.

3.7.2. ELISA Analysis

Data was imported into GraphPad Prism software, v6 for Macintosh (GraphPad Software, La Jolla California USA), where a linear regression was performed of a standard curve, which was calculated from known concentrations of TNF-α run in duplicate, on each ELISA plate.

TNF-α concentration (pg/mL) of unknown samples was then determined by interpolation with the standard curve. The identity of the samples was unknown until all samples had been processed.

3.8. Analysis and Statistics

All statistical tests were performed using GraphPad Prism. A Shapiro-Wilk test was performed to determine if the data was of normal distribution. A parametric unpaired T-test, assuming unequal standard deviation (SD; with Welch's correction) or non-parametric Mann-Whitney test was then performed. Normalised data was analysed by a one-sample t-test. Any outliers within the data were identified by performing a ROUT (1%) test and subsequently omitted from analysis. FACS analysis was performed using Summit (v.4.3, Beckman Coulter).

4. RESULTS

4.1 Optimisation of LPS Stimulation of THP-1 Cells.

To determine the optimal TNF-α release from THP-1 cells, the optimum stimulation time and LPS concentration had to be determined to be within the detection range for ELISA analysis. It can be seen in figure 7 that as expected in the absence of LPS, TNF-α release was below the level of detection. Similarly, with addition of 1 ng/mL LPS, there was minimal release from all time points. However, when 10 ng/mL LPS was added there was a considerable increase in TNF-α that peaked at 4 hours (222.6±43.6 pg/mL) however substantially decreased after 24 hours (34.2±8.9 pg/mL). The largest increase in TNF-α concentration however was seen upon stimulation with 100 ng/mL LPS for 4 hours (508.4±86.4 pg/mL) which again decreased to considerably lower levels following 24 hours (96.3±44.9 pg/mL). Therefore, in future experiments stimulation with 10/100 ng/mL LPS for 4 hours was chosen.

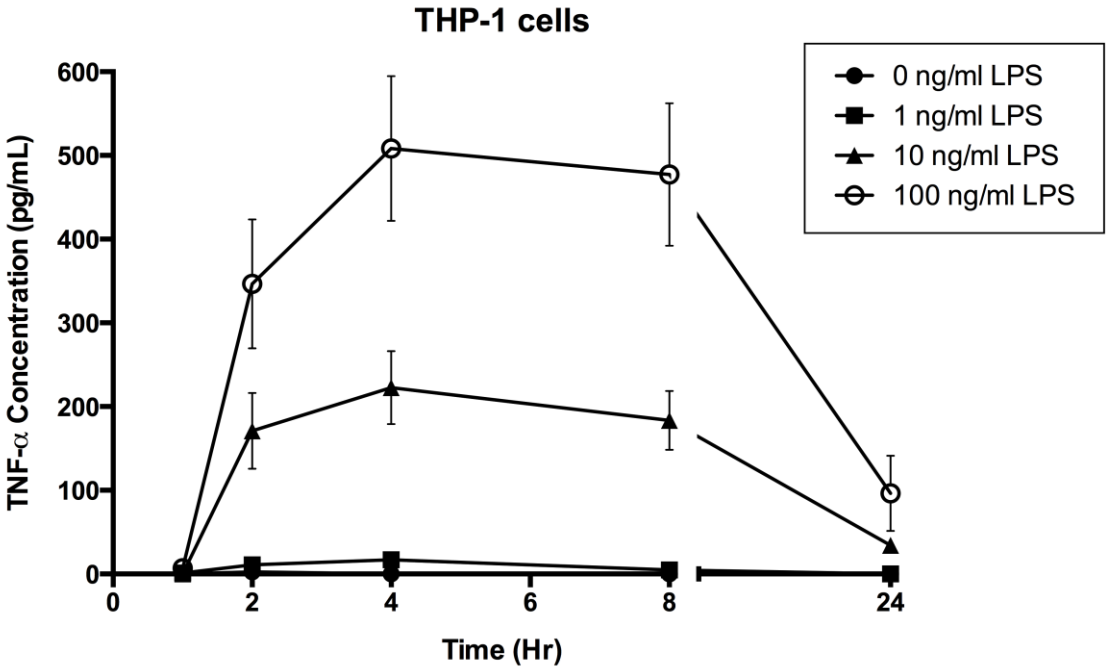

Figure 7: TNF-α release from THP-1 cells with varying concentrations of LPS. THP-1 cells were seeded at a density of 2.5 x 10^5 cells per well of a 48-well

plate. Cells were then stimulated with either 0, 1, 10 and 100 ng/mL of LPS and incubated at 37˚C. The supernatant was collected at various time points during the stimulation period and ELISAs were used to determine TNF-α levels at each time point. It is clear that THP-1 cells were not stimulated in the absence of LPS since no TNF-α was released. Stimulation with 1 ng/mL LPS only elicited a small response, which peaked at 4 hours (16.9±5.7 pg/mL). There was a noticeable increase in TNF-α release when cells were stimulated with 10 ng/mL LPS, which again peaked at 4 hours (222.6±43.6 pg/mL) and declined after 24 hours (34.2±8.9 pg/mL). The largest TNF-α release was seen upon stimulation with 100 ng/mL LPS and again peaked after 4 hours stimulation (508.4±86.6 pg/mL) and similarly declined after 24 hours (96.3±44.9 pg/mL). Samples had not been diluted for ELISA analysis. Data was obtained from 3 independent experiments, with each time point conducted in duplicate. Any outliers were identified using a ROUT test (1%) and subsequently removed. Error bars represent ± standard error of the mean (SEM).

4.2 TNF-α Release From LPS-Stimulated THP-1 Cells Incubated With a Range of Pharmacological Agents.

Stimulated THP-1 cells were incubated with a range of pharmacological agents to see if TNF-α release could be altered. When THP-1 cells were stimulated with 10 ng/mL LPS and incubated with 30 µM 4BP-TQS for 4 hours (figure 8(i)), there was a significant (p=0.002) decrease in TNF-α release compared to control (0.3% DMSO). Upon addition of 5-HT and 5-Chloroindole and PNU and PAM, there was no significant decrease in TNF-α concentration compared to vehicle control (0.1% DMSO). There was a small but insignificant decrease in TNF-α release however, upon addition of 1µM clozapine. The results from each condition were normalised to the vehicle control (figure 8(ii)). Again, there is a distinctive decrease when THP-1 cells were incubated in the presence of 30 µM 4BP-TQS (p=0.01). There was no significant difference when cells were incubated with 5-HT and 5-Chloroindole or PNU and PAM. Clozapine induced a significant reduction (p=0.04) in TNF-α when normalised between experiments.

Cells were also stimulated with 100 ng/mL LPS for 4 hours and again the same trend in TNF-α release with 10 ng/mL can be seen (figures 8 (iii) and (iv)). Incubation with 30 µM 4BP-TQS caused a significant ($p=0.0001$) decrease in TNF-α concentration released from stimulated THP-1 cells. Again there was no change when cells were incubated with 5-HT and 5-Chloroindole but there was a significant decrease ($p=0.05$) in TNF-α release with addition of PNU and PAM. There was a slight decrease when cells were incubated with clozapine however was not significant. When these results were normalised to the vehicle control for each condition (figure 8 (iv)), it is again apparent that 30 µM 4BP-TQS caused a significant reduction in TNF-α release from THP-1 cells ($p=0.01$). Large variability between experiments was seen when cells were incubated with 5-HT and 5-Chloroindole or PNU and PAM. Again a slight decrease in TNF-α concentration was seen with clozapine incubation, however was not significant.

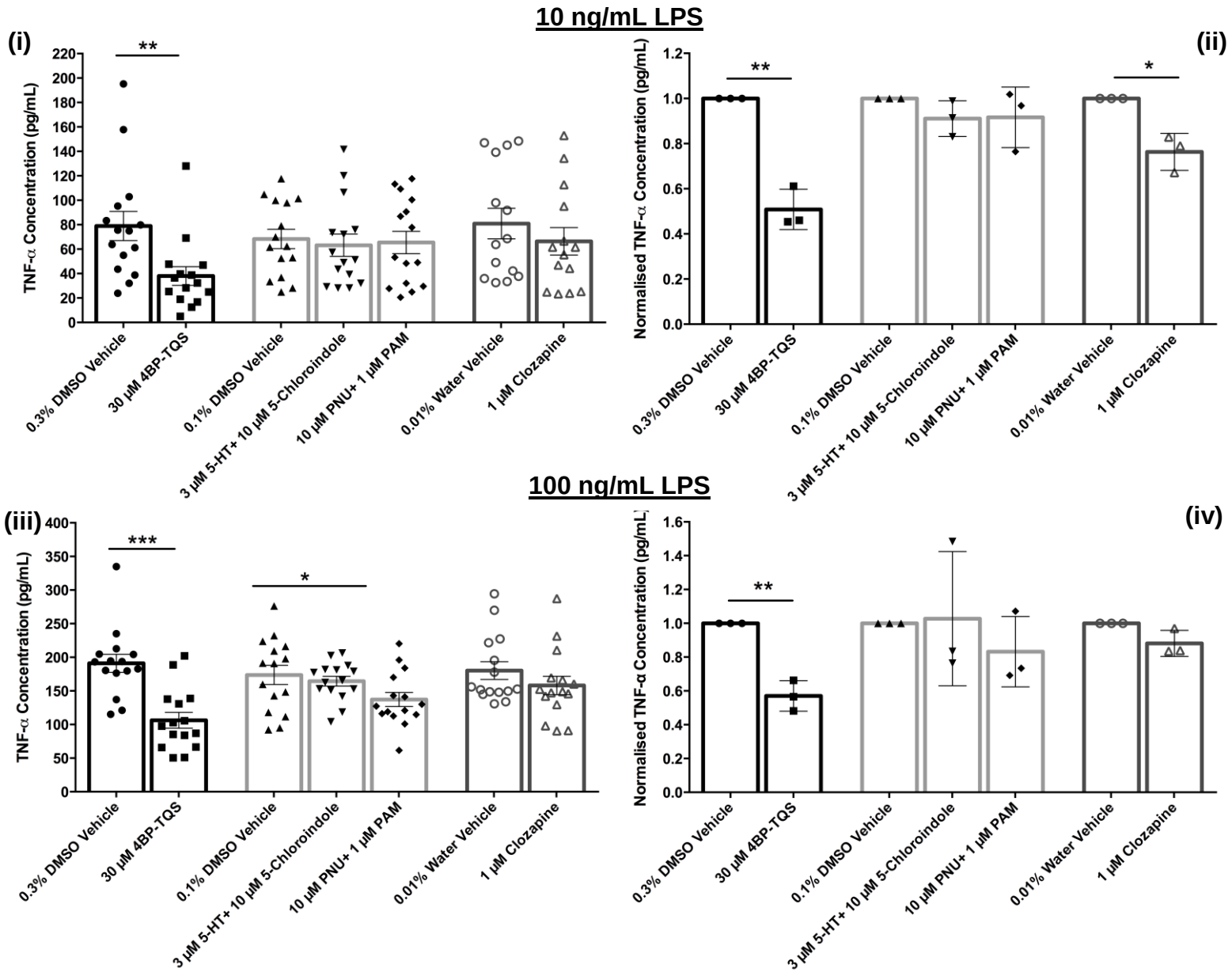
10 ng/mL LPS
(i)
(ii)
TNF-α Concentration (pg/mL)
Normalised TNF-α Concentration (pg/mL)
**
*
0.3% DMSO Vehicle
30 μM 4BP-TQS
0.1% DMSO Vehicle
3 μM 5-HT+ 10 μM 5-Chloroindole
10 μM PNU+ 1 μM PAM
0.01% Water Vehicle
1 μM Clozapine
100 ng/mL LPS
(iii)
(iv)
***

Figure 8: TNF-α release from LPS-stimulated THP-1 cells in the presence of a variety of pharmacological agents. (i) THP-1 cells stimulated with 10 ng/mL LPS for 4 hours. A significant decrease (p=0.002) was observed upon incubation with 4BP-TQS when compared to the 0.3% DMSO vehicle control (0.3%DMSO: 78.7±11.9 pg/mL; 30 µM 4BP-TQS: 38.0±7.6 pg/mL). No other significant differences were seen in TNF-α release with the other agents compared to their respective controls (0.1% DMSO: 68.3±7.9 pg/mL; 3 µM 5-HT+ 10 µM 5-Chloroindole: 63.2±9.1 pg/mL; 10 µM PNU + 1 µM PAM: 65.4±9.1 pg/mL and 0.01% Water: 80.9±12.5 pg/mL; 1 µM Clozapine: 66.4±11.3 pg/mL). **(ii) Normalisation of TNF-α levels to the vehicle control.** The data was then subsequently normalised to the corresponding vehicle control within each experiment performed. Again a significant decrease was seen upon incubation with 30 µM 4BP-TQS (p=0.01). Also a significant decrease was seen in TNF-α release when incubated with 1 µM clozapine (p=0.04). **(iii) THP-1 cells stimulated with 100 ng/mL LPS for 4 hours.** A significant decrease (p= 0.0001) was seen when incubated with 30 µM 4BP-TQS compared to the 0.3% DMSO vehicle control (0.3% DMSO: 191.1±13.4 pg/mL; 30 µM 4BP-TQS; 106.3±11.8 pg/mL). A significant decrease (p=0.05) was also seen when 1µM PNU and 10 µM PAM was incubated with stimulated THP-1 cells compared to the vehicle control (0.1% DMSO: 173.7±14.2 pg/mL; 10 µM PNU+ 1 µM PAM: 137.2±10.5 pg/mL). No significant decrease was seen when incubated with 3 µM 5-HT+ 10 µM 5-Chloroindole however (3 µM 5-HT+ 10 µM 5-Chloroindole: 164.4±7.4 pg/mL) or with 1 µM Clozapine, compared to the vehicle control (0.01% Water: 180.2±13.1 pg/mL; 1 µM Clozapine: 158.1±13.7 pg/mL). **(iv) Normalisation of TNF-α levels to the vehicle control.** A significant decrease in TNF-α release is again apparent following incubation with 4BP-TQS (p=0.01), but not with any of the other compounds. Samples had been diluted 1:4 to be in the detection range for ELISA analysis. Data was obtained from 3 independent experiments, with each condition replicated 5 times in each experiment. Any outliers were identified using a ROUT (1%) statistical test and subsequently removed. For graphs presenting all data points, error bars represent ±SEM and normalised data graphs represent ± SD.

4.3 THP-1 Stimulation With 4BP-TQS and PTX

Following identification that 4BP-TQS reduced significantly TNF-α from LPS-stimulated THP-1 cells, an experiment was conducted to see if this response could be inhibited. THP-1 cells were stimulated with 100 ng/mL LPS for 4 hours in the presence of 30 µM 4BP-TQS and a range of concentrations of PTX. It is apparent that upon addition of 300 nM, 1 and 3 µM PTX, TNF-α release was reduced to a similar level seen with 30 µM 4BP-TQS, compared to vehicle control (0.3% DMSO), therefore showing the effect of 4BP-TQS was not inhibited

(figure 9(i)). To check that PTX alone was not altering TNF-α release, THP-1 cells were incubated solely with 3 µM PTX and it is apparent that there was minimal TNF-α release. Results were normalised to the vehicle control and again it can be seen that upon addition of PTX, TNF-α concentration remained reduced and was not rescued to values similar to the vehicle control (figure 9 (ii)).

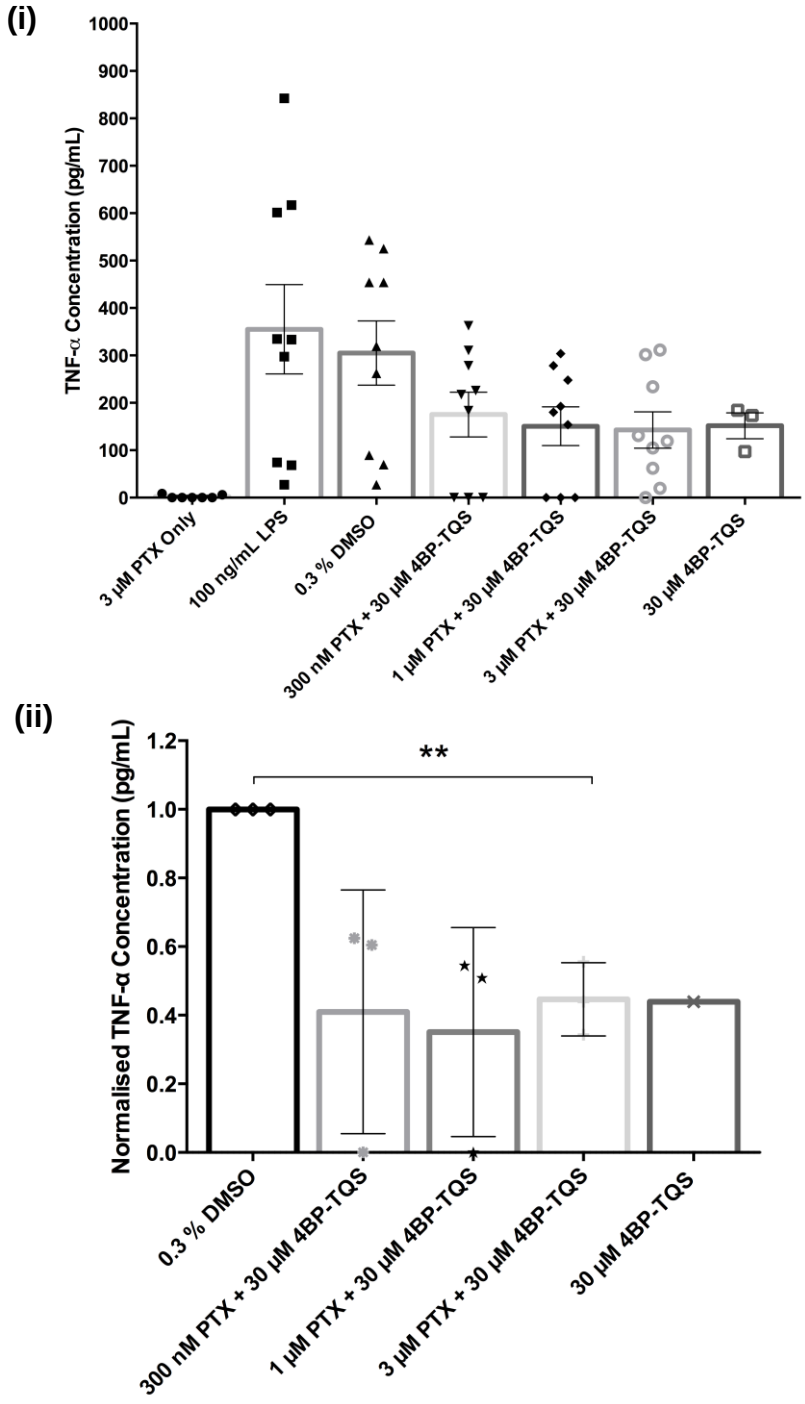

Figure 9: Incubation with PTX and 30 µM 4BP-TQS does not inhibit TNF-α from 100 ng/mL LPS-stimulated THP-1 cells. (i) Upon incubation with 300 nM, 1 and 3 µM PTX and 30 µM 4BP-TQS, there was no significant increase in TNF-α levels compared to the 0.3% DMSO vehicle control (0.3% DMSO: 305.1±67.8 pg/mL; 300 nM PTX+ 30 µM 4BP-TQS: 175.3±47.2 pg/mL; 1 µM PTX+ 30 µM 4BP-TQS: 150.7±40.8 pg/mL; 3 µM PTX+ 30 µM 4BP-TQS: 142.7±38.4 pg/mL) and to 30 µM 4BP-TQS alone (30 µM 4BP-TQS: 151.6±27.4 pg/mL). TNF-α levels were measured from THP-1 cells that had been incubated with 3 µM PTX in the absence of 100 ng/mL LPS stimulation to confirm that PTX did not cause a direct effect on THP-1 cells. It can be seen that cells were not affected since TNF-α was not produced in absence of stimulation (3 µM PTX: 2.2±1.4 pg/mL). **(ii)** Data was normalised to the vehicle control and it is apparent that incubation with PTX in combination with 30 µM 4BP-TQS did not inhibit the reduction in the levels of TNF-α which is caused by 4BP-TQS. A significant reduction was seen between the control and 3 µM PTX and 30 µM 4BP-TQS ($p=0.01$). Samples had been diluted 1:4 to be in the detection range for ELISA analysis. Data was obtained from 3 independent experiments (1 experiment for 30 µM 4BP-TQS alone). Each condition was performed in triplicate within each experiment. Any outliers were identified using a ROUT (1%) statistical test and subsequently removed. Error bars in graphs showing all data points (i) represent ± SEM and normalised data (ii) represent ± SD.

4.4 4BP-TQS Concentration Curve

To determine the minimum concentration of 4BP-TQS needed to cause a reduction in TNF-α, THP-1 cells were stimulated (100 ng/mL LPS, 4 hours) in the presence of 1, 3, 10, 30 and 100 µM 4BP-TQS. Figure 10 shows that 1 µM 4BP-TQS increased the TNF-α concentration compared to the vehicle control (0.1% DMSO). However 3, and 10 µM had a slight decrease in TNF-α release and it is clear that 100 µM 4BP-TQS had the largest reduction in TNF-α. There is large variability within the results however so replications are needed.

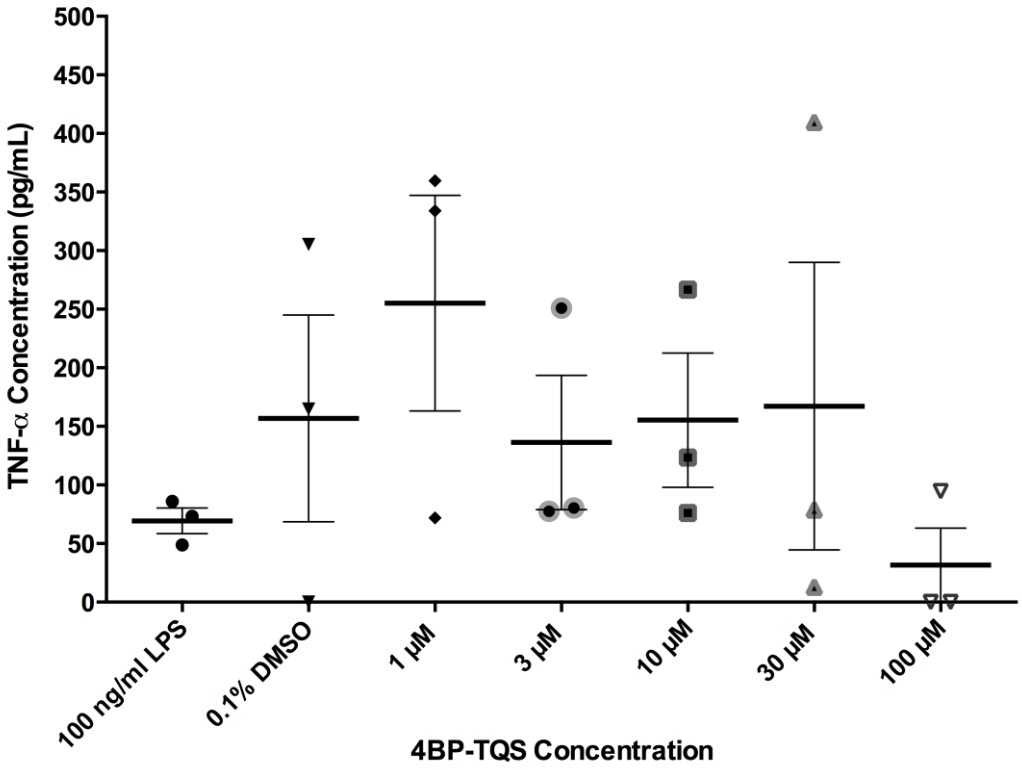

Figure 10: TNF-α levels from LPS-stimulated THP-1 cells incubated with increasing concentration of 4BP-TQS. It is apparent that upon incubation with 1 µM 4BP-TQS (255.2±92.0 pg/mL), there is an increase in the TNF-α levels compared to the 0.1% DMSO control (156.7±88.2 pg/mL) indicating this concentration of 4BP-TQS is not sufficient to reduce TNF-α release. There is a slight decrease upon application with 3 (136.2±57.3 pg/mL) and 10 µM (155.3±57.3 pg/mL) but increase with 30 µM 4BP-TQS (167.3±122.8 pg/mL). The largest and consistent reduction in TNF-α concentration was seen however with 100 µM 4BP-TQS (31.6±31.6 pg/mL). Large variability is seen within the other concentrations and should therefore be repeated. Samples were diluted 1:4 to be in the detection range for ELISA analysis. Data was obtained from 1 independent experiment. Each condition was repeated in triplicate. Error bars represent ± SEM.

4.5 Confirmation of Cell Viability Following 4BP-TQS Incubation

To confirm that 4BP-TQS was not toxic to THP-1 cells during the 4-hour stimulation, cell viability was measured using SYTOX Blue staining and analysed by flow cytometry. Figure 11 shows forward and side scatter plots of THP-1 cells for each condition and histograms

documenting the fluorescence emission from SYTOX Blue, indicating the percentage of dead cells. Gating was applied to distinguish THP-1 cells. It is clear that there was less than 1% cell death exhibited in all conditions.

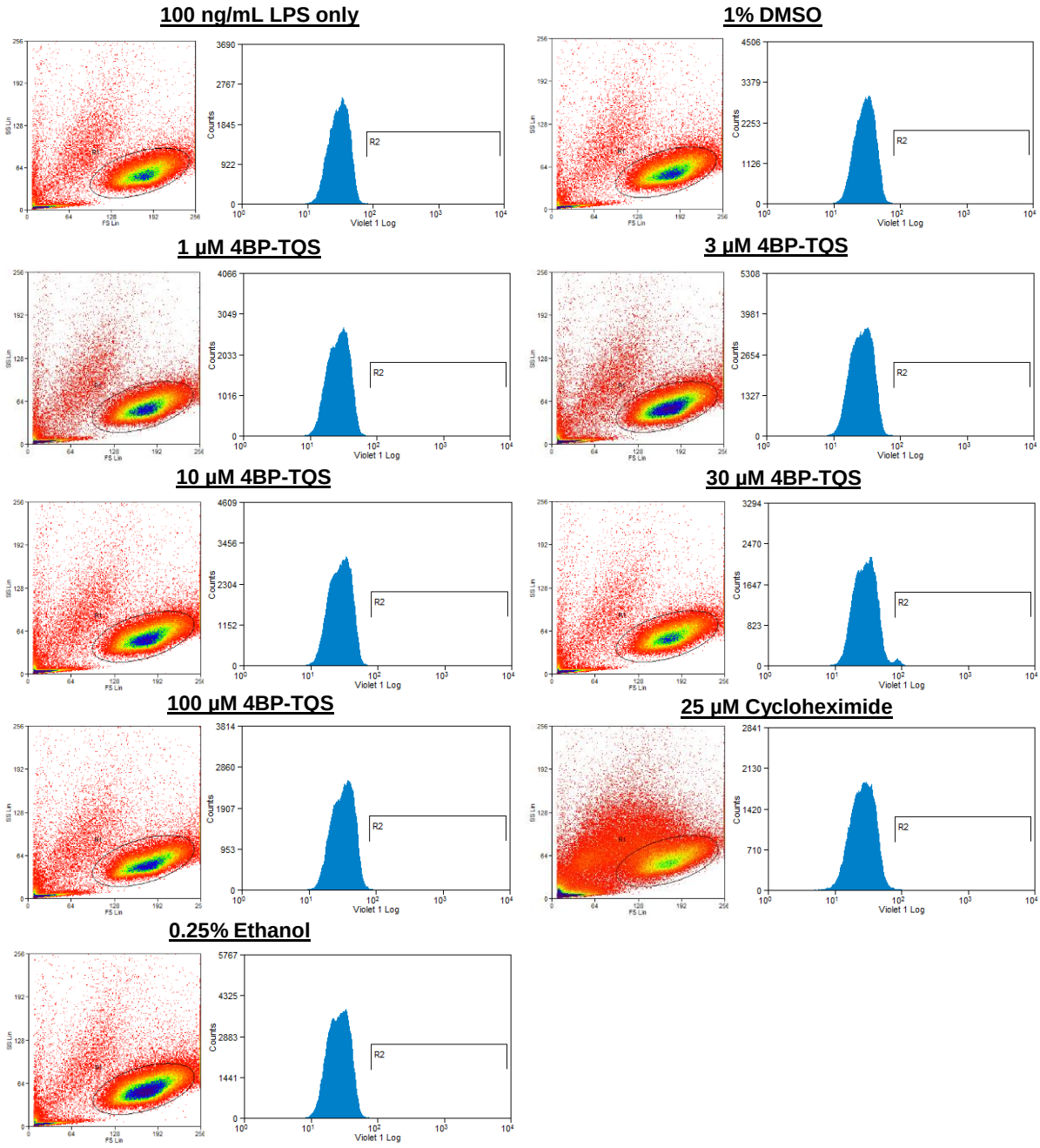

Condition	100 ng/mL LPS	1% DMSO	1 µM 4BP-TQS	3 µM 4BP-TQS	10 µM 4BP-TQS	30 µM 4BP-TQS	100 µM 4BP-TQS	25 µM Cyclohex-imide	0.25% Ethanol
Average Cell death (%)	0.32	0.24	0.23	0.20	0.79	0.94	0.45	0.61	0.19

Figure 11: Flow cytometry was used to assess cell viability following 4BP-TQS incubation. Following 4-hour stimulation, THP-1 cells were stained with SYTOX blue to assess cell viability in the various conditions. It is apparent that less than 1% cell death was exhibited. 25 µM cycloheximide (and its vehicle control 0.25% ethanol) was used as a positive control for cell death, as it is a known inhibitor of protein synthesis. However cell death was not exhibited in this condition. The granularity of the cells however has been significantly altered, indicated by the increased side scatter of the cells. Data was obtained from 1 independent experiment, in which each condition was replicated 5 times.

4.6 THP-1 Stimulation With 4BP-TQS and MLA

To observe whether 4BP-TQS-induced reduction in TNF-α release from THP-1 cells could be blocked, cells were stimulated with 100 ng/mL LPS for 4 hours in presence of a potent nAChR antagonist, MLA. It is clear from figure 12(i) that there was a reduction in TNF-α upon incubation with 10 µM 4BP-TQS compared to the vehicle control (0.1% DMSO), however this did not achieve statistical significance. When THP-1 cells were incubated with 10 µM 4BP-TQS and 100 nM MLA however, TNF-α concentration was comparable to vehicle control levels (0.1% DMSO and 0.01% water). Upon application of 100 nM MLA, TNF-α was significantly ($p=0.05$) reduced compared to the vehicle control (0.01% water).

When results were normalised to vehicle controls (figure (ii)), it was again apparent that upon incubation with 10 µM 4BP-TQS that TNF-α concentration was reduced in comparison to the vehicle control but levels were increased when 100 nM MLA was added in combination with 10 µM 4BP-TQS. Incubation with 100 nM MLA was shown to reduce TNF-α release from THP-1 cells, however large variability between experiments is shown.

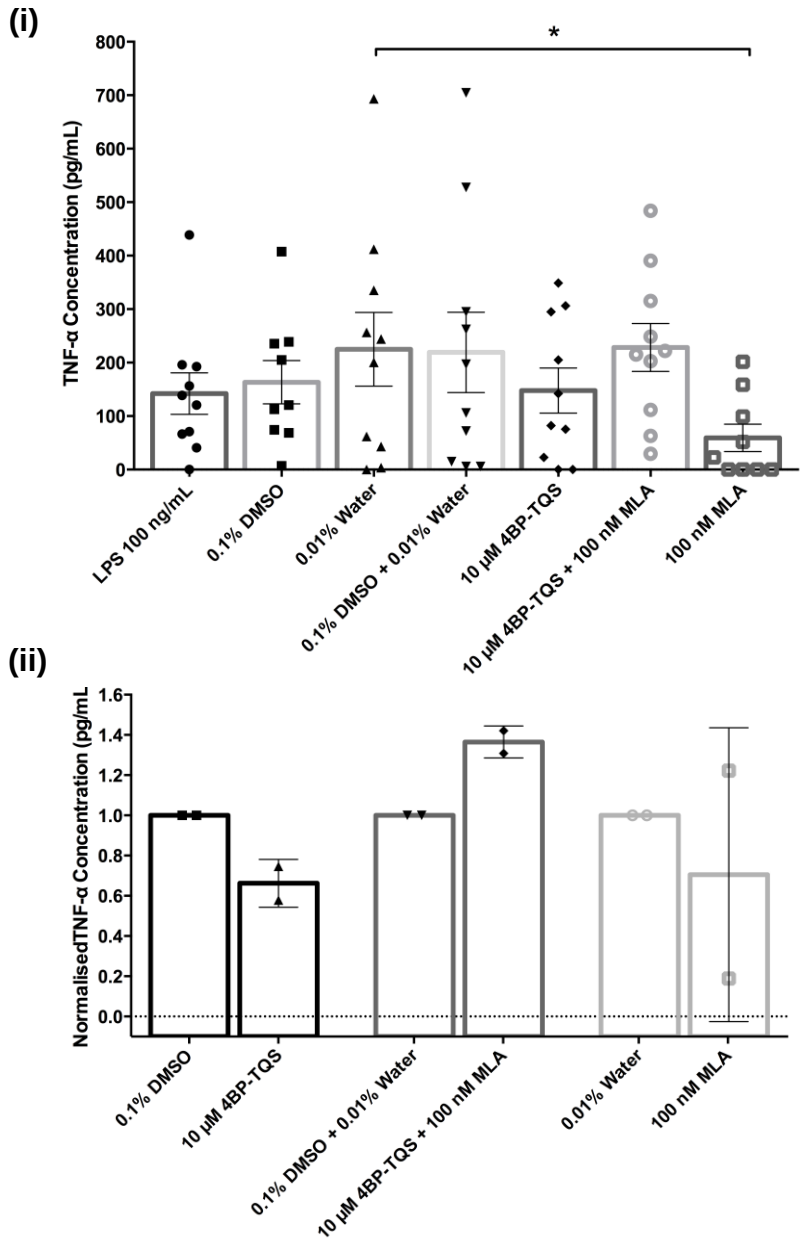

Figure 12: TNF-α release from 100 ng/mL LPS-stimulated cells in the presence of a potent nAChR antagonist. (i) Incubation of stimulated THP-1 cells with 10 µM 4BP-TQS showed a decrease in TNF-α release, however was not significant compared to the 0.1% DMSO vehicle control (0.1% DMSO: 163.3±40.5 pg/mL; 10 µM 4BP-TQS: 147.7±42.1 pg/mL). An increase in TNF-α levels was seen however upon co-incubation with 100 nM MLA compared to 10 µM 4BP-TQS incubation alone and similar levels were seen to the 0.1%DMSO+ 0.01% water vehicle control (0.1%+ 0.01% water: 219.1±75.0 pg/mL; 10 µM 4BP-TQS+ 100 nM MLA: 228.2±44.8 pg/mL). A significant decrease (p=0.05) was seen upon incubation of stimulated cells with 100 nM MLA alone, compared to the 0.01% water vehicle control (0.01% water: 225.1±68.9 pg/mL; 100 nM MLA: 59.4±25.6 pg/mL). **(ii)** Data from each condition was normalised to the

vehicle control for each experiment performed. It is clear that incubation with 10 µM 4BP-TQS caused a reduction in TNF-α release, which was restored when 100 nM MLA was incubated in combination. There was a decrease in TNF-α levels upon incubation with 100 nM MLA alone, however a large variability between experiments is evident. Samples were diluted 1:4 to be in the detection range for ELISA analysis. Data was obtained from 2 independent experiments. Each condition was replicated 5 times within each experiment. Any outliers were identified using a ROUT (1%) statistical test and subsequently removed. Error bars in graphs showing all data points (i) represent ± SEM and normalised data (ii) represent ± SD.

4.7 TNF-α Concentration Released From Neuroleptic-Naïve FEP Patients and Control LPS-Stimulated Monocytes.

Monocytes were harvested from whole blood samples obtained from 10 FEP patients and 9 controls, and stimulated with 10 ng/mL LPS for 24 hours. TNF-α production was measured using ELISAs (figure 13).

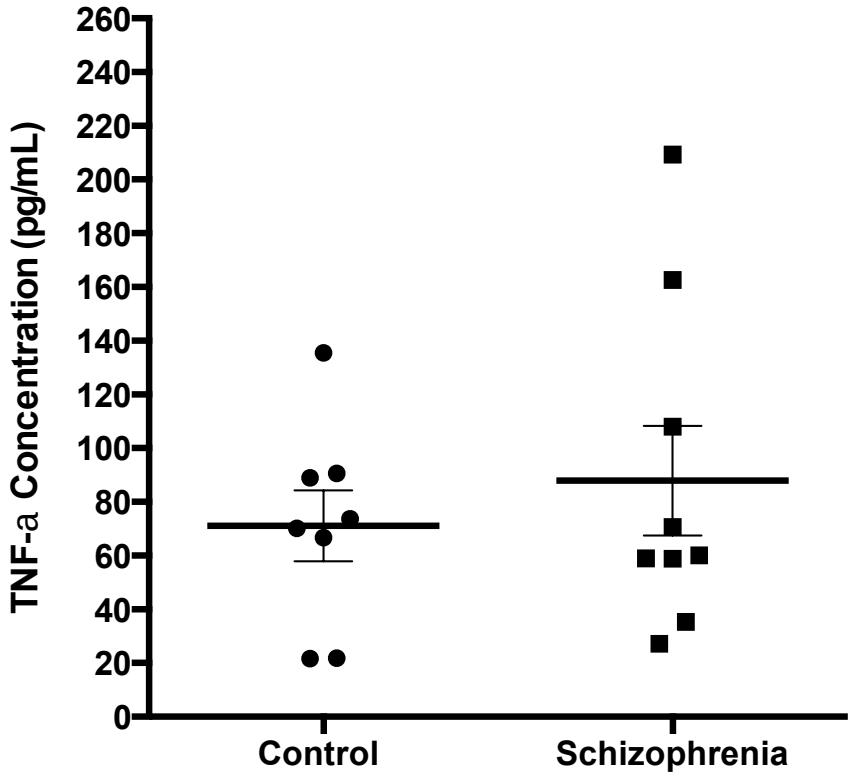

Figure 13: TNF-α release from LPS-stimulated monocytes obtained from neuroleptic-naïve FEP patients and control individuals. Primary monocytes were harvested from whole blood obtained from 10 FEP neuroleptic-naïve schizophrenic patients and 9 healthy controls. Monocytes were then stimulated with 10 ng/mL LPS for 24 hours. Supernatants were then collected and TNF-α levels were then measured using ELISAs. It is clear that there is only a slight increase in TNF-α concentration in the FEP neuroleptic-naïve patients compared to the healthy controls, and was not statistically significant (Control: 71.1±13.2 pg/mL; Schizophrenia: 87.9±20.4 pg/mL). Samples were diluted 1:50 to be in the detection range for ELISA analysis. One outlier was detected in each condition (ROUT test (1%)) and subsequently removed from analysis. Error bars represent ± SEM.

It is apparent that there is a small increase in the mean TNF-α release from FEP patients compared to the matched controls. However, there is wide distribution within the data and statistical analysis showed this increase to be non-significant.

4.8 TNF-α Concentration According to Patient Demographics

Results obtained from measuring monocyte TNF-α concentration from each patient was sorted according to patient demographics such as smoking status, age, gender and body mass index (BMI), seen in figure 14.

Patient smoking status showed a significant ($p=0.02$) increase in TNF-α concentration amongst smokers compared to those who were non-smoking (figure 13 (i)). Gender also appeared to be a determinant of TNF-α release amongst schizophrenia patients (figure (ii)). It is apparent that males have a higher TNF-α release than females, however this was not significant as more female samples are required. Patient age was also considered and it is clear that there is an increase in TNF-α in age categories 24-29 and over 30 years old, however large patient variability is seen (figure (iii)). Patient BMI was also accounted for, and

TNF-α release was increased in patients who were overweight, however again there is large variability within the data and is therefore not significant (figure (iv)).

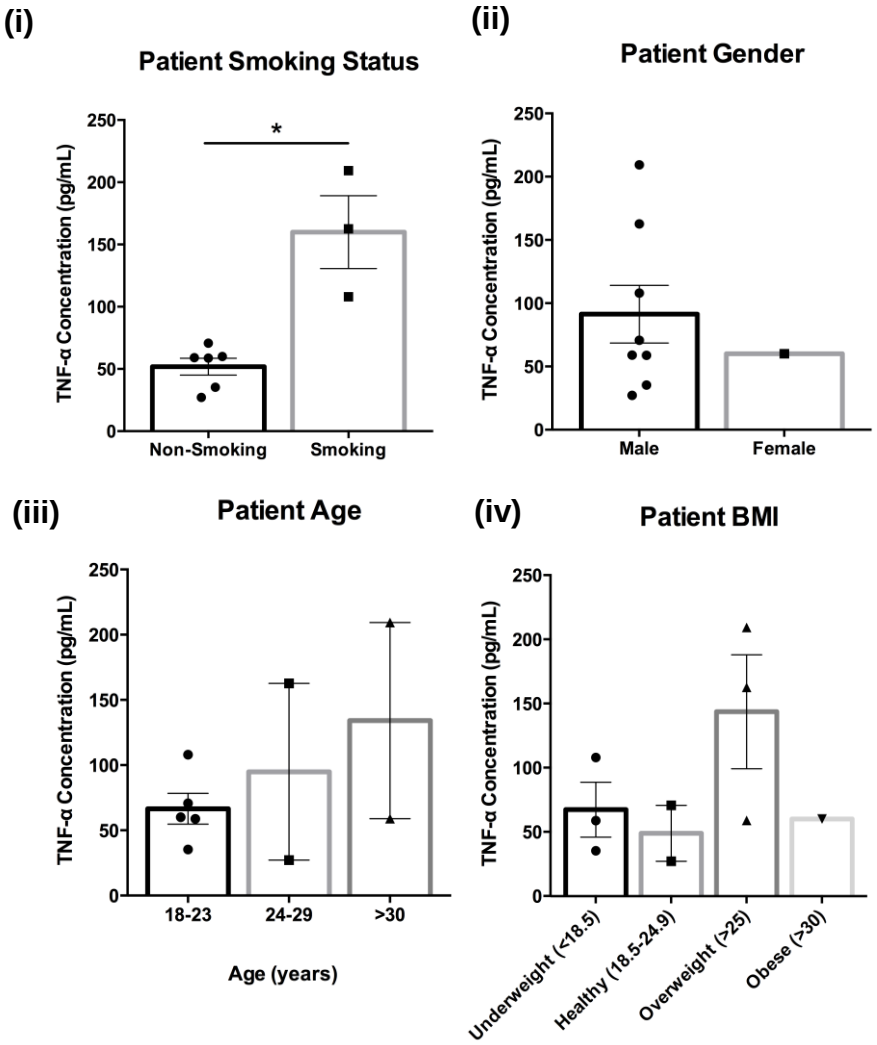

Figure 14: TNF-α release from 9 FEP neuroleptic-naïve schizophrenia patients according to smoking-status, gender, age and BMI. TNF-α levels from FEP schizophrenic patients were classified according to 4 categories, which are often not controlled for in many published studies. **(i) Patient smoking status.** The smoking status of patients was seen to affect the TNF-α release from monocytes. A significant increase (p=0.02) in TNF-α release from patients who were smokers compared to those who were non-smokers (Non-smoking: 51.8±6.8 pg/mL; Smoking: 160.0±29.3 pg/mL). **(ii) Patient gender**. Male patients had increased TNF-α release compared to the female patient however was not significant as more female patients would need to be sampled. (Male: 91.4±22.8 pg/mL; Female: 60.0 pg/mL). **(iii) Patient age**. Patients were separated into 3 age categories and TNF-α levels are seen to increase with age. However this

observation was not significant due to large variability between patients (18-23 years: 66.6±11.9 pg/mL; 24-29 years: 94.9±67.7 pg/mL; >30 years: 134.2±75.1 pg/mL). **(iv) Patient body mass index**. Patients were separated into categories, which are used to classify body mass index. From the data, an increase in TNF-α levels was seen in the overweight category, however this was not significant due to large patient variability (Underweight: 67.4±21.4 pg/mL; Healthy: 48.9±21.7 pg/mL; Overweight: 143.7±44.4 pg/mL; Obese: 60.0 pg/mL). Error bars represent ±SEM.

5. DISCUSSION

5.1 LPS-Stimulation of THP-1 Cells

THP-1 monocytic cells were chosen in this project to provide a cell culture model, to represent primary monocytes, which are often difficult to obtain. There are many additional advantages to using THP-1 cells over primary monocytes. THP-1 cells have a uniform genetic background, therefore removing any donor variability within results as well as removing the risk of any common blood contaminants, such as lymphocytes, which can occur in monocyte preparations[63]. Furthermore, studies have shown that THP-1 cells have a similar transcriptional response to monocytes and macrophages, obtained from donor peripheral blood, when stimulated with LPS[63]. Therefore these cells were chosen to characterise TNF-α response in the presence of a range of pharmacological agents.

To obtain the optimal TNF-α release from LPS-stimulated THP-1 cells to be in the ELISA detection range, a LPS-stimulation time course was conducted with varying concentrations of LPS (figure 7). Application of 100 ng/mL LPS produced the highest TNF-α response (508.4±86.6 pg/mL) compared to lower concentrations. Interestingly, the TNF-α concentration release from THP-1 cells peaked at 4 hours of LPS stimulation in all conditions where a response was elicited. After 4 hours, TNF-α was seen to reduce and after 24 hours, TNF-α production had decreased to low levels (96.3±44.9 pg/mL). TNF-α is known to be a primary moderator of the innate immune response and rapidly released in response to LPS stimulation[64], which these data reiterate. These results are also consistent with those in the literature[63]. Consequently from these results, a 4-hour stimulation period was chosen to use in THP-1 LPS stimulation experiments.

This experiment could be repeated in primary monocytes to see if the same TNF-α release pattern would be observed therefore providing validity to this *in vitro* model. Additionally, a TNF-α expression time course could be conducted in primary monocytes obtained from schizophrenia patients to see if there are any abnormalities in TNF-α release over time and whether there is a sustained increase in TNF-α, which could potentially contribute to the inflammatory phenotype seen in patient blood.

5.2 TNF-α Production Related to Administration of Pharmacological Agents

A variety of pharmacological compounds were incubated with THP-1 cells for 4 hours to observe any alterations in TNF-α production and release. These drug concentrations were chosen as they had been previously used in the laboratory and shown to be optimum concentrations however following the preliminary results presented in this study, then it would be prudent to re-calculate concentration curves for these drugs under the specific conditions used in these experiments.

Results show that upon application of 30 µM 4BP-TQS, TNF-α levels were significantly decreased upon stimulation with 10 ng/mL ($p=0.002$) and 100 ng/mL LPS ($p=0.0001$) for 4 hours, compared to the vehicle control (figure 8). 4BP-TQS has been shown to be a potent agonist of α7-nAChRs[65, 66]. Traditionally, endogenous ligands and agonists bind to the receptors binding site (orthosteric site). However, it has been shown that nAChRs also contain multiple additional binding sites (allosteric sites)[27]. Molecules that bind within this site typically exert their activity only if an agonist is bound at the orthosteric site, and can indirectly modulate receptor activity by either enhancing or reducing agonist activity[27, 67]. Positive allosteric modulators (PAMs) act to positively enhance and amplify agonist response,

whereas negative allosteric modulators (NAMs) act to reduce the response. When bound to the allosteric site in the absence of an agonist, allosteric modulators exhibit no effect on receptor activity[68].

4BP-TQS however, has been previously shown to bind to this allosteric site on α7-nAChRs and can exert potent agonist activity in the absence of endogenous ligands, inducing a direct effect on receptor activity[65, 66]. The data (figure 8) confirms that activation of the nAChR inhibits pro-inflammatory cytokine release from THP-1 cells following LPS-stimulation. Additionally, this effect can be induced not only through orthosteric ligands, such as nicotine but can also be regulated in absence of agonist binding, providing an alternative mechanism of regulation. This potentially provides a novel mechanism, which could be exploited for therapeutic use.

From the cell viability results (figure 11), it is apparent that 4BP-TQS is not toxic to THP-1 cells even at high concentrations (100 µM). However, it is apparent from the incubation with 25 µM cycloheximide, a protein synthesis inhibitor, that this toxic compound did not kill the THP-1 cells as expected. This could be because the 4-hour incubation was too short to do significant damage to THP-1 cell viability. Therefore this experiment could be repeated with longer incubation time of over 24 hours to check that 4BP-TQS does not affect cell viability over a longer stimulation period.

Additional experiments with 4BP-TQS could be conducted using monocytes harvested from donors to see if this nAChR allosteric agonist can elicit the same effect seen in this *in vitro*

model. Furthermore, it should be repeated with monocytes harvested from schizophrenia patients to see if 4BP-TQS can reduce the elevated pro-inflammatory response.

LPS-stimulated THP-1 cells were also incubated with a combination of nAChR allosteric modulators, PNU-282987 and PNU-120596 (PAM). It can be seen from the results that TNF-α release was significantly decreased when stimulated with 100 ng/mL LPS for 4 hours compared to the vehicle control. PNU-282987 is a selective and potent agonist of the α7 subtype of nAChRs[69] whose activity is enhanced in the presence of PNU-120596, a selective α7 PAM[27]. This result therefore reinforces that TNF-α release from THP-1 cells can be altered through manipulation of α7-nAChRs. However, reduction in TNF-α upon incubation with PNU and PAM was not as prominent as observed by application of allosteric agonist 4BP-TQS and, upon normalisation of the data, considerable variability was seen between experiments involving PNU and PAM incubation (figure 8 (iv)). Therefore to obtain a firm conclusion, more replicates are required. Interestingly, PNU-282987 has been shown to restore sensory gating deficits *in vivo*[27] and so this compound could potentially provide a treatment aimed to target cognitive effects of schizophrenia, as well as reducing inflammatory response.

Incubation with 5-HT and a potent 5-HT_3 receptor allosteric modulator[70], 5-Chloroindole showed a small but insignificant decrease in TNF-α release when stimulated with 10 and 100 ng/mL LPS compared to the vehicle control (figure 8 (i) and (iii)). Serotonin is a monoamine neurotransmitter known to be involved in many neurological processes including learning and memory, mood[71] and has been heavily implicated in treating depression. Therefore, 5-HT derived treatments have been used to relieve the negative symptoms associated with

schizophrenia[72, 73]. In this experiment, 5-HT was used to investigate whether this compound may also have an effect on the inflammatory response, however the data suggest that it does not.

THP-1 cells were also incubated with clozapine, an atypical anti-psychotic given to schizophrenic patients that have not responded to other treatments. Clozapine is a broad-spectrum antagonist known to bind to many dopaminergic, serotoninergic and GABA receptors[74] and has been shown to reduce many negative symptoms of schizophrenia including depression through antagonism of the 5-HT_A receptor[72]. Studies have shown that clozapine can actually increase the plasma levels of TNF-α[75]. Within this experiment clozapine was administered at a concentration found within patient plasma. The data (figure 8) appear to show a small decrease in TNF-α release compared to the vehicle control. Clozapine however is known to have many adverse side effects such as agranulocytosis and seizures and is predominately linked with weight-gain in medicated individuals[50, 75]. It is therefore believed that this increase in cytokine levels could be associated with increased weight and therefore may explain why elevated levels were not seen within this model. Because clozapine has shown mixed results in its ability to reduce pro-inflammatory cytokines in addition to its severe side-effects, it is therefore suggested that research into treatments involving α7-nAChR agonists should be prioritised. Current investigations show promising α7-nAChR treatments such as GTS-21 (DMXBA)[76, 77] which has shown to improve cognition and the P50 deficit in clinical trials, however these compounds require further investigation since the drug has a relatively short half-life, so would require frequent dosage[77] which would be unrealistic for patients.

5.3 Inhibition of 4BP-TQS Induced TNF-α Reduction.

Further to the discovery that 4BP-TQS significantly reduced TNF-α release from LPS-stimulated THP-1 cells, experiments were performed to investigate whether this reduction could be blocked using nAChR antagonists and to confirm TNF-α release was via α7-nAChRs.

Picrotoxin has been previously shown to be an effective inhibitor of the α7 nAChR subunit[78]. PTX is a known potent neurotoxin and a channel blocker of many ligand-gated ion channels, including nAChRs[78]. Figure 9 shows that the addition of 0.3, 1 and 3 µM of PTX was not able to inhibit reduction of TNF-α from THP-1 cells and concentrations were similar to those seen with 4BP-TQS alone. However, upon normalisation to the vehicle control, it is apparent that there is considerable variation between experiments and it is advised that more replicates are conducted. Additionally, higher concentrations of PTX could be needed however could not be investigated due to project time constraints.

Methyllycaconitine is a potent competitive orthosteric antagonist of α7-nAChRs[79]. The data (figure 12) demonstrate that the application of 10 µM 4BP-TQS is able to reduce the TNF-α levels, as previously documented. In comparison, upon application of MLA and 4BP-TQS, there is an increase in the production of TNF-α. Upon normalisation to the vehicle control for each condition, it is clear that MLA causes a marked increase in TNF-α levels, suggesting that antagonist activity of MLA, in combination with 4BP-TQS, is increased. When MLA is applied to LPS-stimulated cells however, there is a significant decrease ($p=0.05$) in TNF-α levels, which contradicts the hypothesis that MLA should antagonise the nAChR anti-inflammatory response. However, upon normalisation of the data compared to the vehicle

control, considerably large variability is evident and therefore more replications are needed before a definitive conclusion can be drawn.

5.4 TNF-α Release from LPS-Stimulated Monocytes From Neuroleptic-Naïve FEP Patients.

5.4.1 TNF-α Concentration From FEP Neuroleptic-naïve Monocytes Compared to Healthy Controls.

This investigation is one of the few to quantify TNF-α release from LPS-stimulated monocytes from 10 FEP, neuroleptic-naïve patients which have been controlled for demographics such as age, gender, BMI and smoking-status. This study provides a significant benefit over previous investigations as these studies have failed to control for such factors that would produce erroneous measurements of TNF-α. As such, previous research is unlikely to represent an accurate and realistic picture of the role of inflammatory cytokines in schizophrenia cases.

Figure 13 shows TNF-α release from 8 control individuals compared to levels obtained from 9 FEP patients (an outlier from each condition had been statistically removed). It is apparent that there is a small increase in TNF-α amongst patients, however this was not significantly different when compared to the controls. This suggests that when cytokine status is investigated at the first onset of schizophrenia, before commencing medication, that there is no significant increase in pro-inflammatory cytokines and that the increases in TNF-α concentrations seen in the literature are potentially due to medication or sampling from patients at a different stage in disease course. Additionally, these results are obtained from a

single-cell population of monocytes, and an increase in TNF-α could be apparent in the serum or plasma obtained from these patients, which has been shown in the literature.

Future investigations should initially measure TNF-α levels from plasma obtained from these FEP patients and control individuals to test whether TNF-α is elevated, as reported in the literature. Other pro-inflammatory cytokines, such as IL-6, released from monocytes have been shown to be more consistently elevated in schizophrenia studies[41, 80]. Future experiments should therefore assess whether concentrations of these cytokines are elevated in FEP neuroleptic-naïve patients compared to healthy controls. A Luminex multiplex assay should also be performed to investigate levels of numerous pro-inflammatory, and anti-inflammatory cytokines simultaneously from both monocyte and serum preparations. From these results, certain cytokines of interest, providing a better model for the inflammatory response associated with schizophrenia, could then be investigated further.

5.4.2 TNF-α Release From FEP Neuroleptic-naïve Patients According to Demographic Factors.

Once TNF-α levels had been measured for both controls and patients, the sample identities were revealed, and the patient data was categorised according to smoking status, gender, age and BMI (figure 14). It is clear that patients who smoked nicotine had a significant increase ($p=0.02$) in TNF-α release. This data appears contradictory to the phenomenon of nicotine agonism of nAChRs, which produces a reduction in pro-inflammatory cytokines. A possible explanation for this is that if these patients are chronic smokers, then the overall pro-inflammatory response could be elevated since nicotine has many other adverse side-effects that contribute to the inflammatory response (e.g. cardiovascular and respiratory

complications). Furthermore, Van der Zanden *et al.* (2012)[81] have shown that LPS-stimulated THP-1 monocyte release was inhibited by nAChR activation however was not constantly observed in primary monocytes from smoking individuals, which suggests that patient variability could play a role in this unpredicted response. Therefore for further investigation, it is advised that the sample numbers be increased for both the FEP patients and control individuals to provide a better representation of the population and aid in the omission of anomalous data.

None of the other schizophrenia patient demographics produced any significant differences in TNF-α release however an increase in BMI was seen to elevate TNF-α levels suggesting that BMI does play a role in the increase of pro-inflammatory cytokines of patients. However large variability was seen amongst patients and further data would be required to be able to draw any definitive or firm conclusions. This data needs to be compared with data obtained from the demographically controlled healthy individuals to provide a true comparison. Unfortunately this data could not be made available at the time of writing.

6. CONCLUSION

The data presented in this study represent a substantial development in our ability to investigate the role of pro-inflammatory cytokines in the development of schizophrenia. An abnormal increase in pro-inflammatory cytokines, such as TNF-α, can hinder both the early development of the brain and periods of neuronal plasticity in later life leading to an increased risk of schizophrenia. Many studies have documented an elevated release of TNF-α in schizophrenia patients however there is a certain amount of ambiguity within these studies as others have claimed no significant difference. It is believed that these discrepancies are likely to be as a result of a failure on behalf of these investigations to control for factors that can affect cytokine concentrations, such as medication. This study therefore aimed to remove this uncertainty in TNF-α determination in schizophrenia and is one of the few studies to investigate TNF-α release from primary monocytes from neuroleptic-naïve FEP patients who had been demographically matched to healthy controls. The subsequent findings show a small increase in TNF-α release from 9 FEP patients although was not statistically significant when compared to 8 healthy controls. It is recommended however that the sample size be increased to provide a better representation of the population.

In addition to these results, it was discovered that the nAChR allosteric agonist, 4BP-TQS was significantly able to reduce TNF-α from THP-1 monocytes. Further research needs to be conducted into whether this compound could potentially be adapted to provide a treatment targeted at reducing the inflammatory response that affects the positive, negative and cognitive symptoms seen in schizophrenia. Nicotine, a principal agonist of the nAChRs, is widely used among schizophrenic patients for this purpose, however this study showed that TNF-α release was significantly *increased* amongst smokers, suggesting that prolonged

nicotine usage can actually have the opposite effect. Consequently, it would be beneficial to further research additional nAChR agonists to remove these adverse effects apparent in self-medicalization treatments and currently prescribed anti-psychotics, such as clozapine.

7. LIST OF REFERENCES

1. Meyer, U., Schwarz, M.J. and Müller, N. (2011) *Inflammatory processes in schizophrenia: a promising neuroimmunological target for the treatment of negative/cognitive symptoms and beyond.* Pharmacology & Therapeutics, **132**(1): p. 96-110.
2. American Psychiatric Association. (1994) *Diagnostic and statistical manual of mental disorders.* http://www.nlm.nih.gov/research/umls/sourcereleasedocs/current/DSM4/ Last accessed (14.05.14).
3. Tandon, R., Nasrallah, H.A. and Keshavan, M.S. (2009) *Schizophrenia,"just the facts" 4. Clinical features and conceptualization.* Schizophrenia Research, **110**(1): p. 1-23.
4. Solinski, S., Jackson, H. and Bell, R. (1992) *Prediction of employability in schizophrenic patients.* Schizophrenia Research, **7**(2): p. 141-148.
5. Brüne, M., et al. (2011) *Social skills and behavioral problems in schizophrenia: the role of mental state attribution, neurocognition and clinical symptomatology.* Psychiatry Research, **190**(1): p. 9-17.
6. Howes, O.D. and Kapur, S. (2009) *The dopamine hypothesis of schizophrenia: version III—the final common pathway.* Schizophrenia Bulletin, **35**(3): p. 549-562.
7. Laruelle, M. (2014) *Schizophrenia: from dopaminergic to glutamatergic interventions.* Current Opinion in Pharmacology, **14**: p. 97-102.
8. Schwarz, M. (2007) *The immunological basis of glutamatergic disturbance in schizophrenia: towards an integrated view.* Neuropsychiatric Disorders An Integrative Approach. Springer, p. 269-280.
9. Wright, P., et al. (1995) *Maternal influenza, obstetric complications, and schizophrenia.* American Journal of Psychiatry, **152**(12): p. 1714-1720.
10. Kunugi, H., Nanko, S. and Murray, R.M. (2001) *Obstetric complications and schizophrenia: prenatal underdevelopment and subsequent neurodevelopmental impairment.* The British Journal of Psychiatry, **178**(40): p. s25-s29.
11. Craddock, N., O'Donovan, M. and Owen, M. (2005) *The genetics of schizophrenia and bipolar disorder: dissecting psychosis.* Journal of Medical Genetics, **42**(3): p. 193-204.
12. Owen, M., Craddock, N. and O'Donovan, M. (2005) *Schizophrenia: genes at last?* TRENDS in Genetics, **21**(9): p. 518-525.
13. Vereczkei, A. and Mirnics, K. (2011) *Genetic predisposition to schizophrenia: what did we learn and what does the future hold.* Neuropsychopharmacology Hungary, **13**(4): p. 205-210.
14. Upthegrove, R., Manzanares-Teson, N. and Barnes, N.M. (2014) *Cytokine function in medication-naive first episode psychosis: A systematic review and meta-analysis.* Schizophrenia Research, **155**(1): p. 101-108.

15. Upthegrove, R. and Barnes, N.M. (2014) *The immune system and schizophrenia: an update for clinicians.* Advances in Psychiatric Treatment, **20**(2): p. 83-91.
16. Meneghin, A. and Hogaboam, C.M. (2007) *Infectious disease, the innate immune response, and fibrosis.* Journal of Clinical Investigation, **117**(3): p. 530-538.
17. Zhang, J.-M. and An, J. (2007) *Cytokines, inflammation and pain.* International Anesthesiology Clinics, **45**(2): p. 27-37.
18. Serhan, C.N. and Savill, J. (2005) *Resolution of inflammation: the beginning programs the end.* Nature Immunology, **6**(12): p. 1191-1197.
19. Miller, B.J., et al. (2011) *Meta-analysis of cytokine alterations in schizophrenia: clinical status and antipsychotic effects.* Biological Psychiatry, **70**(7): p. 663-671.
20. O'Brien, S.M., Scully, P. and Dinan, T.G. (2008) *Increased tumor necrosis factor-alpha concentrations with interleukin-4 concentrations in exacerbations of schizophrenia.* Psychiatry Research, **160**(3): p. 256-262.
21. Potvin, S., et al. (2008) *Inflammatory cytokine alterations in schizophrenia: a systematic quantitative review.* Biological Psychiatry, **63**(8): p. 801-808.
22. Hagberg, H., Gressens, P. and Mallard, C. (2012) *Inflammation during fetal and neonatal life: implications for neurologic and neuropsychiatric disease in children and adults.* Annals of Neurology, **71**(4): p. 444-457.
23. Raison, C.L. and Miller, A.H. (2013) *Malaise, melancholia and madness: The evolutionary legacy of an inflammatory bias.* Brain, Behavior, and Immunity, **31**: p. 1-8.
24. Müller, N. (2011) *Inflammation and schizophrenia: pathophysiological and therapeutic aspects.* Minerva Psichiatrica, **52**: p. 205-218.
25. Brown, A.S. and Derkits, E.J. (2010) *Prenatal infection and schizophrenia: a review of epidemiologic and translational studies.* American Journal of Psychiatry. **167**(3): p. 261-280.
26. Dantzer, R., et al. (2008) *From inflammation to sickness and depression: when the immune system subjugates the brain.* Nature Reviews Neuroscience, **9**(1): p. 46-56.
27. Faghih, R., Gopalakrishnan, M. and Briggs, C.A. (2008) *Allosteric modulators of the α7 nicotinic acetylcholine receptor.* Journal of Medicinal Chemistry, **51**(4): p. 701-712.
28. Schaaf, C.P. (2014) *Nicotinic acetylcholine receptors in human genetic disease.* Genetics in Medicine, P. 1-8, Doi:10.1038/gim.2014.9.
29. Posadas, I., López-Hernández, B. and Ceña, V. (2013) *Nicotinic Receptors in Neurodegeneration.* Current Neuropharmacology, **11**(3): p. 298-314
30. Ulloa, L. (2005) *The vagus nerve and the nicotinic anti-inflammatory pathway.* Nature Reviews Drug Discovery, **4**(8): p. 673-684.

31. Erulkar, S. (2013) *Nervous system (anatomy).* http://www.britannica.com/EBchecked/topic/409665/nervous-system . Last accessed (14.05.14).
32. Leonard, S., et al. (1996) *Nicotinic receptor function in schizophrenia.* Schizophrenia Bulletin, **22**(3): p. 431-446.
33. Leonard, S., et al. (2000) *Smoking and schizophrenia: abnormal nicotinic receptor expression.* European Journal of Pharmacology, **393**(1): p. 237-242.
34. Berrettini, W.H. (2005) *Genetic bases for endophenotypes in psychiatric disorders.* Dialogues in Clinical Neuroscience, **7**(2): p. 95-101.
35. Adler, L.E., et al. (1993) *Normalization of auditory physiology by cigarette smoking in schizophrenic patients.* The American Journal of Psychiatry, **150** (12): p. 1856-1861.
36. Brunzell, D.H. and McIntosh, J.M. (2012) *Alpha7 nicotinic acetylcholine receptors modulate motivation to self-administer nicotine: implications for smoking and schizophrenia.* Neuropsychopharmacology, **37**(5): p. 1134-1143.
37. Ripoll, N., Bronnec, M. and Bourin, M. (2004) *Nicotinic receptors and schizophrenia.* Current Medical Research and Opinion®, **20**(7): p. 1057-1074.
38. D'Souza, M.S. and Markou, A. (2012) *Schizophrenia and tobacco smoking comorbidity: nAChR agonists in the treatment of schizophrenia-associated cognitive deficits.* Neuropharmacology, **62**(3): p. 1564-1573.
39. Kelly, C. and McCreadie, R. (2000) *Cigarette smoking and schizophrenia.* Advances in Psychiatric Treatment, **6**(5): p. 327-331.
40. Freedman, R., et al. (1995) *Evidence in postmortem brain tissue for decreased numbers of hippocampal nicotinic receptors in schizophrenia.* Biological Psychiatry, **38**(1): p. 22-33.
41. Krause, D.L., et al. (2012) *Intracellular monocytic cytokine levels in schizophrenia show an alteration of IL-6.* European Archives of Psychiatry and Clinical Neuroscience, **262**(5): p. 393-401.
42. Müller, N., et al. (2012) *Impaired monocyte activation in schizophrenia.* Psychiatry Research, **198**(3): p. 341-346.
43. Giebelen, I.A., et al. (2007) *Local stimulation of [alpha] 7 cholinergic receptors inhibits LPS-induced TNF-[alpha] release in the mouse lung.* Shock, **28**(6): p. 700-703.
44. Marrero, M.B., et al. (2011) *Application of alpha7 nicotinic acetylcholine receptor agonists in inflammatory diseases: an overview.* Pharmaceutical Research, **28**(2): p. 413-416.
45. Borovikova, L.V., et al. (2000) *Vagus nerve stimulation attenuates the systemic inflammatory response to endotoxin.* Nature, **405**(6785): p. 458-462.

46. Wang, H., et al. (2003) *Nicotinic acetylcholine receptor α7 subunit is an essential regulator of inflammation.* Nature, **421**(6921): p. 384-388.
47. Wilke, I., et al. (1996) *Investigations of cytokine production in whole blood cultures of paranoid and residual schizophrenic patients.* European Archives of Psychiatry and Clinical Neuroscience, **246**(5): p. 279-284.
48. Kawashima, K., et al. (2012) *Critical roles of acetylcholine and the muscarinic and nicotinic acetylcholine receptors in the regulation of immune function.* Life Sciences, **91**(21): p. 1027-1032.
49. Levin, E.D. (2002) *Nicotinic receptor subtypes and cognitive function.* Journal of Neurobiology, **53**(4): p. 633-640.
50. Kluge, M., et al. (2009) *Effects of clozapine and olanzapine on cytokine systems are closely linked to weight gain and drug-induced fever.* Psychoneuroendocrinology, **34**(1): p. 118-128.
51. Asher, C. and Gask, L. (2010) *Reasons for illicit drug use in people with schizophrenia: Qualitative study.* BMC Psychiatry, **10**:94, p. 1-15.
52. Di Nicola, M., et al. (2013) *Serum and gene expression profile of cytokines in first-episode psychosis.* Brain, Behavior, and Immunity, **31**: p. 90-95.
53. Gregor, M.F. and Hotamisligil, G.S. (2011) *Inflammatory mechanisms in obesity.* Annual Review of Immunology, **29**: p. 415-445.
54. Pollmächer, T., et al. (1997) *Smoking affects plasma-soluble interleukin-2 receptor levels in patients with schizophrenia.* Archives of General Psychiatry, **54**(1): p. 89-89.
55. Fain, J.N. (2006) *Release of interleukins and other inflammatory cytokines by human adipose tissue is enhanced in obesity and primarily due to the nonfat cells.* Vitamins & Hormones, **74**: p. 443-477.
56. Yoshikawa, H., et al. (2006) *Nicotine inhibits the production of proinflammatory mediators in human monocytes by suppression of I-κB phosphorylation and nuclear factor-κB transcriptional activity through nicotinic acetylcholine receptor α7.* Clinical & Experimental Immunology, **146**(1): p. 116-123.
57. Álvarez, A., et al. (2007) *Serum TNF-alpha levels are increased and correlate negatively with free IGF-I in Alzheimer disease.* Neurobiology of Aging, **28**(4): p. 533-536.
58. Rutgeerts, P., Van Assche, G. and Vermeire, S. (2004) *Optimizing anti-TNF treatment in inflammatory bowel disease.* Gastroenterology, **126**(6): p. 1593-1610.
59. Song, X.-Q., et al. (2009) *The interaction of nuclear factor-kappa B and cytokines is associated with schizophrenia.* Biological Psychiatry, **65**(6): p. 481-488.
60. Life Technologies. (2014) *SYTOX® Blue Dead Cell Stain, for flow cytometry.* http://www.lifetechnologies.com/order/catalog/product/S34857 Last accessed (14.05.14).

61. World Health Organisation. (2010) *ICD-10 Version:2010*. http://apps.who.int/classifications/icd10/browse/2010/en. Last accessed (14.05.14).
62. Munoz, N.M. and Leff, A.R. (2007) *Highly purified selective isolation of eosinophils from human peripheral blood by negative immunomagnetic selection.* Nature Protocols, **1**(6): p. 2613-2620.
63. Schildberger, A., et al. (2013) *Monocytes, peripheral blood mononuclear cells, and THP-1 cells exhibit different cytokine expression patterns following stimulation with lipopolysaccharide.* Mediators of Inflammation, v**2013**: p.1-10.
64. DeForge, L. and Remick, D.G. (1991) *Kinetics of TNF, IL-6, and IL-8 gene expression in LPS-stimulated human whole blood.* Biochemical and Biophysical Research Communications, **174**(1): p. 18-24.
65. Gill, J.K., et al. (2012) *A series of α7 nicotinic acetylcholine receptor allosteric modulators with close chemical similarity but diverse pharmacological properties.* Molecular Pharmacology, **81**(5): p. 710-718.
66. Gill, J.K., et al. (2011) *Agonist activation of α7 nicotinic acetylcholine receptors via an allosteric transmembrane site.* Proceedings of the National Academy of Sciences, **108**(14): p. 5867-5872.
67. Hu, M., Gopalakrishnan, M. and Li, J. (2009) *Positive allosteric modulation of α7 neuronal nicotinic acetylcholine receptors: lack of cytotoxicity in PC12 cells and rat primary cortical neurons.* British Journal of Pharmacology, **158**(8): p. 1857-1864.
68. Pałczyńska, M.M., et al. (2012) *Activation of α7 nicotinic receptors by orthosteric and allosteric agonists: influence on single-channel kinetics and conductance.* Molecular Pharmacology, **82**(5): p. 910-917.
69. Bodnar, A.L., et al. (2005) *Discovery and structure-activity relationship of quinuclidine benzamides as agonists of α7 nicotinic acetylcholine receptors.* Journal of Medicinal Chemistry, **48**(4): p. 905-908.
70. Newman, A.S., et al. (2013) *5-Chloroindole: a potent allosteric modulator of the 5-HT3 receptor.* British Journal of Pharmacology, **169**(6): p. 1228-1238.
71. Gordon, J. and Barnes, N.M. (2003) *Lymphocytes transport serotonin and dopamine: agony or ecstasy?* Trends in Immunology, **24**(8): p. 438-443.
72. Igbal, N. and van Praag, H.M. (1995) *The role of serotonin in schizophrenia.* European Neuropsychopharmacology, **5**: p. 11-23.
73. Abi-Dargham, A., et al. (1997) *The role of serotonin in the pathophysiology and treatment of schizophrenia.* The Journal of Neuropsychiatry and Clinical Neurosciences, **9**(1): p.1-17.

74. Coward, D. (1992) *General pharmacology of clozapine.* The British Journal of Psychiatry,**17**: p. 5-11.

75. Lett, T., et al. (2011) *Pharmacogenetics of antipsychotic-induced weight gain: review and clinical implications.* Molecular Psychiatry, **17**(3): p. 242-266.

76. Jonge, W. and Ulloa, L. (2007) *The alpha7 nicotinic acetylcholine receptor as a pharmacological target for inflammation.* British Journal of Pharmacology, **151**(7): p. 915-929.

77. Olincy, A. and Freedman, R. (2012) *Nicotinic mechanisms in the treatment of psychotic disorders: a focus on the α7 nicotinic receptor*. Novel Antischizophrenia Treatments. Springer, p. 211-232.

78. Erkkila, B.E., Weiss, D.S. and Wotring, V.E. (2004) *Picrotoxin-mediated antagonism of α3β4 and α7 acetylcholine receptors.* Neuroreport, **15**(12): p. 1969-1973.

79. Alkondon, M., et al. (1992) *Blockade of nicotinic currents in hippocampal neurons defines methyllycaconitine as a potent and specific receptor antagonist.* Molecular Pharmacology, **41**(4): p. 802-808.

80. Müller, N., et al. (2000) *The immune system and schizophrenia: an integrative view.* Annals of the New York Academy of Sciences, **917**(1): p. 456-467.

81. Van der Zanden, E.P., et al. (2012) *Nicotinic acetylcholine receptor expression and susceptibility to cholinergic immunomodulation in human monocytes of smoking individuals.* Neuroimmunomodulation, **19**(4): p. 255-265.